PL-TR-93-2071

SENSITIVITY TESTING OF A SINGLE-DOPPLER TEMPERATURE RETRIEVAL AND FORECAST SYSTEM

Thomas M. Hamill
Thomas Nehrkorn

Atmospheric and Environmental Research, Inc
840 Memorial Drive
Cambridge, MA 02139

1 February 1993

Scientific Report No. 4

Approved for public release; distribution unlimited

PHILLIPS LABORATORY
Directorate of Geophysics
AIR FORCE MATERIEL COMMAND
HANSCOM AIR FORCE BASE, MA 01731-3010

"This technical report has been reviewed and is approved for publication."

ALLAN J. BUSSEY
Contract Manager

JOSEPH W. SNOW
Chief, Satellite Meteorology Branch
Atmospheric Sciences Division

ROBERT A. McCLATCHEY
Director, Atmospheric Sciences Division

This report has been reviewed by the ESC Public Affairs Office (PA) and is releasable to the National Technical Information Service (NTIS).

Qualified requestors may obtain additional copies from the Defense Technical Information Center. All others should apply to the National Technical Information Service.

If your address has changed, or if you wish to be removed from the mailing list, or if the addressee is no longer employed by your organization, please notify PL/TSI, 29 **Randolph Road,** Hanscom AFB, MA 01731-3010. This will assist us in maintaining a current mailing list.

Do not return copies of this report unless contractual obligations or notices on a specific document requires that it be returned.

REPORT DOCUMENTATION PAGE	*Form Approved OMB No. 0704-0188*

1. AGENCY USE ONLY (Leave blank)	2. REPORT DATE	3. REPORT TYPE AND DATES COVERED
	1 February 1993	Scientific No. 4

4. TITLE AND SUBTITLE
Sensitivity Testing of a Single Doppler Temperature Retrieval and Forecast System

5. FUNDING NUMBERS
F19628-91-C-0011
PE 62101F
PR 6670
TA 17
WU CA

6. AUTHOR(S)
Thomas M. Hamill and Thomas Nehrkorn

7. PERFORMING ORGANIZATION NAMES(S) AND ADDRESS(ES)
Atmospheric and Environmental Research, Inc.
840 Memorial Drive
Cambridge, MA 02139

8. PERFORMING ORGANIZATION REPORT NUMBERS
(none)

9. SPONSORING / MONITORING AGENCY NAMES(S) AND ADDRESS(ES)
Phillips Laboratory
29 Randolph Road
Hanscom AFB, MA 01731-3010
Contract Manager: Allan Bussey/GPA

10. SPONSORING / MONITORING AGENCY REPORT NUMBER
PL-TR-93-2071

11. SUPPLEMENTARY NOTES

12a. DISTRIBUTION / AVAILABILITY STATEMENT
Approved for public release; distribution unlimited

12b. DISTRIBUTION CODE

13 ABSTRACT *(Maximum 200 words)*

Results are presented from the second year of a three-year contract to explore the feasibility of local thunderstorm forecasting based on the assimilation of single-Doppler radar data. The method used can assimilate Doppler radial winds, derive a tangential component, infer temperature distributions from the wind, and assimilate the resultant information.

The underlying analysis and assimilation methodology is explained in detail. This is then followed with a set of sensitivity experiments using simulated Doppler radar data generated from a numerical model forecast. A simple 2-D experiment is first presented which confirms the benefit of temperature assimilation to complement wind data assimilation. Second, a set of 3-D model experiments is presented to test the sensitivity of the model to observational data type and error characteristics. The results suggest that forecast accuracy is relatively insensitive to the observational error, though this result is in part due to the inherent smoothing built into the objective analysis and the assumption of no biases in the wind observations.

14. SUBJECT TERMS
Numerical weather prediction
Doppler radar data analysis
Mesoscale meteorology
Thunderstorm forecasting

15. NUMBER OF PAGES
94

16. PRICE CODE
-

17. SECURITY CLASSIFICATION OF REPORT	18. SECURITY CLASSIFICATION OF THIS PAGE	19. SECURITY CLASSIFICATION OF ABSTRACT	20. LIMITATION OF ABSTRACT
Unclassified	Unclassified	Unclassified	SAR

TABLE OF CONTENTS

LIST OF TABLES

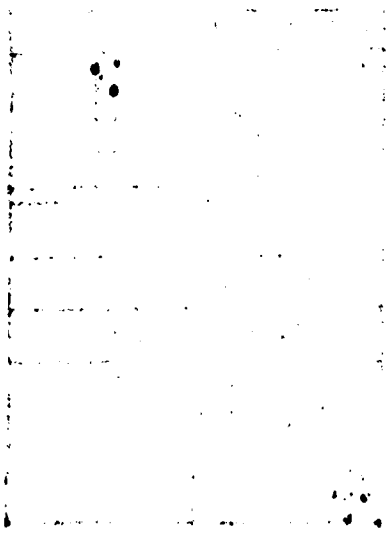

LIST OF FIGURES

LIST OF FIGURES
(continued)

LIST OF FIGURES
(continued)

1. Introduction

This technical report is a follow-on to Phillips Laboratory Technical Report PL-TR-92-2029 (Hamill, 1992). It summarizes the second year of research into the feasibility of thunderstorm prediction based on the continuous assimilation of single-Doppler radar information into a numerical forecast model. The hope of this project is that it will demonstrate a usable assimilation and forecast technique, one that can accurately describe current boundary layer airflow and subsequently predict the onset of convection for many weather regimes. The underlying premise is that thunderstorms typically are generated in areas of instability and low-level convergence, and effectively using Doppler winds and derived temperatures may improve the prediction of these features.

As was shown in Liou (1989), Cotton et al. (1989), and our previous report, assimilation using Newtonian nudging (Stauffer and Seaman, 1990) of the observed Doppler wind velocities alone is usually insufficient; temperature information is also needed. Without temperature information, circulation patterns developed from the assimilation of wind data may not be sustained. In the preconvective boundary layer, areas with low-level convergence are usually also areas with positive buoyancy. As was shown in Cotton et al. (1989), nudging the winds alone in this situation may actually create a cold anomaly through adiabatic cooling, resulting in the circulation reversing direction after the nudging is stopped. Our own assimilation experiments (Hamill, 1992) for a seabreeze simulation also showed generally inferior forecasts from assimilation experiments using wind data alone, compared to those nudging to observed winds and temperatures.

There is an effective way to "retrieve" atmospheric temperatures provided the winds are known with reasonable accuracy (Gal-Chen, 1978). Using the available wind information, and the u and v equations of motion, a Poisson equation can be formulated and solved for pressure perturbations, and temperature deviation derived from these pressure perturbations. This procedure will be outlined more completely in Section 2.

The literature has many examples of successful retrievals (e.g., Hane and Scott, 1978; Roux, 1985). However, only recently has attention been paid to how to perform them when only one radar is available. Since the NEXRAD (Next Generation Weather Radar, or WSR-88D) radar network is not dense enough to give dual- or triple-Doppler coverage to many areas, this is more than an academic concern; most of the country will be observed by only one radar. Thus, if retrieval technology is to be used operationally in the next few decades, the problem of how to successfully deduce temperatures from one radar's winds must be solved.

An interesting theoretical question is why use of the retrieved temperature information should lead to improved forecasts: all the information that is used as input to the retrieval (the 4-D structure of the wind field, and the governing equations) is available and used in some fashion in model runs with nudging of the

wind data alone. However, it appears from the results of both our own and other research experiments that this information is not used to its fullest extent with simple Newtonian nudging of winds.

The adjoint technique provides, in principle, a more direct way to relate the wind information to the corresponding mass field through the equations of motions. This is a very active area of research (Qiu and Xu, 1992; Sun et al., 1991; Kapitza, 1991). In the long run this approach has more potential to accurately determine the 4-D wind and temperature structure. However, the dynamic retrieval technique is computationally more efficient, and we believe it has more potential over the short term for practical application.

Thus, the prototype forecast system we have designed is relatively simple, and built around a dynamic temperature retrieval technique. Our objective is to extract as much information as possible about the 3-D windflow from a single-Doppler radar. Data is processed through two algorithms, one of which produces observations with not only radial but also tangential wind velocities. Both types of Doppler-derived observations are combined with a model forecast through a simple objective analysis, and the resultant wind analyses drive the Gal-Chen temperature retrieval. With high-resolution analyzed fields of wind and temperature, the simple mesoscale forecast is then nudged, hopefully resulting in a more realistic description of the atmosphere and ultimately resulting in a more realistic forecast. Crook and Tuttle (1992) recently presented encouraging results from a similar system.

The intent of this technical report is to give a more complete description of a prototype Doppler assimilation system and to determine the performance that can be expected with such a model. Over the past year it was decided to focus on tests with synthetic Doppler data, rather than progressing on to real-data tests. By using synthetic rather than real Doppler data, we can simulate changes in radar resolution and observational error characteristics. In so doing, we can learn more quickly and profitably about the general characteristics of our single-Doppler retrieval forecast system.

This research takes place at a time of skepticism about the usefulness of mesoscale models in operational thunderstorm prediction. The objections are best stated by Brooks et al. (1992). The authors believe that the highly nonlinear processes involved in convection, the difficulty in determining accurate initial and boundary conditions, and the inability to formulate a suitably complex forecast algorithm preclude the success of forecasts from conventional numerically based forecast models. They argue that a more fruitful approach will be the application of Monte-Carlo techniques, now commonly used in medium range forecasting (e.g., Tracton et al., 1989). Because predictability error growth for synoptic scales is large at day 5 and beyond, current work in medium range forecasting is focused on assessing the most likely forecast and the confidence in that forecast from many runs of a model with slightly different initial conditions. In the same way, the large

predictability error growth for small-scale features may favor the use of multiple integrations and statistical evaluation methods rather than a single model forecast.

Note, however, that the goal of the current project has been defined somewhat more narrowly. This project focuses on predicting the **onset** of convection, where and when the first convective elements may appear, rather than precise forecasts of their subsequent development and interaction. This may have a better chance of success due to the (presumed) smaller predictability error growth during the preconvective phase. Other authors have had some notable success with predicting the onset of convection using a numerical forecast model (Lyons et al., 1992), so despite the technical problems of single-Doppler data assimilation, there is a reasonably good chance of successfully demonstrating skill in the retrieval and the forecast of convective onset.

The rest of the report is organized as follows: Section 2 of this report will describe the new front-end wind analysis, retrieval, and nudging software added to the Phillips Lab., 3-D (PL-3D) model (Hamill, 1992; Gustafson et al., 1991) to test the assimilation of single-Doppler data. Sections 3-4 describe assimilation experiments and results for 2-D and 3-D simulations, respectively. Section 5 provides conclusions.

2. Description of New Data Assimilation System for the PL-3D Model

2.1 Background

Before describing the software used for the dynamic retrieval, we first review some of the underlying scientific and data processing issues. In general, there are two problems with single-Doppler retrievals our software design must address: (1) difficulty in determining tangential wind components from the Doppler data, and (2) sensitivity of the retrieval to the wind errors, which are certainly larger than for dual-Doppler retrievals.

The difficulty in determining an accurate tangential wind component may be alleviated through the assimilation of wind observations generated by the TREC algorithm (Tuttle and Foote, 1990), discussed in more detail in Section 2.2.1. However, we note now that TREC has a number of limitations, including a degradation of quality when the radar scans are spaced too closely (say, less than 3 minutes apart) or too widely (more than 5 minutes apart). Many research radars have the capability to scan every 3-5 minutes, but the National Weather Service currently plans to only perform one volume scan every 10 minutes in clear-air mode with NEXRAD. Hence, our testing include tests of retrieval accuracy when TREC data is not available. In such cases, only the radial wind information (processed through the SPRINT algorithm described in Section 2.2.2) is available, and the tangential component supplied by a model forecast first guess is used unmodified.

The second problem is the lessened accuracy of the retrieval with the larger wind errors that can be expected using single-Doppler data (as opposed to dual- or triple-Doppler). Errors can be introduced in the gridding process, by inaccurate data, or result from the lack of data.

The gridding process often introduces undesirable interpolation errors. As shown in Section 2, part of the dynamic temperature retrieval is using the Doppler observed winds to determine the magnitude of terms in the u and v equations of motion. Gal-Chen (1978) showed that many nonlinear terms (e.g., u*dv/dy) are more accurately calculated when done directly from the radar data before gridding rather than after. Such calculations are impossible with only a single-Doppler's radial velocities, since the full u, v, and w components are needed for the calculations. The TREC algorithm will produce raw u and v wind components, but testing has showed these observations, even in the best conditions, to be too noisy and sparse to be relied on alone. Further, all Doppler observations, be it radial velocities or derived TREC observations, will not be uniformly available throughout the domain, especially far from the radar, where a coarse spacing of scans in the vertical will result in little boundary layer wind information (Figure 8). This all argues against developing the single-Doppler retrieval scheme to work with data in the radar projection.

Wind analyses are also affected by data inaccuracy and unrepresentativeness. All measurements naturally have some error; with Doppler data this error is primarily due to poor signal-to-noise ratio from insufficient scatterers (inaccuracy) or due to the sampling of data over a small volume and short amount of time (unrepresentativeness). Gal-Chen and Kropfli (1984) found this problem to affect the accuracy of their calculations in radar space and used two filters on the retrieved velocities before using them in the dynamic retrieval. For our scheme, this provided another reason to design one software solution to synthesize the observations of different types with a useful model first guess. Hence, we use an objective analysis scheme for determining the Doppler winds. Similarly, the lack of data can also be dealt with through objective analyses, which will default back to a model first guess when new data is lacking.

Our approach is a new approach for determining winds with single-Doppler retrievals. The approach tested here objectively analyzes u and v wind components using the output from two wind algorithms, TREC and SPRINT, with the first guess supplied by ongoing forecasts from the PL-3D model. Our assumption is that after many iterations of analyzing the wind and nudging the model to these wind analyses, the numerical model will develop a consistent and accurate windflow such that the missing or inaccurate tangential component is well-predicted by the model. Our hypothesis is that a consistent wind analysis determined in this way will derive an accurate calculation of the forcing functions, and thus an accurate temperature retrieval and subsequent forecast. The sensitivity tests in Section 4 will test this hypothesis.

2.2 New PL-3D Model Modules

This section describes the retrieval and assimilation code added to the PL-3D model. The PL-3D model was recoded to allow Newtonian nudging to wind and temperature data derived from a Doppler radar. The wind information is derived through the objective analysis and the temperatures through a dynamic retrieval methodology. This is a multi-step procedure, illustrated in Figure 1. We now discuss each of the steps and their implementation. The first two steps, the extraction of Doppler observations by TREC and SPRINT code, will be performed off-line; all following steps will be performed during the integration of the forecast model, at regular time intervals (say, every 5 or 10 minutes).

2.2.1 TREC Processor

TREC is the "Tracking of Radar Echoes by Correlation" (Tuttle and Foote, 1990). This technique can be used to infer a 2-D wind field from successive scans of measured reflectivities. It does this through a cross-correlation of subsets of a scan of Doppler data at time T to all surrounding subsets for a scan at time $T+\Delta T$; the displacement vector (i.e., "wind") is from the center of the originating box to the center of the box with the maximum correlation. This scheme is both very useful and very finicky. It is useful because it is currently the only scheme which can

derive relatively high-resolution boundary layer wind observations with both radial and *tangential* components. However, the TREC scheme is sensitive to ground clutter, works best with closely timed radar scans (3-5 minutes between successive scans is ideal) and requires clear-air inhomogeneities or scatterers such as bugs to use as passive tracers.

For the sensitivity tests discussed in Section 4, it was necessary to generate synthetic TREC observations. Following a procedure typical with Observing System Simulation Experiments (OSSEs), a special version of the forecast model was run; this was considered the ground truth data, i.e., the "nature run". To then generate TREC observations from the nature run, the user defines a radar location, an observation spacing typical of TREC data, and a typical observational error characteristic. Wind "observations" are then extracted from the nature run for regularly spaced points along regularly spaced radii through an interpolation of the eight surrounding model gridpoints. A user-defined error may also be added to these observations.

2.2.2 *SPRINT (Sorted Position Radar INTerpolation)*

This software, developed at the National Center for Atmospheric Research, performs a Cartesian rectification of Doppler measurements (Mohr et al., 1986). It is used to grid the Doppler radial velocities at regular time intervals, making them available to the objective analysis software. SPRINT software is typically used in the gridding of dual-Doppler data; however, for our purposes here it will be used to grid single-Doppler radial wind components.

Generating synthetic SPRINT observations is relatively simple. Actual SPRINT software reads in one or more radar's velocity data and interpolates the data to a grid. Since we are simulating the winds observed and gridded from a single-Doppler radar, simulated SPRINT data is generated directly from gridded nature run output. This output is filtered to extract the radial wind velocity for that gridpoint. If errors are desired, a random error is added to all gridpoints in the nature run data, and this field is then smoothed with a 3*3 boxcar filter, simulating the smoothing that would occur along the radar ray to minimize noise. The resultant field is then used as input data for extracting the gridded radial velocities.

2.2.3 *Objective Analysis*

This step adjusts a model first guess of the wind field to wind velocity observations from TREC and gridded radial velocities from SPRINT. This objective analysis is based on the technique of successive corrections (Cressman, 1959) but differs in some substantive ways from the basic Cressman scheme. The major differences are as follows:

a. Analysis in radial/tangential coordinate system. It is traditional to perform the objective analysis on the u- and v-components of the wind. With the current

code the analysis is done on radial and tangential components and converted back to u/v as a last step. This is done because the TREC scheme supplies observations with both a radial and tangential component, but the SPRINT output has only radial velocities. Analyzing in the conventional u/v coordinate system would require a prior step of inferring some tangential component of the wind for the SPRINT observations - a step liable to induce error.

b. Use of only one SPRINT observation. For the SPRINT observations, only the derived radial velocity at a particular gridpoint is allowed to affect the analysis at that gridpoint; neighboring gridpoints' radial velocities are not used. Once again, this is due to the incomplete wind information having only radial velocities. Nearby gridpoints, especially close to the radar, will have a radial direction different from the radial direction at the analysis point; thus, it will not have complete information on the radial velocity at the original analysis point.

c. Use of nonstandard summation relation. The standard Cressman summation relation is:

$$G(i,j) = \frac{\sum_{n=1}^{nobs} \left(W * \left(D(x_n,y_n) - G(x_n,y_n) \right) \right)}{\sum_{n=1}^{nobs} \left(W \right)} \qquad (2.1)$$

Here G is the first guess at gridpoint (i,j), W is the standard isotropic Cressman weighting function dependent on the distance between the observation and the analysis point, and D is the observed velocity at location (x_n,y_n). Instead a nonstandard summation relation is used of the form:

$$G(i,j) = \frac{(Num_t(i,j) + Num_s(i,j))}{(Den_t(i,j) + Den_s(i,j))} \qquad (2.2)$$

The subscripts "t" and "s" refer to TREC and SPRINT, respectively. Each numerator and denominator term is calculated separately to allow differential weighting according to quality (explained later):

$$Num_t(i,j) = \sum_{n=1}^{nobs} \left(W_t^{2*} \left(D(x_n,y_n) - G(x_n,y_n) \right) \right) / \sum_{n=1}^{nobs} \left(W \right)$$

(when $\sum W_t > 1.0$)

and

$$Num_t(i,j) = \sum_{n=1}^{nobs} (W_t^{2*} (D(x_n,y_n) - G(x_n,y_n))) \qquad (2.3)$$

(when $\sum W_t \leq 1.0$)

Similarly,

$$Den_t(i,j) = 1.0 \qquad \text{(when } \sum W_t > 1.0\text{)}$$

$$Den_t(i,j) = \sum_{n=1}^{nobs} (W_t) \qquad \text{(when } \sum W_t \leq 1.0\text{)} \qquad (2.4)$$

Here the weight is not only a function of horizontal distance between the gridpoint and the observation, but also a function of data quality and the vertical separation between the observation and the gridpoint, i.e.,

$$W_t = W_h * W_v * W_d \qquad (2.5)$$

where the subscripts h, v, and d refer to the horizontal, vertical, and data quality weights, respectively. The vertical weight and data quality factor are explained later. For SPRINT observations, the weighted residual is expressed simply as:

$$Num_s(i,j) = W_d{}^2 * (D(i,j) - G(i,j)) \qquad (2.6)$$

where W_d is simply the data quality weight for SPRINT observations, and

$$Den_s(i,j) = W_d \qquad (2.7)$$

Equation (2.2) is a rather odd-looking way of expressing a Cressman relation. Were only TREC observations used and were the observations randomly distributed, the more standard form of (2.1) could be used. However, only one SPRINT observation is available at a given gridpoint, whereas this gridpoint can be influenced by dozens of TREC observations. Uncorrected, this could have a deleterious influence on the quality of the objective analysis. Let us presume that a SPRINT radial velocity is more reliable than many nearby TREC observations' radial velocities. It would be hard to set a generalized data quality factor for SPRINT or TREC observations that would properly weight one against the other and correctly decrease the influence of the greater number of TREC observations. To address this, after the numerator and denominator in (2.2) have been tallied for all the TREC observations (not including the SPRINT obs) the sum of weights (denominator) is examined. If the sum of weights is less than 1.0, nothing is changed. However, if the sum of weights exceeds 1.0, both Num_t and Den_t are normalized, i.e. the denominator is set to 1.0 and the numerator adjusted accordingly. Thus, for each analysis point there are multiple TREC observations; however, the SPRINT observations are generated only for radial velocities, and there is only one observation, valid at the gridpoint.

When TREC observations are now combined with the SPRINT observation in (2.2), their combined relative weight does not exceed that of a single SPRINT observation with a perfect quality control factor. This procedure is analogous (although not mathematically equivalent) to the formation of a TREC superobservation located directly at the gridpoint. The normalization takes into account the correlation of TREC errors, and ensures that the SPRINT observation is not swamped by the greater number of TREC observations, allowing relative TREC and SPRINT data quality factors to be more easily estimated and more appropriately used.

d. Use of quality factors. The TREC and SPRINT codes have both been tailored to produce a quality factor W_d for each observation, ranging from 0.0 to 1.0. This quality factor is used directly as a weight to apply to the given observation; a weight of 1.0 thus indicates that the observation is completely trustworthy (no error) while a weight of 0.0 would conversely indicate that an observation has no useful information content. There are currently separate quality factors for SPRINT and TREC observations, and they are also a function of forecast time, since during the start of the model forecast period the first guess is relatively inaccurate compared with the observations, but much less so as the assimilation period continues. For real-data tests, the data quality factor may also be set individually for each observation based on data noisiness or other criteria. In a sense, use of quality factors allows a simplified optimum interpolation (Gandin, 1963) to be run, neglecting of course the more complex correlation of errors within and between data types. For the sensitivity tests described in this report, we have used a time-invariant quality control factor of 1.0.

e. Use of a vertical weighting coefficient. We have developed a vertical weighting coefficient which allows the observation increments to be applied not only to the level of the observation but to surrounding vertical levels. This weight is of the form:

$$W_v = 1.0 \; / \; [\, 1.0 + C_v * (D_h)^2 \,] \qquad (2.8)$$

where

W_v = derived vertical weight
C_v = weighting coefficient (m^{-2})
D_h = height difference between observation and analysis level (m)

Figure 2.2 shows the vertical weight as a function of height difference for a C_v of $5.0*10^{-6}\ m^{-2}$.

2.2.4 Dynamic Retrieval of Temperature Observations

Following the method of Gal-Chen (1978) and the derivation of Liou (1989), temperature observations can be derived from gridded wind data. To illustrate consider that the u- and v-equations of motion can be written as:

$$\frac{\partial u}{\partial t} + \theta \frac{\partial \pi}{\partial x} = - u \frac{\partial u}{\partial x} - v \frac{\partial u}{\partial y} - w \frac{\partial u}{\partial z} + fv + turb(u,v,w,K) \qquad (2.9)$$

$$\frac{\partial v}{\partial t} + \theta \frac{\partial \pi}{\partial y} = - u \frac{\partial v}{\partial x} - v \frac{\partial v}{\partial y} - w \frac{\partial v}{\partial z} - fu + turb(u,v,w,K) \qquad (2.10)$$

Rearranging , we get

$$\frac{\partial \pi}{\partial x} \sim= [-\frac{\partial u}{\partial t} - u \frac{\partial u}{\partial x} - v \frac{\partial u}{\partial y} - w \frac{\partial u}{\partial z} + fv + turb(u,v,w,K)] \; / \; <\theta> = F \qquad (2.11)$$

$$\frac{\partial \pi}{\partial y} \sim= [-\frac{\partial v}{\partial t} - u \frac{\partial v}{\partial x} - v \frac{\partial v}{\partial y} - w \frac{\partial v}{\partial z} - fu + turb(u,v,w,K)] \; / \; <\theta> = G \qquad (2.12)$$

π here is the Exner function and K an eddy exchange coefficient. Turbulence parameterization and use of K are described more completely in Tripoli and Cotton (1982). Since we are seeking θ, we cannot explicitly use it here and thus approximate it with a previously calculated horizontal mean $<\theta>$. With the available Doppler information, we can derive all the terms of F and G; the horizontal winds are derived from an objective analysis of Doppler radar data, the vertical velocities through the procedure described below, and the local time derivatives through comparisons of successive scans of Doppler wind analyses. If the calculations of F and G are perfect (implying perfect observations and perfect numerical calculations) then F and G are related by:

$$\partial F/\partial y = \partial G/\partial x = \partial^2 \pi/\partial x^2 \qquad (2.13)$$

Because of errors in the data, the analysis of the data, and the numerical approximations, this equation is not satisfied. It can be satisfied in the least-squares sense, resulting in a Poisson equation

$$\partial F/\partial x + \partial G/\partial y = \partial^2 \pi'/\partial x^2 + \partial^2 \pi'/\partial y^2 \qquad (2.14)$$

with Neumann boundary conditions

$$\partial \pi'/\partial x = F \quad \text{and} \quad \partial \pi'/\partial y = G \qquad (2.15)$$

Here π' is used rather than π since the solution is not unique - only the horizontal deviation from the mean can be considered unique. To remove this non-uniqueness, we impose the constraint that the horizontal mean of the derived pressure is equal to that of the model first guess.

With the Exner function determined, temperature can be retrieved, as will be shown later.

Specific algorithmic steps in the dynamic retrieval are shown in Figure 3 and summarized below:

a. Calculation of vertical velocity: The PL-3D model normally calculates the vertical velocity from an upward integration of the continuity equation. For consistency, this was preserved here. However, because Doppler-derived wind analyses may be noisy, we chose to impose constraints on the diagnosed vertical velocities. This hopefully will result in more accurate temperature retrievals, because of more reliable estimates of the vertical advection. After a preliminary vertical velocity w'_{nud} is diagnosed from the continuity equation, a constraint (Gal-Chen and Kropfli, 1984) is applied of the form:

$$w_{nud}(k) = w'_{nud}(k) - E * D_w * V_r(k) \qquad k \le k_{max} \tag{2.16}$$

$$w_{nud}(k) = w(k) + (1.0 - E) * D_w \qquad k > k_{max} \tag{2.17}$$

where

E = nondimensional, user-selected damping coefficient $(0.0 \le E \le 1.0)$
$D_w = w'_{nud}(k_{max}) - w(k_{max})$ (ms^{-1})
$w(k)$ = model-produced vertical velocity (ms^{-1})
$V_r(k) = Z(k) / Z(k_{max})$
$Z(k)$ = MSL height (m)

This equation preserves the Doppler-derived vertical velocity near the ground, but as the model layer height approaches a prespecified height level ($Z(k_{max})$), w_{nud} is effectively damped. The higher the value of E, the greater the amount of damping. For computational efficiency, u and v were not readjusted to be consistent with the new vertical velocity through the continuity equation. Since the only use of w is in the calculation of vertical advection terms for the forcing function, this should not introduce any dynamical inconsistencies. The adjustment of u and v could, however, become necessary in order to lessen the amount of gravity wave generation when the analyses are used to nudge the forecast model.

b. Calculation of u and v forcing functions. The forcing functions F and G in equations (2.11) and (2.12) must be calculated using the available Doppler radar. There are four general terms: the local rate of change, advection, coriolis, and turbulence. Existing PL-3D code is used to calculate all terms except the local rate of change; this is calculated using a backward difference with the previous analysis:

$$\partial u/\partial t = (u_t - u_{t-1}) / \Delta t \tag{2.18}$$

$$\partial v/\partial t = (v_t - v_{t-1}) / \Delta t \tag{2.19}$$

c. Dynamic Retrieval of Pressure Perturbations. Using standard numerical techniques such as sequential over-relaxation (Vemuri and Karplus, 1981) equation (2.14) is now solved for π' level by level. So that the vertical finite differencing is not spuriously affected by differences between an analysis level (say, level k) and a non-analysis level (say, k+1), the retrieval is confined to one level above the minimum analysis level and one level below the maximum analysis level (k-1).

d. Extraction of Temperature Observations. The hydrostatic equation

$$\partial\pi/\partial z = -g/\theta \tag{2.20}$$

can be written in finite difference form and solved for the mean layer temperature θ_{lyr} for each of the layers from k_{min} to k_{max} according to

$$\theta_{lyr}(k) = \frac{-g * (z(k) - z(k-1))}{\pi(k) - \pi(k-1)} . \tag{2.21}$$

Level temperatures are now deduced from averages of the surrounding layers, i.e., for levels k_{min} to k_{max} -1:

$$\theta(k) = [\, \theta_{lyr}(k) - \theta_{lyr}(k+1) \,] / 2 \tag{2.22}$$

A final check is made to ensure that no biases were introduced in the vertical interpolation. Temperatures are reset according to

$$\theta(k) = \theta(k) - \langle \theta(k) \rangle + \langle \theta_{mod}(k) \rangle \tag{2.23}$$

where brackets denote a horizontal average, and $\theta_{mod}(k)$ is the model-supplied temperature (recall that the dynamic retrieval only yields information on deviations from the horizontal mean of pressure, and thus, temperature). Thus we derive finally a set of temperature observations compatible with the observed winds.

2.2.5 Newtonian Nudging of u, v, and t

Following the discussion in Hamill (1992) the model is now nudged to the new data adjusting the model's time tendencies for u, v, and t according to:

$$F_{tot} = F_{mod} + (X_{obs} - X_{mod}) * R * W_t \tag{2.24}$$

where

F_{tot} = $\partial X/\partial t$ = total local tendency for the gridpoint at a given timestep

F_{mod} = normal model terms of the local tendency (e.g., advection, coriolis)

X_{obs} = observed field's value for a gridpoint at time (t)

X_{mod} = model forecast value for a gridpoint at time (t)

R = nudging coefficient

W_t = weight applied to this timestep

The residual ($X_{obs} - X_{mod}$) are calculated at the time when the Doppler analysis and temperature retrieval are performed, and this residual is used until the next analysis time. To deweight this residual as we progress forward in time, W_t starts at 1.0 at the time of the analysis but tapers off to zero, approaching zero right at the time of the next Doppler analysis and retrieval.

2.3 Other Coding Modifications and PL-3D Deficiencies

Since the PL-3D model is a hydrostatic model using water vapor only as a tracer, it has a number of drawbacks which can affect the accuracy of the simulations. Some are obvious; the nonlinear interactions that happen after first cumulus development but before the onset of convection cannot be adequately handled with such a simple model.

Some other problems do exist with the model, or at least the usage of it here. For example, we encountered computational instability when running the model at a 4 km horizontal resolution; we believed that this grid length combined with the strong local heating and forcing were inducing nonhydrostatic effects which even the inclusion of a superadiabatic checking routine could not eliminate.

3. 2-D Tests of Temperature Retrieval and Forecast Accuracy

Before performing full 3-D simulation experiments with the new retrieval system, some prototype tests were tried with a 2-D version of the system. Previously (Hamill, 1992) it was noted that there were circumstances where forecasts, including temperature data assimilation, improved on forecasts with just wind data assimilation or with no data assimilation at all. However, the temperature retrieval scheme tested here actually derives its observations from the wind field. The previous OSSE tests were performed before the dynamic retrieval software was coded, so retrieved temperature observations were simulated by using temperature forecasts directly from a forecast model. There are additional sources of error not accounted for with the previous OSSE tests. For example, with the new dynamic retrieval system, horizontal biases cannot be eliminated. The retrieval scheme can generate a relatively accurate field of temperature deviations from the horizontal average, but if the horizontal average itself is in error, the retrieved temperatures will reflect this. Thus, as a first step, the new temperature retrieval software was again tested on a simple 2-D seabreeze case to prove the concept of the benefit of temperature data assimilation again before proceeding with the 3-D simulations. The hypothesis is that there should still be a positive influence from temperature data assimilation, even with horizontal bias errors.

In the 2-D OSSE documented here, a seabreeze experiment very similar to the one documented in Hamill (1992) was run. A 5 km, 2-D version of the model was again run, with 32 gridpoints in the horizontal and 18 in the vertical. The vertical grid spacing was 200 m for the lowest four levels, and 350 m above this. The domain was split into half water (the left half) with a water temperature of 296 K, and half land. For the nature run, a 7-hour forecast was started from quiescent initial conditions and a 7 AM starting time. As shown in Figures 4 (a) - (f), a seabreeze circulation rapidly develops and moves inland during the forecast.

Our actual forecasts were performed on the same domain and started at 10 AM, with a slightly less stable boundary layer profile and a 2.5 ms^{-1} offshore flow, simulating a wind error that should affect the position and development of the seabreeze front without additional information supplied through data assimilation. We performed three simple experiments to test the assimilation effects:

(1) No data assimilation,
(2) Wind assimilation, and
(3) Wind and temperature data assimilation (temps derived through dynamic retrieval).

For each of the assimilation experiments, there was a 2-hour nudging period from hours 0-2 of the forecast. Nudging data from this time was taken straight from the 3- to 5-hour data of the nature run. New wind information was supplied every 5 minutes for levels 2-12 (200 - 2350 m) of the model, and for the simulation, including the dynamic temperature retrieval, temperature information is available at

levels 3-11 (400 - 2000 m). The wind information here was error-free; simulations with errors are included in the later 3-D simulations. The nudging coefficient was set at $5.56 * 10^{-4}$ sec^{-1} (1/1800 sec). In a sense this simulation can be taken to represent a best-possible case scenario, with high-resolution, error-free data. This test is merely designed to reconfirm the hypothesis of the benefit of temperature data assimilation with bias-prone temperature observations.

Figure 5 illustrates a 4-hour forecast of the model for the test with no data assimilation. Some errors are evident; the comparable data from the nature run (Figure 4 (f)) is 2 degrees cooler over water, and the forecast position of the center of circulation is almost 15 km too close to the coast. There is a similar coastward displacement of the location of maximum updraft, where presumably convection would preferentially initiate. Further, the entire seabreeze front has not propagated inland far enough.

Figure 6 similarly illustrates a 4-hour forecast with wind data assimilation. Though again this model forecast is not cool enough over water and the circulation and seabreeze front is not far enough inland, the forecast is more accurate than the test without any data assimilation. The center of circulation is now only about 10 km too close to the coast.

The 4-hour forecast for the wind and temperature assimilation experiment is shown in Figure 7. This test run improves slightly the position error of the center of circulation from the wind only test; the center in this test is almost 20 km inland, an error of approximately 5 km. The temperature field, with the exception of inadequate cooling in the lowest layers over water, is exceptionally well forecast. The inadequate cooling is likely due to the inability to perform temperature retrievals at the lowest levels. In all, this experiment is the most accurate. This result reconfirms last year's conclusions on the potential benefit of temperature assimilation. Temperature observations derived through the dynamic retrieval, with accurate wind observations, may lead to substantial improvements in forecast quality.

4. 3-D Tests of Temperature Retrieval and Forecast Accuracy

With the 2-D tests used as a proof of concept, a set of 3-D sensitivity tests were conducted using the new temperature retrieval and assimilation code. Rather than proceeding to test the retrieval software and forecast assimilation process with actual Doppler data, the new software was tested with synthetic data so wind error characteristics could be manually adjusted. The setup of this experiment simulated the use of single-Doppler data and the attendant wind errors that can be expected from use of this data.

4.1 Experiment Design

A set of assimilation experiments was performed to determine the accuracy of Doppler temperature retrievals and model forecast quality when assimilating Doppler winds and derived temperatures. To test the retrieval, we performed a set of runs of the dry, hydrostatic PL-3D model with and without Doppler assimilation. We have chosen a domain centered over Tampa Bay, FL, and shown in Figure 8. The forecast was carried out on a 1/15th degree grid (Δx = 6.56 km, Δy = 7.40 km), and the vertical grid spacing was 200 m in the boundary layer tapering off to 350 m at 1750 m AGL. All model terrain heights were set to 0.0. Local water temperatures were set at 296 K.

For the nature run, our model was started with a hypothetical initial time of 7 AM on July 17, 1987, and a 7-hour forecast was run. The model was initialized with no winds and a slightly stable lapse rate. The initial land temperature was 295.2 K.

The time/date of forecast model start was 3 hours later, or 10 AM. A 4-hour forecast was run, with the first two hours of the forecast an assimilation period. This corresponds to hours 3-5 of the nature run. The model here was initialized with a land temperature of 298.2 K and a 2.0 ms^{-1} easterly flow, again to simulate some wind error in the initial conditions. For experiments with data assimilation and nudging, the analysis and retrieval scheme described in Section 2 was used.

Table 1 shows a matrix of assimilation experiments performed. The first experiment was simply to run the model without any data assimilation whatsoever; this will help quantify the benefit of all the latter experiments, with their differing data configurations and error characteristics. As shown, the rest of the table is filled with experiments assimilating TREC data (exp. 2-5), SPRINT data (exp. 6-9), or both (exp. 10-12). Differing vertical resolutions of TREC and SPRINT observations were tested to determine how sensitive the retrieval accuracy will be to the number of vertical radar scans. These experiments are designed to answer questions about how precisely the vertical wind structure must be deduced. Similarly, the amount of wind error was varied to determine the sensitivity of the retrieval to wind accuracy. These tests attempted to quantify the expected benefit of data ranging from ideal data

Exp #	Data: TREC, SPRINT	# levels radar	Wind error type	Radar elevation angle (degrees)	Notes (reason for test)
1	none	none	–	–	Model execution without any radar data assimilation; baseline case.
2	T	3	mod	0.3, 1.0, 3.0	Simulate TREC data from CP-3, CaPE expt.
2N	T	3	mod	0.3, 1.0, 3.0	No observations allowed over water; objective analysis tuned to new data density.
3	T	5	none	0.3, 0.8, 1.3, 1.8, 2.3	What if NEXRAD scans were at 5 min intervals? Test upper bound of usefulness of TREC data if such data were available.
4	T	5	mod	0.3, 0.8, 1.3, 1.8, 2.3	Test realistic simulation of TREC data alone.
5	T	5	high	0.3, 0.8, 1.3, 1.8, 2.3	Test upper limits of error.
6	S	3	mod	0.3, 1.0, 3.0	Test typical case for CP-3 with simulated 0.3, 1.0 and. 3.0 elevation angle data.
6N	S	3	mod	0.3, 1.0, 3.0	No observations allowed over water.
7	S	5	none	0.3, 0.8, 1.3, 1.8, 2.3	Test for minimum error possible with realistic set of NEXRAD scan angles.
7 UV	S	5	none	0.3, 0.8, 1.3, 1.8, 2.3	Same as (7) above, but nudge only the winds with no retrieved temperatures.
8	S	5	mod	0.3, 0.8, 1.3, 1.8, 2.3	Test realistic scenario of retrieval accuracy when only 5 levels of Doppler data are available every 10 minutes (10 min spacing means TREC unworkable) .
9	S	5	high	0.3, 0.8, 1.3, 1.8, 2.3	Test upper limits of error and its effects.
10	T,S	3	mod	0.3, 1.0, 3.0	Test realistic CP-3 CaPE scenario.
11	T,S	5	none	0.3, 0.8, 1.3, 1.8, 2.3	Test theoretical lower bound of error possible NEXRAD if scans were temporally closer (and TREC could be run).
11 UV	T,S	5	none	0.3, 0.8, 1.3, 1.8, 2.3	Same as (11) above, but nudge only the winds with no retrieved temperatures.
12	T,S	5	mod	0.3, 0.8, 1.3, 1.8, 2.3	Test typical expected error with NEXRAD if scans were temporally closer.

Table 1: A matrix of assimilation experiments carried out to test the sensitivity of the PL-3D model to various data configurations. Column 1 gives the experiment number, column 2 the type of data assimilated (T=TREC, S=SPRINT), column 3 the number of vertical levels of radar data, column 4 the amount of error added to the wind observations (see Table 2), and column 6 comments on what information is to be gleaned from this particular test.

to very poor data. We tested with the best possible information and vertical resolution, and then with less resolution, higher errors, and missing data types to quantify this. Two tests (2N and 6N) did not allow any observations over water, a reasonable assumption with short wavelength Doppler radars.

Synthetic TREC and SPRINT observations were created every 5 minutes during the 2-hour assimilation period. These observations were generated using data from hours 3-5 of the nature run for points over land. Table 2 shows the TREC and SPRINT error characteristics used in the experiments. As mentioned in Section 2, TREC observations were generated at regular spacings (every 5 km) along constant

Type of error	(SPRINT) Max Percent Random Error Added	(TREC) Max Percent Random Error Added	(TREC) Percent Observations Randomly Deleted
None	0.0	0.0	0.0
Mod	20.0	30.0	40.0
High	35.0	65.0	60.0

Table 2: Description of the categories listed in Table 1: the percent random error added to the derived wind observations before input into the objective analysis software.

radii. SPRINT data were generated directly from the model gridded fields, but to simulate interpolation errors, some of the new horizontal levels of synthetic SPRINT data did not use the model data directly, but rather had their wind velocities determined through a vertical interpolation from the surrounding layers. For the experiments with radar sweeps at 5 elevation angles, as in experiment 7 in Table 1, every other layer was determined through interpolation, i.e., real radial data were generated for levels 2, 4, 6, etc., and interpolated at levels 3, 5, etc. For the experiments with sweeps at 3 elevation angles, as in experiment 6, data were available only at levels 2, 5, and 9; all other level winds were determined through interpolation.

For all experiments, the TREC and SPRINT wind observations were filtered through the objective analysis software, which blends the observations together with a first guess supplied by the forecast model. The objectively analyzed winds were then used as input to the temperature retrieval, and the model was subsequently nudged to the winds and derived temperatures. Setting the objective analysis parameters to give the best analysis possible was difficult; the quality of the analysis can be controlled by adjusting the number of passes, the influence radius of each pass, the vertical weighting coefficient, the buddy check difference, and the data quality factors for TREC and SPRINT data. Influence radii and the vertical weighting coefficient were adjusted for different tests based upon the data distribution, and for the tests with no data over water, the summation relation discussed in Benjamin and Seaman (1985) was used for latter correction passes to minimize the effects of discontinuities.

TREC and SPRINT data quality factors (DQFs), discussed in 2.2.3 (d), were set as time-invariant functions of 1.0 for this case study.

Once the objective analysis and subsequent dynamic retrieval were performed, the model was nudged to the new data. A nudging coefficient of $5.56 * 10^{-4}$ ($1/1800\ sec^{-1}$) was used, and for these tests, E, the analysis quality factor, was set

to 1.0 (see Section 2.2.5). For this case, retrievals and nudging were performed from levels 2 to 12 in the model.

4.2 Evaluation Procedure

The quality of the retrievals and the subsequent forecasts were judged in a number of ways;

a. Manual interpretation. Horizontal and vertical cross-sections of potential temperature and wind were evaluated in a straightforward sense to determine what the errors were in terms of positions of convergence zones, temperature gradients, etc.

b. RMS error and bias of temperatures and wind forecasts. We verified the accuracy of 4-hour forecasts wind and temperature RMS and bias in the center of the domain, from gridpoint 7 to 18 in the x-direction, gridpoints 5 to 16 in the y-direction, and 3 to 8 in the z-direction. This yielded a quantitative evaluation of forecast accuracy which presumably would reflect the accuracy of determining the position of convective initiation.

c. Temperature retrieval accuracy, as judged from horizontal plots of the error of the derived temperature observations.

d. Momentum checking. Following Gal-Chen and Kropfli (1984) and Gal-Chen (1986), a momentum check was used of the form:

$$E_r = \frac{\iint \left(\frac{\partial \pi'}{\partial x} - F\right)^2 + \left(\frac{\partial \pi'}{\partial y} - G\right)^2 dxdy}{\iint F^2 + G^2 dxdy} \qquad (4.1)$$

The authors suggest that: for a perfect fit, E_r is 0.0; with random white noise, E_r = .5; even when the fit is perfect, however, and pressure perturbations are solved by finite difference, $E_r \cong .25$. A suggested upper bound for acceptable momentum check is $E_r \cong .35$.

4.3 Results

4.3.1 Manual Interpretation and Discussion

We first display and discuss the results from the nature run and then for each forecast, concentrating primarily on the accuracy of forecasting the regions of strongest upward motion, since these are preferred areas for thunderstorm development. For each case, a horizontal cross-section of winds and potential temperature is displayed for level 2 (250 m AGL), and a vertical cross-section at coordinate y = 13, very near the radar coordinate (x=10.25, y=13.25).

a. Nature run. This simulation is supposed to represent the hypothetical real evolution of the atmosphere. Figures 9 (a) - (c) show the horizontal cross-sections for 5- to 7-hour forecasts from the nature run, and Figures 9 (d) - (f) the 5- to 7-hour vertical cross-sections. As mentioned earlier, the nature run was started at 7 AM while the forecast runs discussed below start at 10 AM; thus, the 7-hour forecast from the nature run corresponds to the 4-hour forecast from the test cases.

Of note in the horizontal cross-sections is the quickly developing land/sea temperature contrast, with temperatures ranging from less than 297 K over the ocean to greater than 301 K over land. By hour 7 of the simulation, there has been a rapid movement of the seabreeze onshore. As shown in the 7-hour forecast vertical cross-section in Figure 9 (f), the maximum updraft is positioned at ~ + 42 km; at this time, there is one center of circulation around the main seabreeze, though as seen in the cross-sections for hours 5 and 6 (Figures 9 (d) and (e)) there is a secondary circulation nearer the shore, presumably due to the heating over the St. Petersburg peninsula.

b. Experiment 1: Baseline. This simulation, done without the benefit of any data assimilation, illustrates how uncorrected, there can be marked errors in the forecast of the seabreeze front when the forecast model is poorly initialized. Horizontal and vertical cross-sections of the 4-hour forecast are shown in Figures 10 (a) and (b), respectively. As seen in 10 (a), the horizontal temperature gradient is weaker than in the nature run, and the seabreeze has not propagated nearly as far inland. Figure 10 (b) further illustrates the forecast errors; the weakened area of maximum vertical velocity is located at ~ + 29 km, approximately 13 km too close to the coast, and there is a pronounced secondary circulation center over St. Petersburg that does not appear in the nature run. Presumably this secondary circulation has resulted because the initialization with a low-level offshore flow prevented the circulation from moving rapidly onshore, allowing reinforcement of differential surface heating effects.

c. Experiment 2: TREC assimilation, 3 levels. This test, with three levels of radar data at elevation angles typically used during the CaPE experiment (Foote, 1991), is designed to test a typical real-world radar configuration and its expected errors. Four-hour forecasts of the horizontal and vertical cross-sections are shown in Figures 11 (a) and (b). As shown in the horizontal cross-section in Figure 11 (a), the temperatures over land are relatively well forecast, but the temperatures over water are not well forecast. Presumably this temperature error is due to the slightly warm initialization of the lowest layers, which could not be corrected through the dynamic retrieval since the lowest two levels do not have temperatures retrieved due to lower boundary effects. With a weakened land-sea temperature gradient, the onshore flow is not sufficiently accelerated, and the seabreeze does not propagate as far inland as the nature run indicates as ideal. Looking at the vertical cross-section in 11 (b), the secondary circulation over St. Petersburg is greatly reduced, and the maximum updraft is located at + 37 km, about 5 km too close to the coast. Overall, this forecast is much better than the baseline forecast in experiment 1.

d. Experiment 2N: TREC assimilation, 3 levels, no observations over water. This experiment throws away all TREC wind observations over water to test the model sensitivity to data discontinuities. Since a normal Cressman function will not work well with data discontinuities, a modified 5-pass Cressman scheme was used for these tests. For the first two passes, very large influence radii were selected so that points offshore were still affected by onshore data. Latter passes used the relation described in Benjamin and Seaman ($\Sigma W^2 * D / \Sigma W$) (1985) to make corrections at smaller influence radii.

As can be seen in Figures 12 (a) and (b), the horizontal and vertical cross-sections of 4-hour forecasts, the forecast wind pattern is still remarkably similar to that of experiment 2, despite missing observations over water. It is worth noting that, though not tested, the forecast could be expected to be much worse if the objective analysis scheme had not been tailored to handle the data discontinuities. As it stands, however, the forecast is quite similar, with the maximum updraft located at + 37 km, 5 km too close to the coast. In this case, observations over water were clearly not crucial to forecast accuracy.

e. Experiment 3: TREC assimilation, 5 levels, no error. This forecast demonstrates the upper bound on improvement that can be expected from assimilating TREC data alone. Horizontal and vertical 4-hour forecast cross-sections are shown in Figures 13 (a) and (b). As shown, the forecasts again improved significantly on the baseline forecasts; the temperature gradient is slightly stronger, the onshore flow is stronger, and the position of the seabreeze front is much more realistic. In the vertical cross-section shown in Figure 13 (b), the maximum vertical velocity is again at ~ + 37 km, or only 5 km too near the shore. Overall, this forecast shows significant improvement over the baseline, but little or no improvement over the 3-level TREC assimilation experiment with moderate error (experiment 2). Presumably, since the lowest radar level was at 0.3 degrees in both experiments, it captured the important low-level windflow for both and thus led to similar forecasts. The seemingly small effect of the moderate wind errors is discussed more with the next experiment.

f. Experiment 4: TREC assimilation, 5 levels, moderate error. This test case is done under "moderate" error conditions, as explained in Table 2. Presumably a worse forecast would result from not having as high quality TREC data as in experiment 3 above. However, as shown in the horizontal and vertical cross-section forecasts in Figures 14 (a) and (b), the forecasts are almost identical to the forecasts from experiment 3, despite random wind errors of up to 30 percent, and 40 percent of the observations deleted. We believe the surprisingly good results are due to the objective analysis software; for the test case here, the influence radius was chosen large enough for many observations to influence the analysis at each gridpoint, thereby allowing the errors to cancel each other out. Certainly this test may overstate the benefits of assimilating TREC data since systematic or correlated errors were not factored into the test. Also, the objective analysis parameters were chosen

with influence radii large enough to produce this cancellation effect, but at the expense of minimizing small-scale detail.

g. Experiment 5: TREC assimilation, 5 levels, high error. This experiment was conducted with random errors of up to 65 percent of the windspeed added to observations and 60 percent of the observations deleted. Despite this, the results are again very similar to experiment 2 and ideal data conditions. Figures 15 (a) and (b) show horizontal and vertical cross-sections of the resultant 4-hour forecast. Again, this is almost certainly due to the ability of the objective analysis software to combine multiple observations and smooth out the initial errors into a highly accurate wind analysis.

h. Experiment 6: SPRINT assimilation, 3 levels, moderate error. This experiment, along with the next five, were designed to test the benefit of assimilating radial wind information alone into the forecast model. Presumably the forecasts will not produce as realistic temperature observations from the windfield because of the lack of a tangential component, and this will affect the quality of the forecast. This particular test is configured to resemble the data configuration for the CaPE experiment, assuming that TREC data is for some reason unavailable. Figures 16 (a) and (b) show 4-hour forecast horizontal and vertical cross-sections. The vertical cross-section in (b) shows a good forecast of the inward propagation of the seabreeze front, with the maximum vertical velocity correctly placed at ~ + 42 km, but the horizontal cross-section shows that only in the region where the radar is perpendicular to the seabreeze front (for example, right at the vertical cross-section) is the position of the front correctly forecast. Further south and north, the front has not propagated inland far enough, as shown in the horizontal cross-section in Figure 16 (a). This is almost certainly due to the ineffectiveness of adjusting the model to the actual onshore flow north and south of the radar, where the flow is mostly perpendicular to the radar beam.

i. Experiment 6N: SPRINT assimilation, 3 levels, moderate error, no observations over water. Similar to experiment 2N, the observations over water were removed from the objective analysis, testing the sensitivity of the model to this rather realistic data discontinuity. Unlike experiment 2N, however, the basic objective analysis software remained the same; SPRINT data supplies radial velocities only, so this data is not arbitrarily spread to other gridpoints.

Despite the lack of data over water, the forecast frontal positions are remarkably similar to experiment 6, as shown in the 4-hour forecast horizontal and vertical cross-sections of Figures 17 (a) and (b). Again, reinforcing the conclusion from experiment 2N, observations over water were not crucial for defining later convergence zone position over land.

j. Experiment 7: SPRINT assimilation, 5 levels, no error. This experiment adds no errors to the generated radial velocity observations besides those introduced in the normal interpolation process. This test should quantify an upper limit of

accuracy for the SPRINT data assimilation cases when no TREC data are available because of radar timing or other factors. The 4-hour forecast horizontal and vertical cross-sections are shown in Figures 18 (a) and (b). As seen, the overall onshore flow is weaker than in the nature run, and the vertical velocity max is correctly forecast at ~ + 42 km but is too weak. Further, similar to the problem shown in experiment 6, north and south of the radar the front has not propagated far enough inland, again presumably due to the ineffectiveness of the radar in regions of primarily tangential winds.

k. Experiment 7UV: SPRINT wind assimilation, 5 levels, no error. This test is identical to experiment 7, except here only wind information is assimilated; the temperature retrieval and nudging is turned off. This experiment was included to again confirm the hypothesis that temperature data assimilation has a positive impact on the forecast. The horizontal and vertical cross-sections for the 4-hour forecasts are shown in Figures 19 (a) and (b). As exhibited in the vertical cross-section in (b), there is a slight positional error in the forecast of the region of maximum vertical velocity, which is located here at ~ + 37 km, or about 5 km too near the coast, and the updraft strength is too weak. In other parts of the domain, there is a small but noticeable coastward shift in the position of the maximum updraft and seabreeze front.

l. Experiment 8: SPRINT assimilation, 5 levels, moderate error. As shown in Figures 20 (a) and (b), the inclusion of moderate errors to the SPRINT data again does little in this case to degrade the positional accuracy of the seabreeze front from the ideal data configuration in experiment 7.

m. Experiment 9: SPRINT assimilation, 5 levels, high error. Again, as shown in Figures 21 (a) and (b), even relatively large random errors added to the SPRINT data have negligible effects here.

n. Experiment 10: SPRINT and TREC assimilation, 3 levels, moderate error. Here SPRINT and TREC data are combined in the objective analysis, each with moderate error characteristics. The output from this simulation, shown in Figures 22 (a) and (b), are quite similar to the simulation from experiment 2, with TREC data alone, though the seabreeze front appears slightly more displaced onto land than in experiment 2. Overall, the seabreeze front is well-positioned at approximately + 42 km.

o. Experiment 11: SPRINT and TREC assimilation, 5 levels, no error. This experiment defines ideal data conditions, with no error for either observation type. The 4-hour horizontal and vertical cross-sections for this forecast are shown in Figures 23 (a) and (b). The maximum updraft is again at ~ + 37 - 42 km inland. This forecast is almost indistinguishable from the ones with errors (e.g., experiments 4, 5, and 12).

p. Experiment 11UV: SPRINT and TREC wind assimilation, 5 levels, no error. This experiment uses the same wind analysis as experiment 11, but no temperature retrieval is performed, and temperatures are not nudged. Horizontal and vertical cross-sections of the 4-hour forecast are shown in Figures 24 (a) and (b). As shown in (b), the updraft position displaced slightly coastward at + 37 km, but it is stronger in experiment 11 with the temperature assimilation, possibly due to stronger onshore flow associated with the slightly stronger temperature gradient over the shoreline.

q. Experiment 12: SPRINT and TREC assimilation, 5 levels, moderate error. This last test case is performed with both TREC and SPRINT data with moderate errors. The output is shown in Figures 25 (a) and (b), and is virtually the same as experiment 11 output (Figure 23), illustrating again the insensitivity to moderate errors.

Overall, results of these tests were more alike than different, indicating either an insensitivity to observational error or problems formulating the OSSE.

4.3.2 RMS Error and Bias

Four-hour forecasts wind and temperature RMS and bias were verified over the center of the domain, from gridpoints 7 to 18 in the x-direction, gridpoints 5 to 16 in the y-direction, and 3 to 8 in the z-direction. These provide a more quantitative assessment of forecast accuracy. The statistics for each test are provided in Table 3.

The improvement of all the assimilation runs over the baseline (experiment 1) is immediately obvious. The v-component is less well forecast in the other experiments, but because of the general north-south coastline and east-west flow, this is probably less important than the accuracy of the u-component. Otherwise, the table indicates the great similarities in error characteristics; the experiments with TREC data alone (experiments 2-5) all have similar temperature errors, though the additional vertical resolution in experiments 3-5 does decrease the analysis error slightly. The SPRINT experiments seemed to show that temperature assimilation still improves forecast accuracy when only the radial component is assimilated, but as will be shown in the derived temperature plots in the next section, the SPRINT retrieved temperatures do not converge over time to a low error solution as happens when both wind components are used. Statistics also show an increase in error due to the lack of observations over water, as seen in the difference between errors for experiments 6 and 6N.

For the tests combining TREC and SPRINT data (experiments 10-12), the statistics show some expected and some unexpected results. Experiment 11UV shows that both temperature and wind forecast accuracy is improved with the assimilation of temperature data, as expected. The low errors in the low-resolution experiment 10 were unexpected, however. This experiment, using 3 levels of radar

Exp #	RMS Temp	Bias Temp	RMS u-comp	Bias u-comp	RMS v-comp	Bias v-comp
1	0.411	0.355	2.148	-1.571	**0.472**	**0.026**
2	0.224	0.175	0.909	-0.490	0.618	-0.552
2N	0.221	0.173	0.931	-0.481	0.645	-0.576
3	0.213	0.164	0.793	-0.430	0.607	-0.568
4	0.213	0.163	0.779	-0.426	0.605	-0.568
5	0.212	0.169	0.855	-0.458	0.616	-0.571
6	0.167	0.105	0.836	-0.122	0.936	-0.860
6N	0.251	0.209	0.958	-0.244	0.679	-0.578
7	0.167	0.093	0.752	**-0.091**	0.917	-0.845
7UV	0.213	0.155	1.017	-0.124	0.880	-0.802
8	**0.165**	**0.090**	0.741	-0.089	0.922	-0.850
9	0.166	**0.090**	0.748	-0.091	0.926	-0.852
10	0.196	0.136	**0.577**	-0.106	0.721	-0.677
11	0.218	0.165	0.695	-0.326	0.664	-0.624
11UV	0.303	0.251	1.337	-0.799	0.699	-0.593
12	0.217	0.163	0.690	-0.327	0.670	-0.632

Table 3: Bias and RMS error of temperatures (K) and u- and v-wind fields (ms^{-1}) for the 4-hour forecasts from each experiment. Highlighted values indicate the lowest error.

data with moderate error rather than experiment 11's 5 levels with no error, exhibited many of the most accurate forecast parameters. Perhaps this confusing result can be used as a confidence interval of sorts for the forecast scores; for example, the temperature RMS is 0.02 less in experiment 10 than in 11, so perhaps deviations within this range for all experiments should not be considered significant.

4.3.3 Plots of Retrieved Temperatures

Another way of evaluating the success of the retrieval scheme is to plot the differences between the derived temperatures and the ground-truth temperature

data from the nature run. Most of the plots generated were very similar in character, so only a small sample will be shown. Consider Figures 26 (a) and (b), plots of the accuracy of the retrieved temperature at level 3 for times t=330 s and t=3630 s, taken from experiment 3 (5-level TREC with no error). As shown in (a), initially there is a gradient of retrieval error along the coast with an overestimate of the temperatures over water and an underestimate of the temperatures over land. There is also a domain-averaged warm bias corresponding to the overall initial temperature bias at that level (uncorrectable). The gradient of retrieval error is due to the underestimate of the onshore flow, which is due to two problems. First, the model was just started with an offshore wind. The tendency of the Cressman response function, accentuated by the use of a vertical correlation weight, is to not fully correct toward the observed data. Thus, initially the analyzed onshore flow is not strong enough. A second reason for the lack of wind strength is that the radar beam elevation does not allow a full sensing of the low-level wind, overshooting the boundary layer far from the radar. With the strongest winds near the ground, some of this momentum is missed. These two factors, we believe, lead to the observed gradient in retrieval error.

As the model forecast continues, however, the wind analyses become more accurate, despite the strengthening of the circulation. The adjustments the Cressman scheme must make for each iteration become smaller and smaller due to the positive effect of the Newtonian nudging, and the overall onshore flow is captured more accurately. This is reflected in the reduced retrieval error shown in Figure 26 (b), illustrating the decrease in the gradient of retrieval error an hour later. Figures 27 (a) and (b) illustrate that the same principle holds for experiment 7, where the retrieval error at time t=330 s in (a) decreases by time t=3630 s in (b).

4.3.4 *Momentum Checking*

Evaluation of the momentum check was much more complicated than expected. As noted before, for a perfect fit, E_r is 0.0; with random white noise, E_r = 0.5. Even when the fit is perfect, however, and pressure perturbations are solved by finite difference, $E_r \cong .25$; a suggested upper bound for acceptable momentum check is $E_r \cong .35$. We found the majority of points when calculated individually to have low Er's, usually from 0.0 to 0.2, but scattered points often had extremely large values, yielding a much higher overall E_r. This occurred for tests with no observational error as well as tests with large observational errors. We remain somewhat uncertain about how to evaluate these results; since the derived temperature retrievals appear consistent with the input winds, we expect there are no coding problems despite the occasional high E_r's.

4.4 *Discussion of Test Results*

The test results explained in Sections 3 and 4 demonstrated the potential feasibility of a simple forecast system assimilating wind and derived temperature data using Newtonian nudging. However, the sensitivity tests were all quite similar

to each other despite dramatic differences in observational error characteristics. Does this indicate insensitivity to data errors or problems with the methodology of sensitivity testing? While we believe there is reason for optimism as we move forward with real-data tests, it is worth highlighting some of the possible problems with this OSSE.

The sensitivity tests tried to mimic actual weather conditions and data conditions. However, the nature of the atmosphere and the particular characteristics of observing systems and observations could not be precisely duplicated. For example, both TREC and SPRINT data may not be available over large parts of the domain; in our sensitivity tests, the random deletion of data still should leave a generally even distribution in the remaining observations, rather than clusters of observations in areas with reliable radar data and no observations in other areas. Similarly, our method of generating synthetic SPRINT data was simplified; we did not generate synthetic radar data and then perform interpolations back to gridpoints, but rather simply extracted radial velocities from the gridded u and v data. As a result, we may be overestimating the usefulness of SPRINT data by not accounting for the increasing beam elevation with increasing distance from the radar. Our synthetic SPRINT data was available at low levels throughout the domain, whereas in real conditions the atmosphere will be sampled near the ground only for a small volume surrounding the radar.

A second problem with this set of sensitivity tests is that we have modeled one weather situation at one resolution. It remains to be determined whether the Doppler assimilation system will work under a broad variety of conditions. The seabreeze case is one with continual thermal forcing; the tests over a more homogeneous surface may show greater sensitivity to wind and temperature analysis quality. We do know that right now the system has been coded to work only for flat terrain, and the boundary conditions are not interactive, so strong forcing moving in from outside the domain cannot be modeled. Considering the incomplete description of typical SPRINT and TREC observation characteristics, it may be more profitable to simply try real-data experiments rather than attempt to add further complexity to the OSSE experiments.

To limit the complexity of the OSSE, we did not test the system over a wide range of the tunable parameters. Simple trial and error was used to select the best influence radius and vertical weight for this case. However, other parameters such as TREC and SPRINT data qualities and their time dependence were guessed at rather than determined through an analytic process.

5. Conclusions

The second year of this three-year study of the utility of Doppler data assimilation technology for local scale forecasting is complete. During the second year, the data assimilation system was coded, including a unique objective analysis package analyzing data in radial and tangential components, a dynamic temperature retrieval, and a Newtonian nudging scheme. The design of our prototype assimilation system is rather simple yet captures much of the complexity in our test case.

The use of a coupled analysis and Newtonian nudging scheme worked rather well here. Noise was minimal, perhaps because of the smoothness of the input analyses, but also perhaps because the forecast was nudged to a new dataset every 5 minutes. Presumably the errors in the current analysis are not well correlated with the errors in the previous analysis, so the noise caused by nudging to an inappropriate analysis may be cancelled out shortly thereafter when the old analysis is replaced by a new one.

Simple 2-D tests reconfirmed the potential improvement that should come from assimilating temperature as well as wind information. A set of 3-D simulation experiments was less conclusive; temperature assimilation experiments improved on the wind-only forecasts slightly, but not dramatically. Overall, the 3-D simulations were all remarkably similar, which may be an indication of proper design of the assimilation system to minimize insensitivity to error, or it may indicate that the simulation experiment was not sufficiently complex. The sensitivity tests could be extended to other weather regimes, but we believe it will be more useful to start real-data testing rather than broadening the scope of the sensitivity tests further. The bulk of the real-data testing we expect to do with the CaPE dataset, a large convective initiation study dataset over central Florida taken in the summer of 1991. Should the forecast algorithm produce successful results over a range of situations, then we will also concentrate on producing indices which will indicate to the forecaster where convection is likely to occur.

One last lesson: regardless of the success of the forecast, the assimilation system itself may prove useful for users wanting an up-to-date local area analysis. It is easy to envision that such a system may be useful for small regions like Cape Kennedy, FL. This system has the disadvantage of starting off only as accurate as the initial conditions permit, but it may evolve into a highly realistic wind and temperature analysis as the model adjusts over a period of time to the new observations. Though not included here, other observations such as conventional surface observations, profilers, RASS sounders, and such could also be assimilated into such a forecast, leading to even more accurate 3-D analyses.

References

Benjamin, S. G., and N. L. Seaman, 1985: A simple scheme for objective analysis in curved flow. *Mon. Wea. Rev.*, **113**, 1184-1198.

Brooks, H.E., C.A. Doswell, and R. A. Maddox, 1992: On the use of mesoscale and cloud-scale models in operational forecasting. *Wea. Forecasting, 7,* 120-132.

Cotton, W. R., R. McAnelly, C. Tremback, and R. Walko, 1989: A dynamic model for forecasting new cloud development. *AFGL Tech. Report 89-0011*, Phillips Laboratory, Hanscom AFB, MA 01731, 81 pp., ADA213939

Cressman, G. P., 1959: An operational objective analysis system. *Mon. Wea. Rev.*, **87**, 367-374.

Crook, A., and J.D. Tuttle, 1992: Initialization of storm-scale motions in a nonhydrostatic numerical model. Preprints, Cloud Conference, Montreal, 1992.

Foote, G. B., 1991: Scientific overview and operations plan for the convective and precipitation / electrification experiment (CaPE). National Center for Atmospheric Research, Boulder, CO. 145 pp.

Gal-Chen, T., 1978: A method for the initialization of the anelastic equations: implications for matching models with observations. *Mon. Wea. Rev.*, **106**, 587-606.

----- , 1986: Selected comments on the use of the divergence equation to obtain temperature and geopotentials from and observed wind. *Journ. Atmos. Ocean. Tech.*, **3**, 730-733.

----- , and Kropfli, R. A., 1984: Buoyancy and pressure perturbations derived from dual-doppler radar observations of the planetary boundary layer: applications for matching models with observations. *Journ. Atmos. Sci.*, **41**, 3007-3020.

Gandin, L.S., 1963: Objective analysis of meteorological fields. *Gidrometeorologiches-koe zdatelstvo*, Leningrad. English translation by: Israel Program for Scientific Translations, Jerusalem, 242 pp. [NTIS N6618047, Library of Congress QC996.G3313.]

Gustafson, G. B., Moncet, J.-L., Ivaldi, C. F., Huang, H.-C., and Sparrow, J. M., 1991: Mesoscale prediction and satellite cloud analysis for advanced meteorological processing systems. *PL-TR-91-2008*, ADA240510, Phillips Laboratory, Geophysics Directorate, Hanscom

AFB, MA 01731. 112 pp.

Hamill, T. M., 1992: Prediction of thunderstorm initiation through 4-dimensional data assimilation of doppler radar data. *PL-TR-92-2029*, Phillips Laboratory, Geophysics Directorate, Hanscom AFB, MA, 01731. 86 pp. ADA251243

Hane, C.E., Scott, B.C., 1978: Temperature and pressure perturbations within convective clouds derived from detailed air motion information: preliminary testing. *Mon. Wea. Rev.*, **106**, 654-661.

Kapitza, H., 1991: Numerical experiments with the adjoint of a nonhydrostatic mesoscale model. *Mon. Wea. Rev.*, **119**, 2993-3011.

Liou, Y.-C., 1989: Retrieval of three-dimensional wind and temperature fields from one-component wind data using the four-dimensional data assimilation technique. M.S. Thesis, University of Oklahoma, 112 pp.

Lyons, W. A., Pielke, R. A., Cotton, W. R., Keen, C. S., 1992: Final results of an experiment in operational forecasting of sea breeze thunderstorms using a mesoscale numerical model. *Preprints, American Meteorological Society Symposium on Weather Forecasting*, , 181-188.

Mohr, C. G., L. J. Miller, R. L. Vaughan, and H. W. Frank, 1986: The merger of mesoscale data sets into a common cartesian format for efficient systematic analyses. *J. Atmos. Ocean. Tech.*, **3**, 143-161.

Qiu, C-J., and Q. Xu, 1992: A simple ajdoint method of wind analysis for single-doppler data. *J. Atmos. Ocean. Tech.*, **9**, 588-598.

Roux, F., 1985: Retrieval of thermodynamic fields from multiple doppler radar data using the equations of motion and the thermodynamic equation. *Mon. Wea. Rev.*, **113**, 2142-2157.

Stauffer., D. R., and N. L. Seaman, 1990: Use of four-dimensional data assimilation in a limited-area mesoscale model. Part I: experiments with synoptic-scale data. *Mon. Wea. Rev*, **118**, 1250-1277.

Sun, J. Z., D. W. Flicker, and D. K. Lilly, 1991: Recovery of three-dimensional wind and temperature fields from single-Doppler radar data. *J. Atmos. Sci.*, **48**, 876-890.

Tracton, M.S., K. C. Mo, W. Chen, E. Kalnay, R. Kistler, and G. White, 1989: Dynamical extended range forecasting (DERF) at the National Meteorological Center. *Mon. Wea. Rev.*, **17**, 1604-1635.

Tripoli, G. J., and Cotton, W. R., 1982: The Colorado State University EE-Dimensional Cloud / Mesoscale Model - 1982; Part I: General Theoretical Framework and Sensitivity Experiments. *J. Rech. Atmos.*, 16,185-219.

Tuttle, J. D., and G. B. Foote, 1990: Determination of the boundary layer airflow from a single Doppler radar. *Journ. Atmos. Ocean. Tech.*, 7, 218-232.

Vemuri, V., and W. J. Karplus, 1981: *Digital Computer Treatment of Partial Differential Equations*. Prentice Hall, Inc., Englewood Cliffs, NJ, 449 pp.

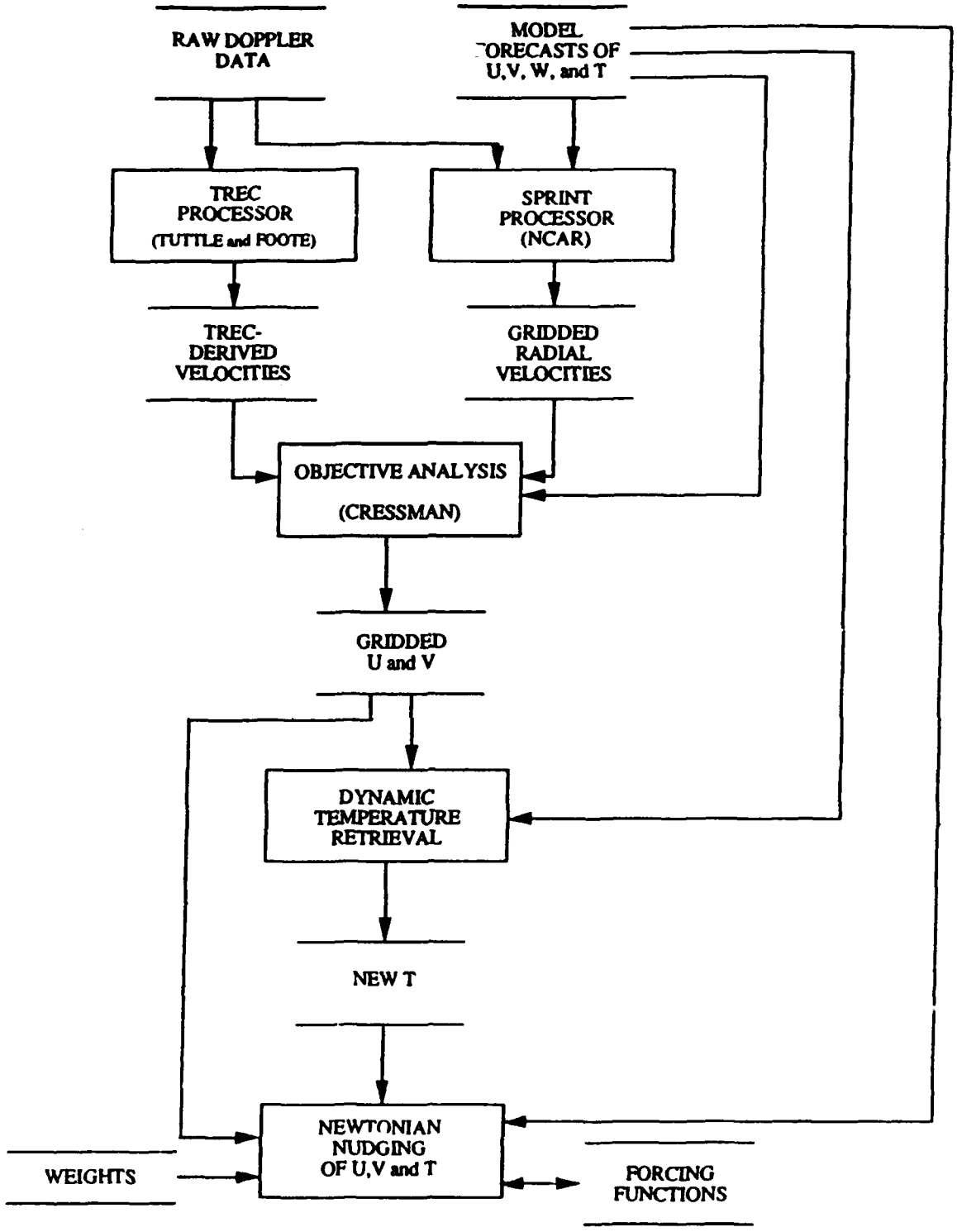

Figure 1: Illustration of the high-level data and processing flow in the new retrieval system. Parallel lines indicate data stores, and boxes describe algorithms. Execution of the algorithm proceeds from top to bottom.

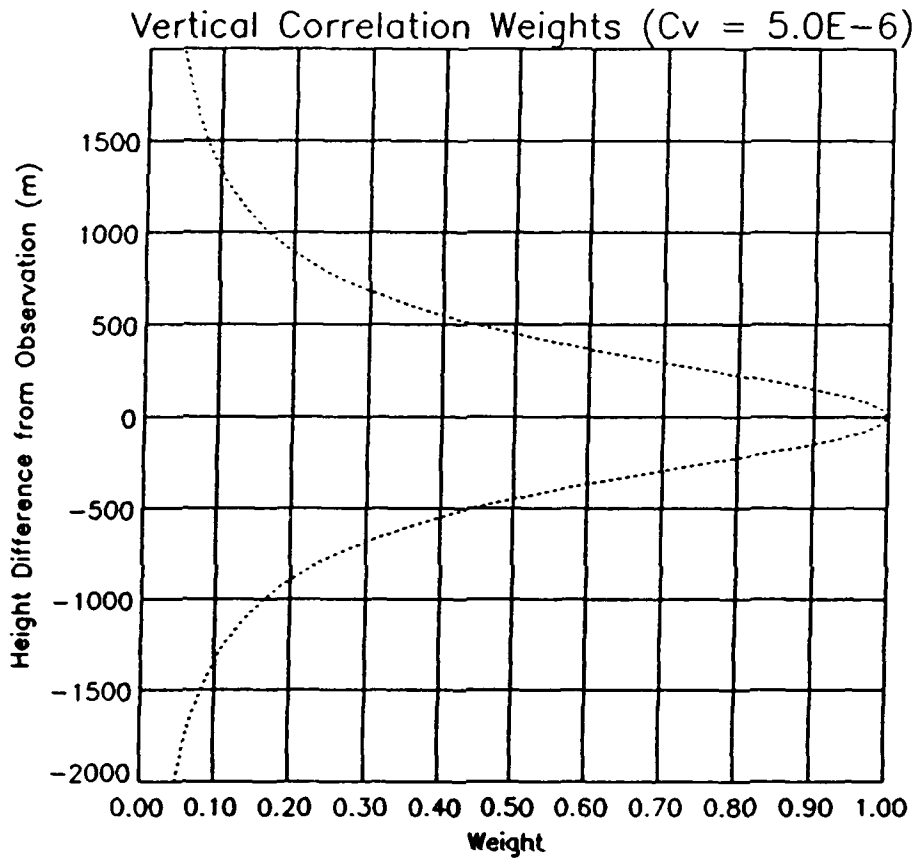

Figure 2: Illustration of the vertical weight as a function of altitude difference from the observation for a weight of $5.0*10^{-6}$ m^{-2}.

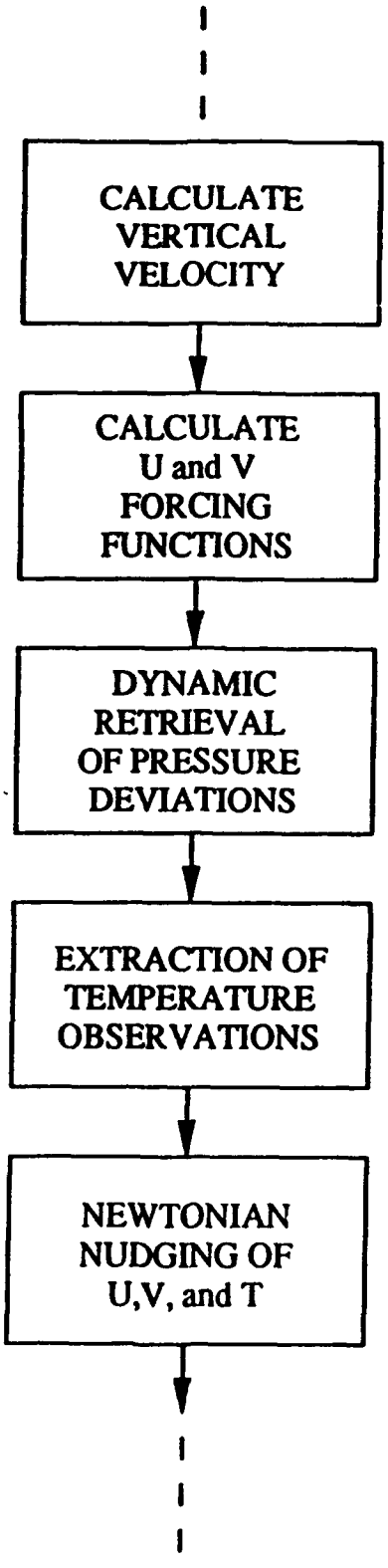

Figure 3: Steps in the dynamic retrieval process. Each step is explained in-depth in the main text.

(a)

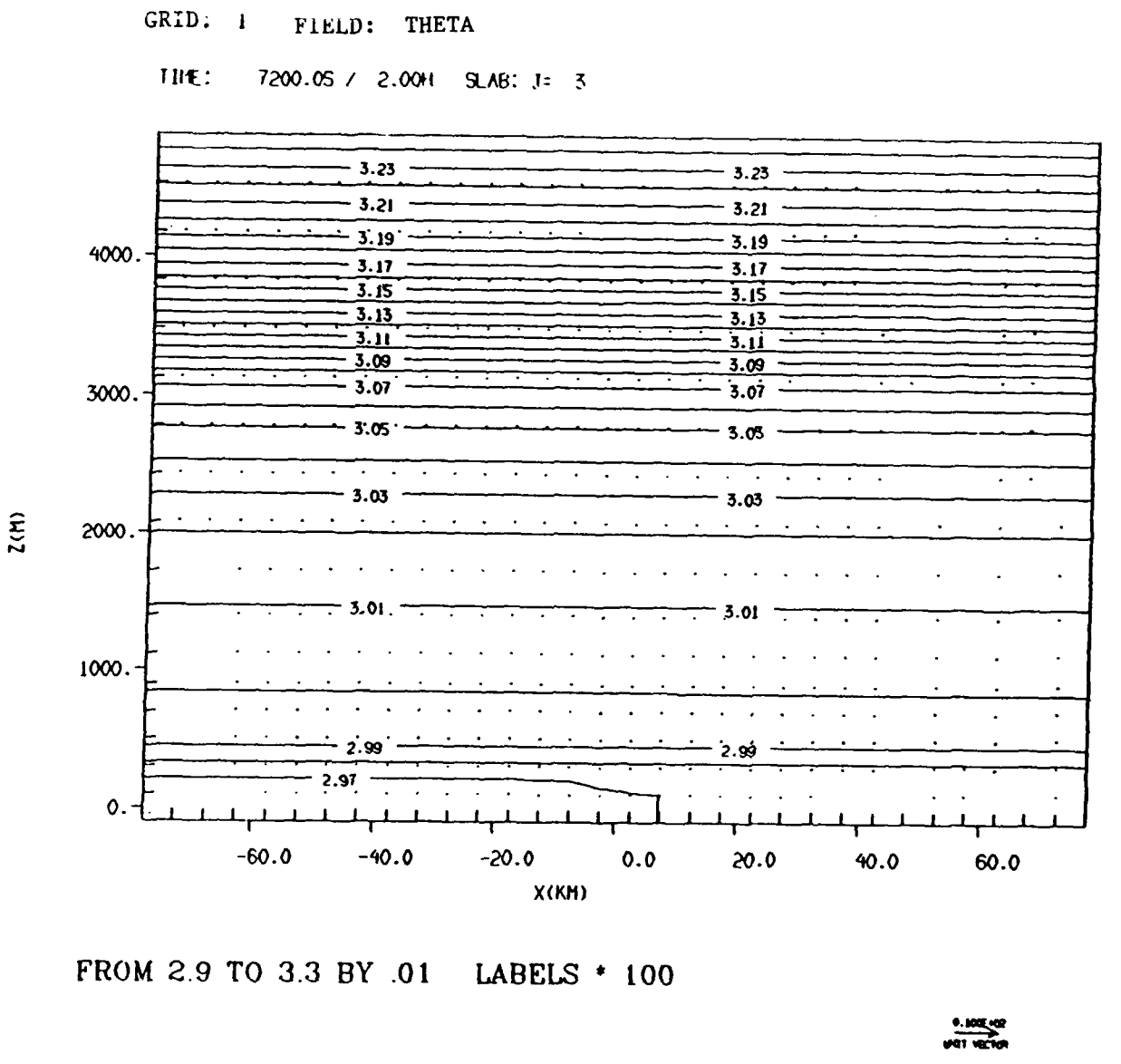

Figure 4: Nature run forecasts for a 2-D seabreeze simulation starting at 0700 LST. Temperatures are in Kelvin/100, and a horizontal unit wind vector is 10 ms^{-1}. (a) 2-hour truth data, (b) 3-hour truth, (c) 4-hour truth, (d) 5-hour truth, (e) 6-hour truth, and (f) 7-hour truth corresponding to 1-hour forecast.

(b)

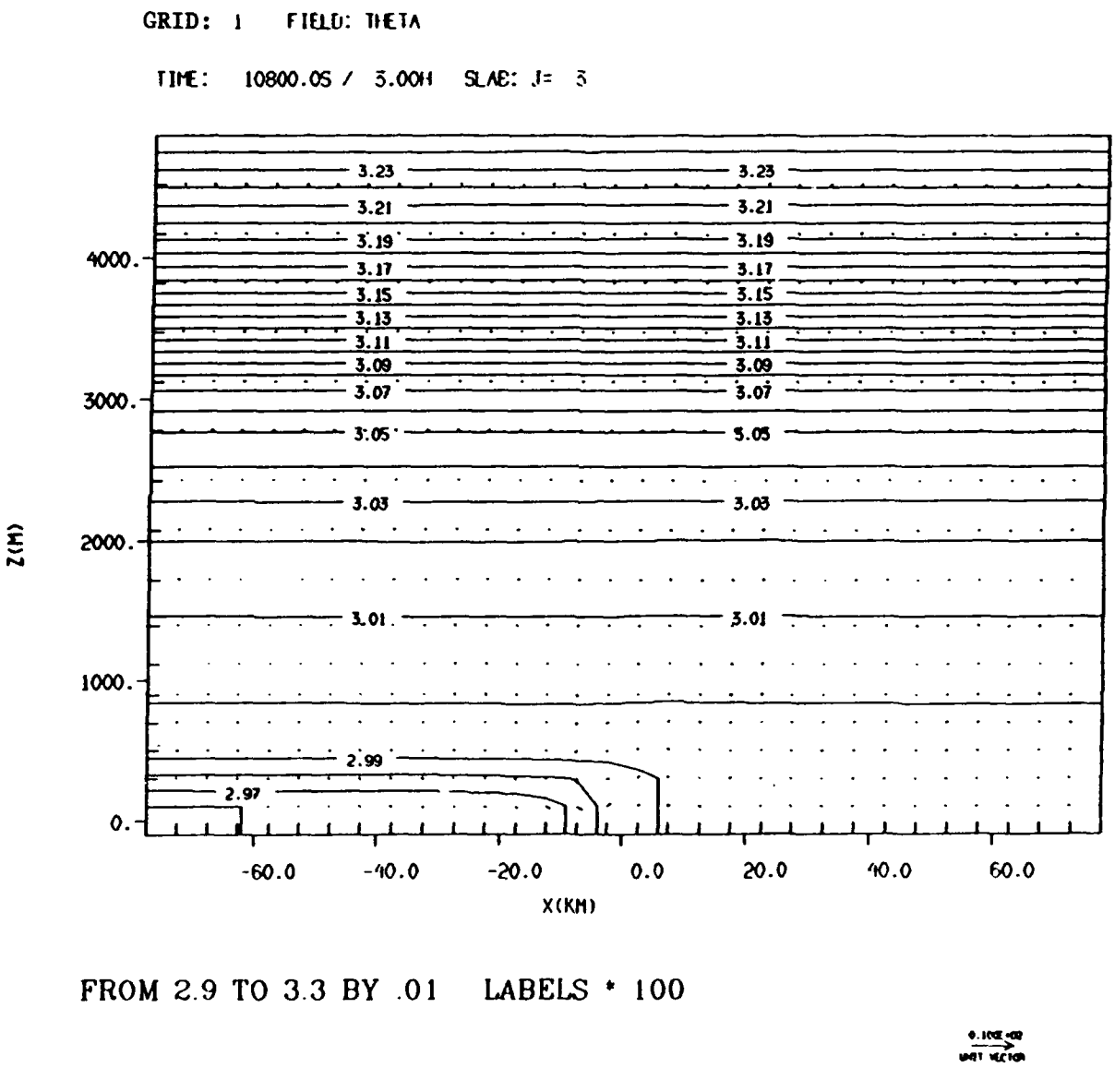

FROM 2.9 TO 3.3 BY .01 LABELS * 100

Figure 4 Continued

(c)

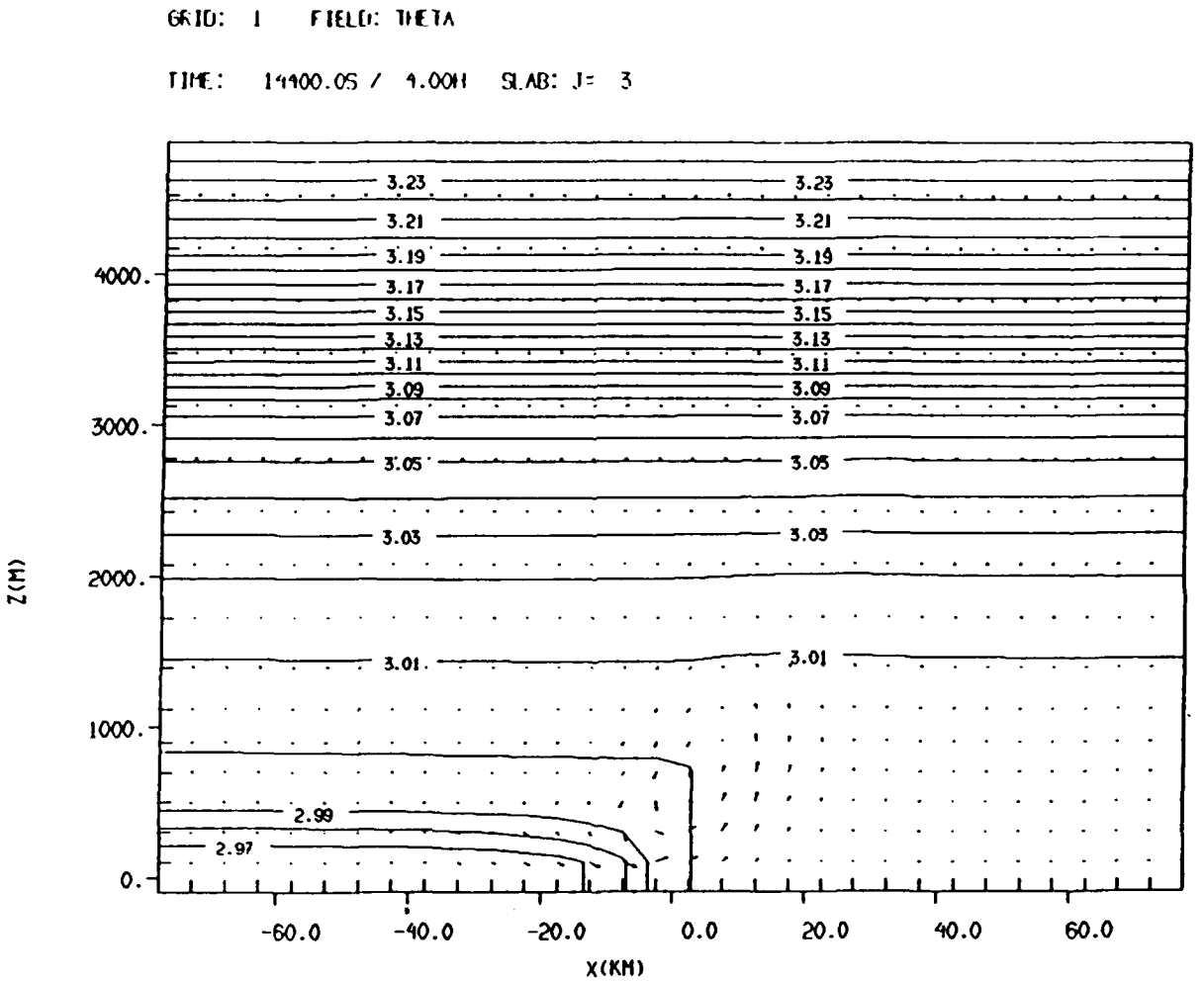

FROM 2.9 TO 3.3 BY .01 LABELS * 100

Figure 4 Continued

(d)

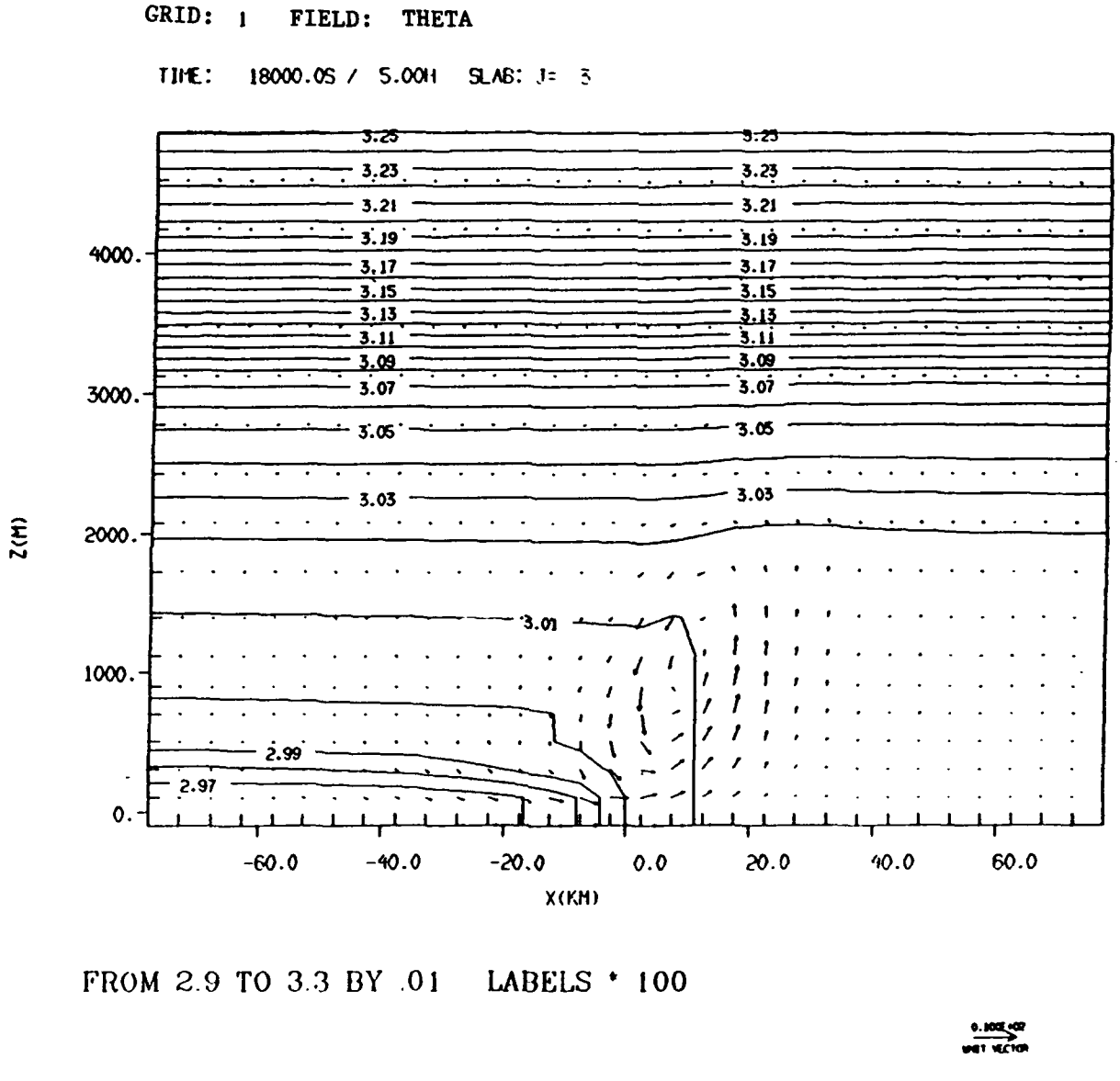

Figure 4 Continued

(e)

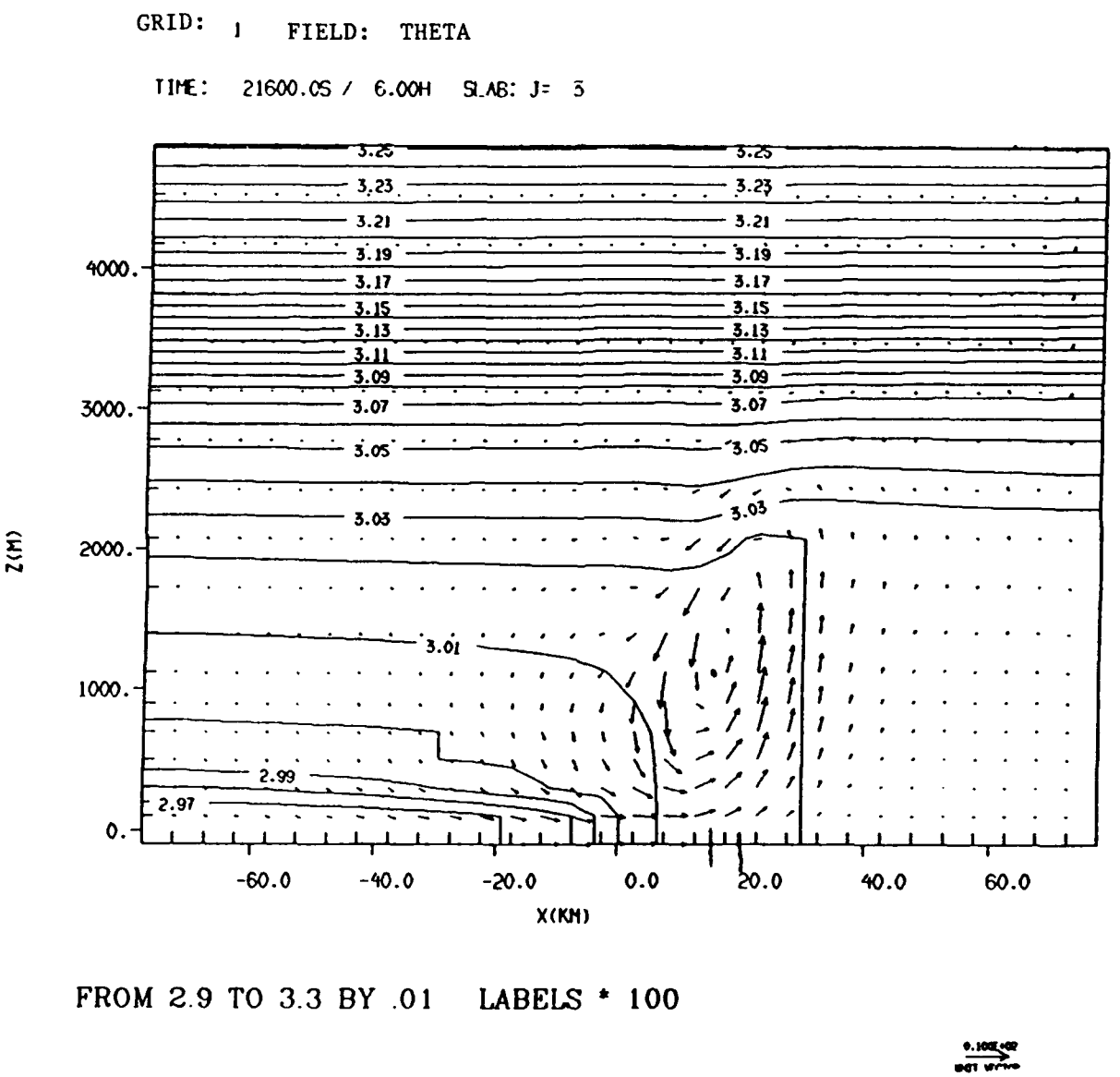

Figure 4 Continued

(f)

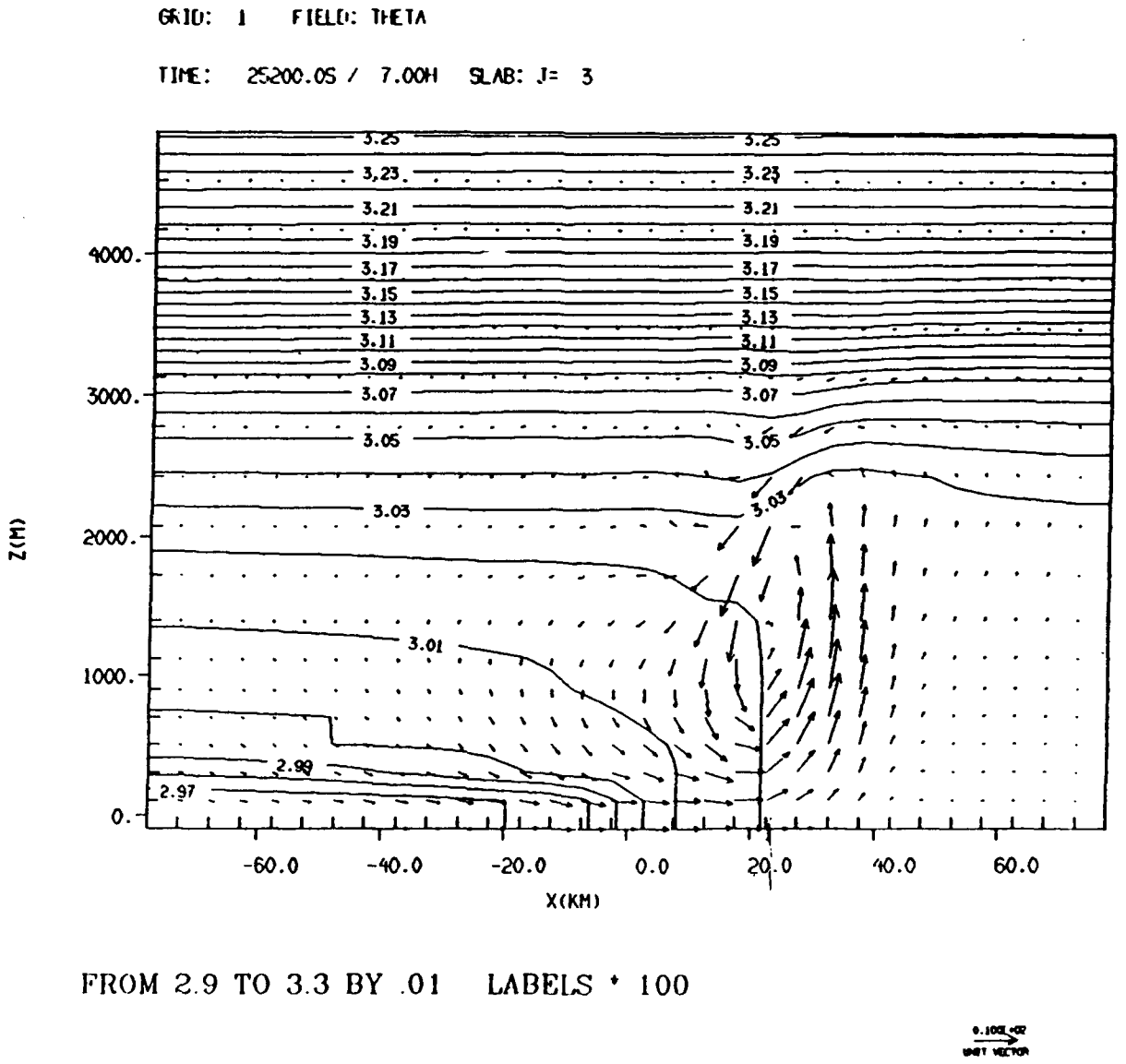

Figure 4 Continued

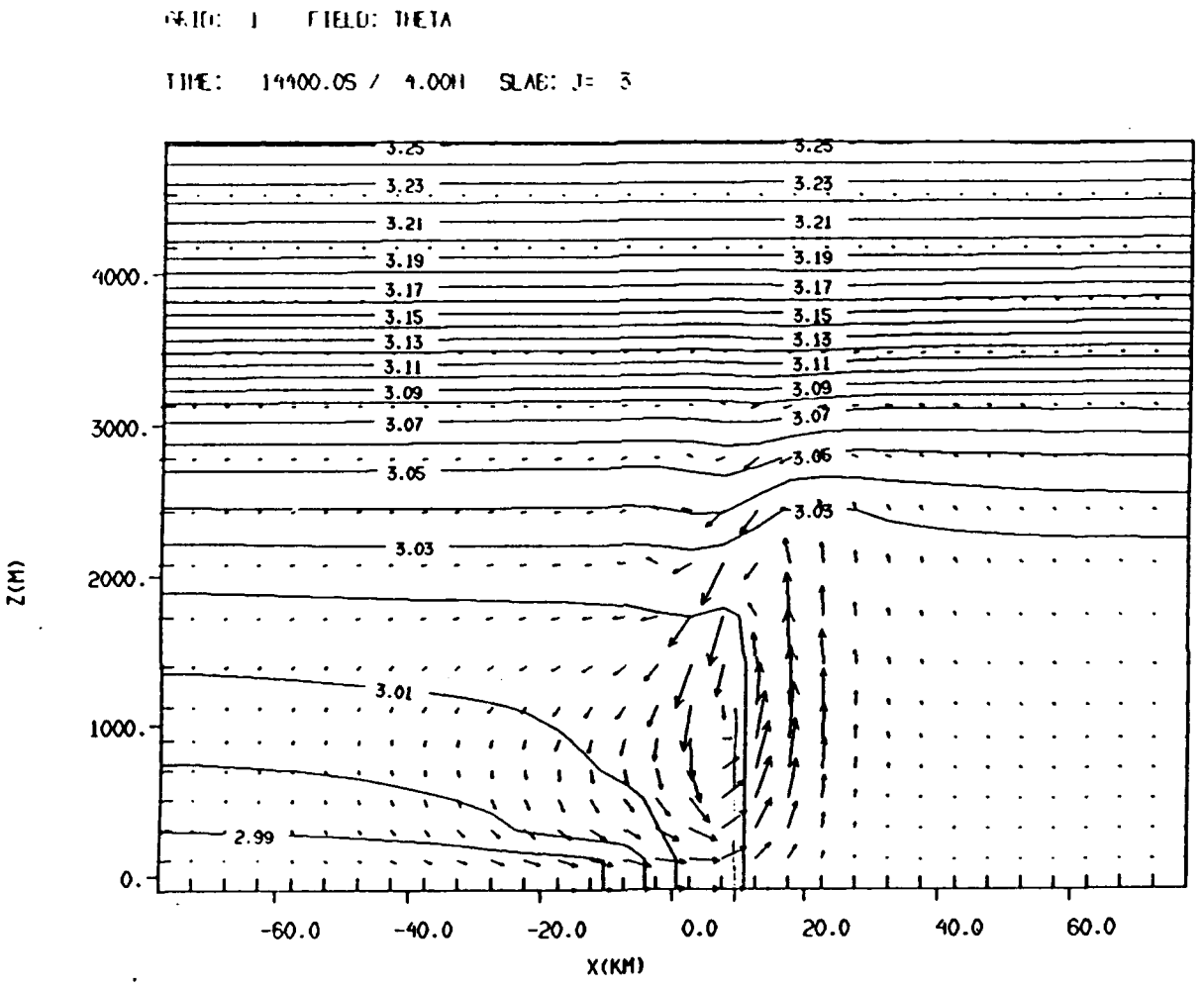

FROM 2.9 TO 3.3 BY .01 LABELS * 100

Figure 5: 4-hour model forecast with no data assimilation.

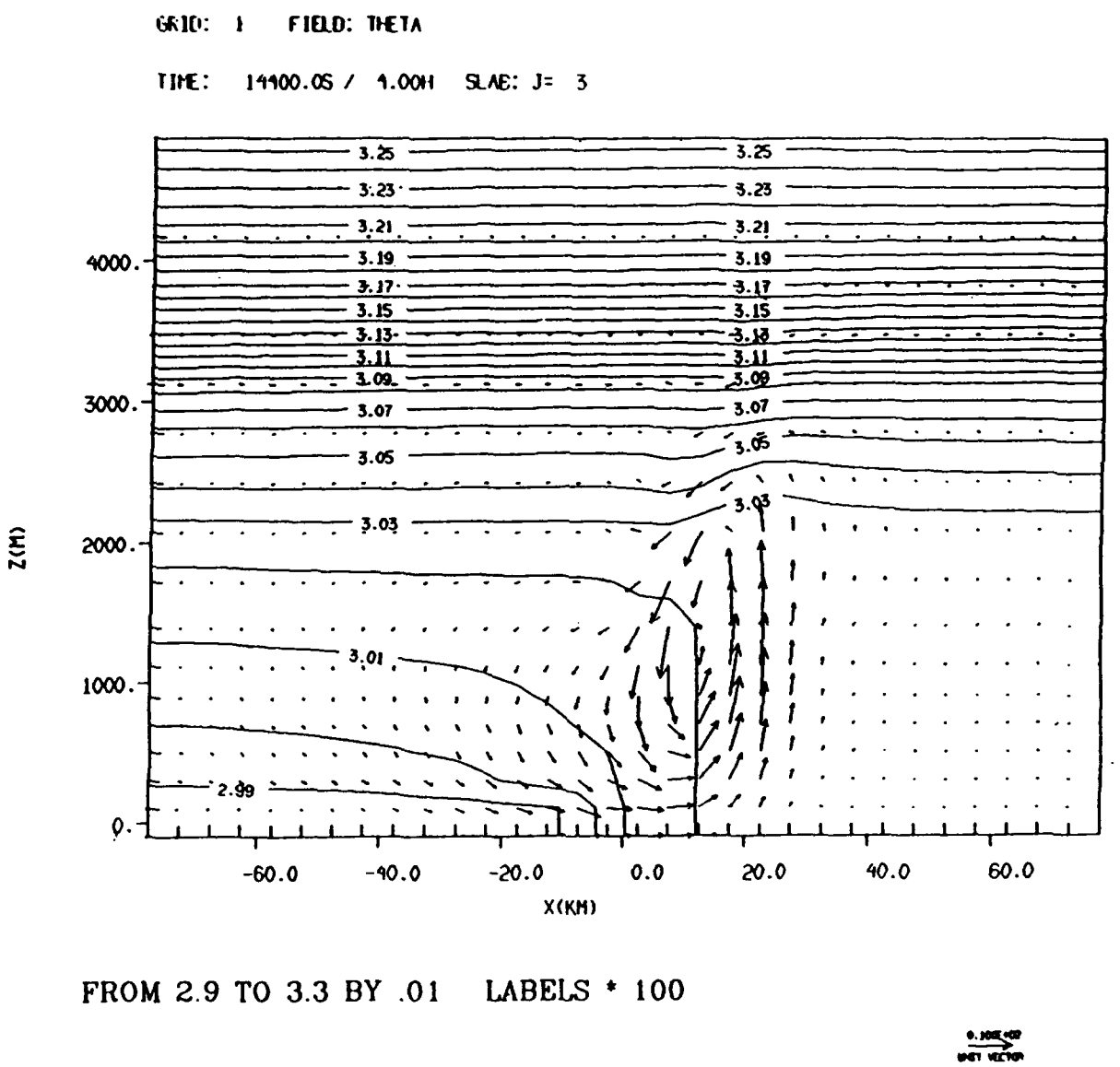

Figure 6: 4-hour model forecast with wind data assimilated.

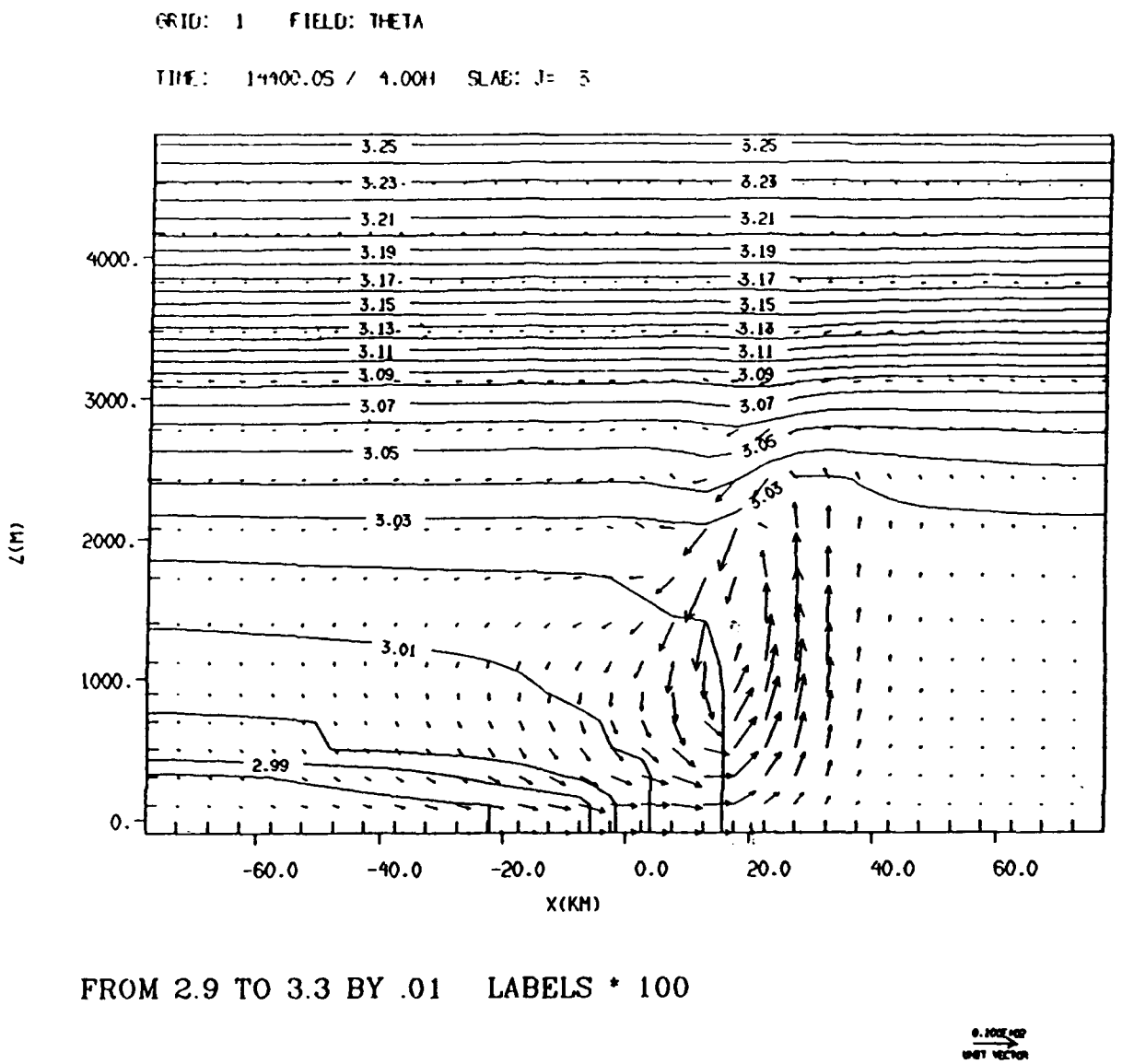

Figure 7: 4-hour model forecast with both wind and temperature data assimilated.

(a)

(b)

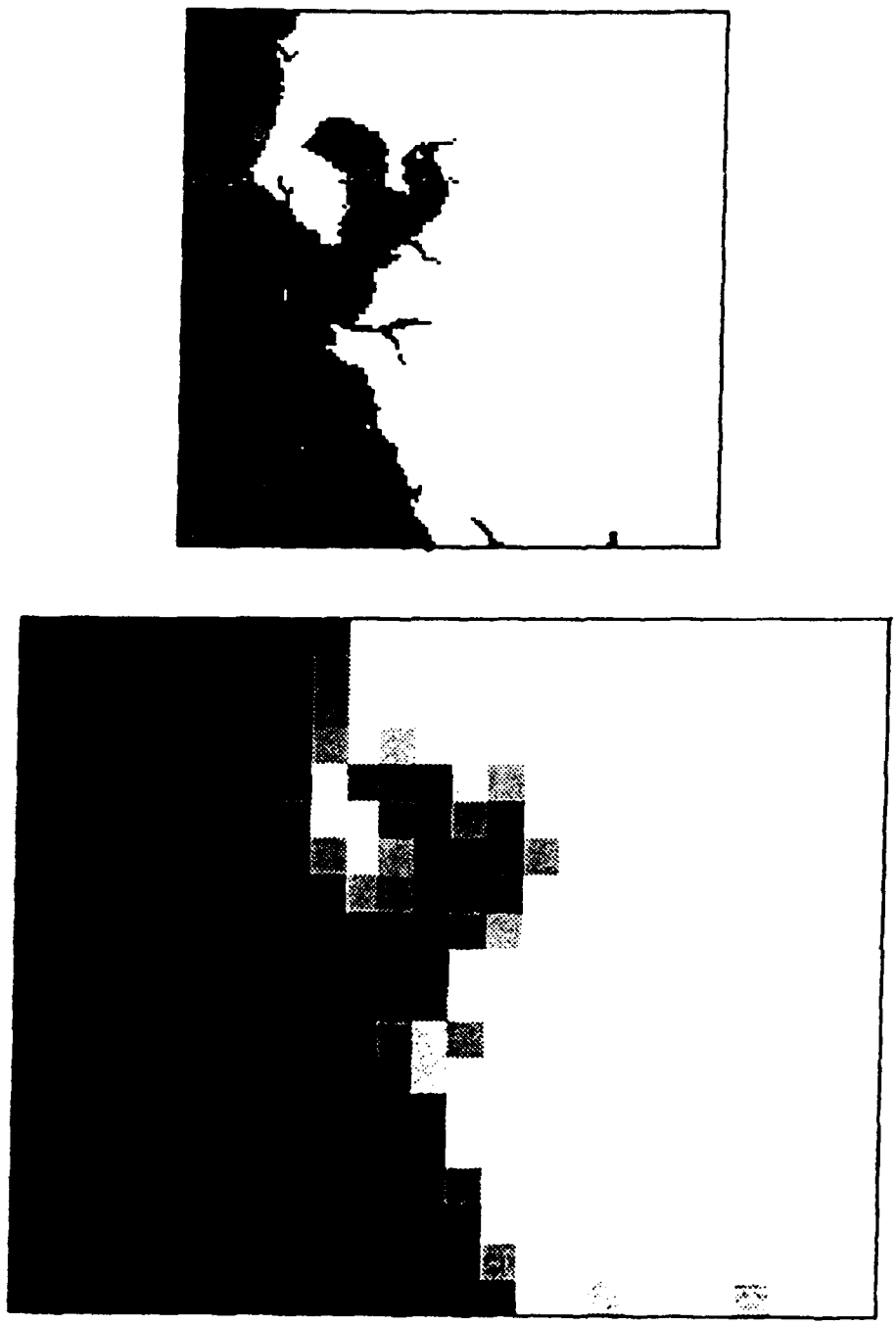

Figure 8: Model terrain in the forecast area. (a) High-resolution map of terrain in the Tampa Bay, FL area, with land in white and water in black, and (b) percentage land at the resolution of the forecast, with shaded from black (0 percent) to white (100 percent).

(a)

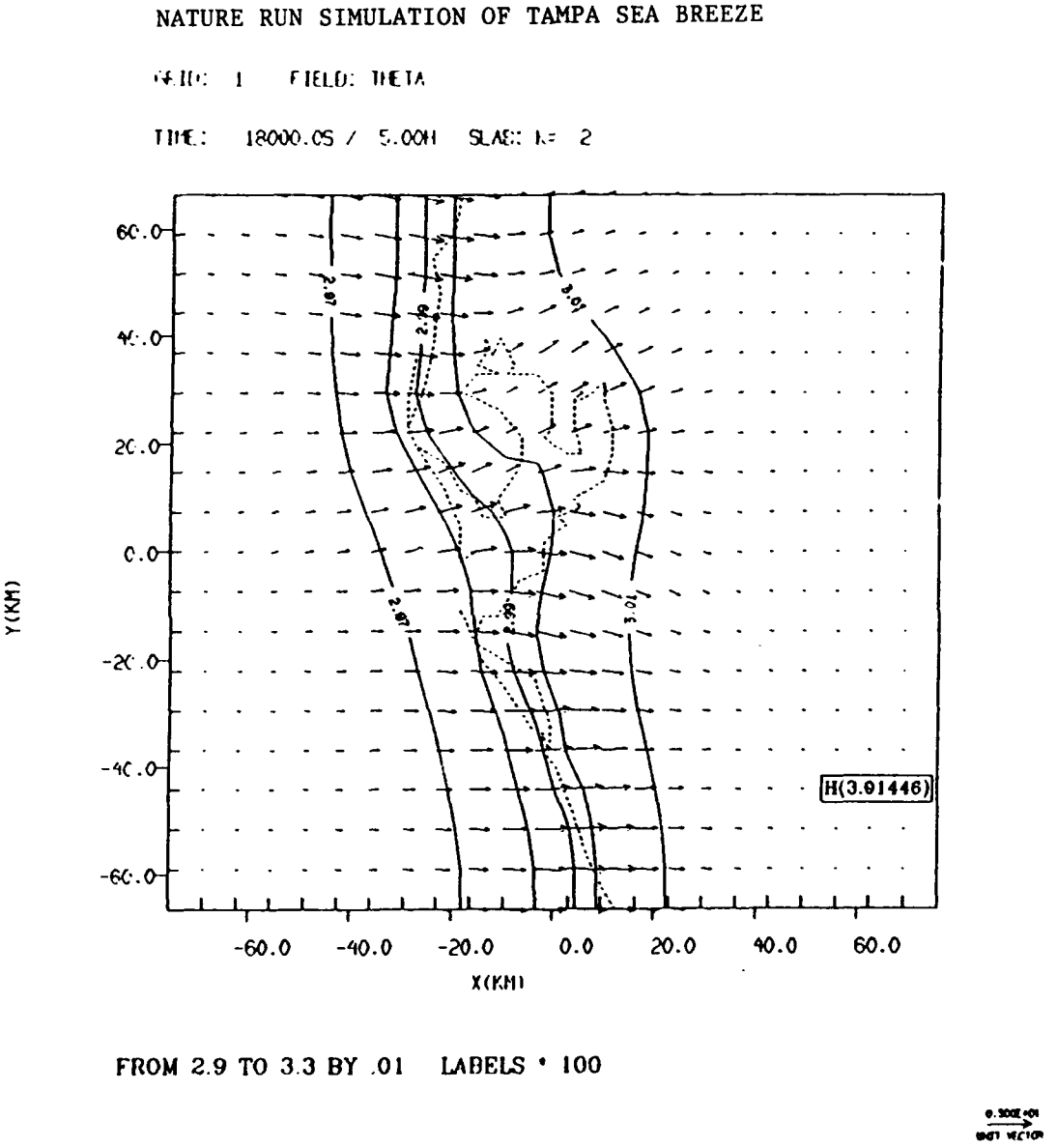

Figure 9: Nature Run ground truth data. Temperatures are in K/100, and horizontal unit wind vectors are 5 ms^{-1}. (a) horizontal cross-section of ground truth data at level 3 for 1200 LST, (b) horizontal cross-section for 1300 LST, (c) horizontal cross-section for 1400 LST, (d) vertical cross-section at y=+22 km for 1200 LST, (e) vertical cross-section for 1300 LST, and (f) vertical cross-section for 1400 LST.

(b)

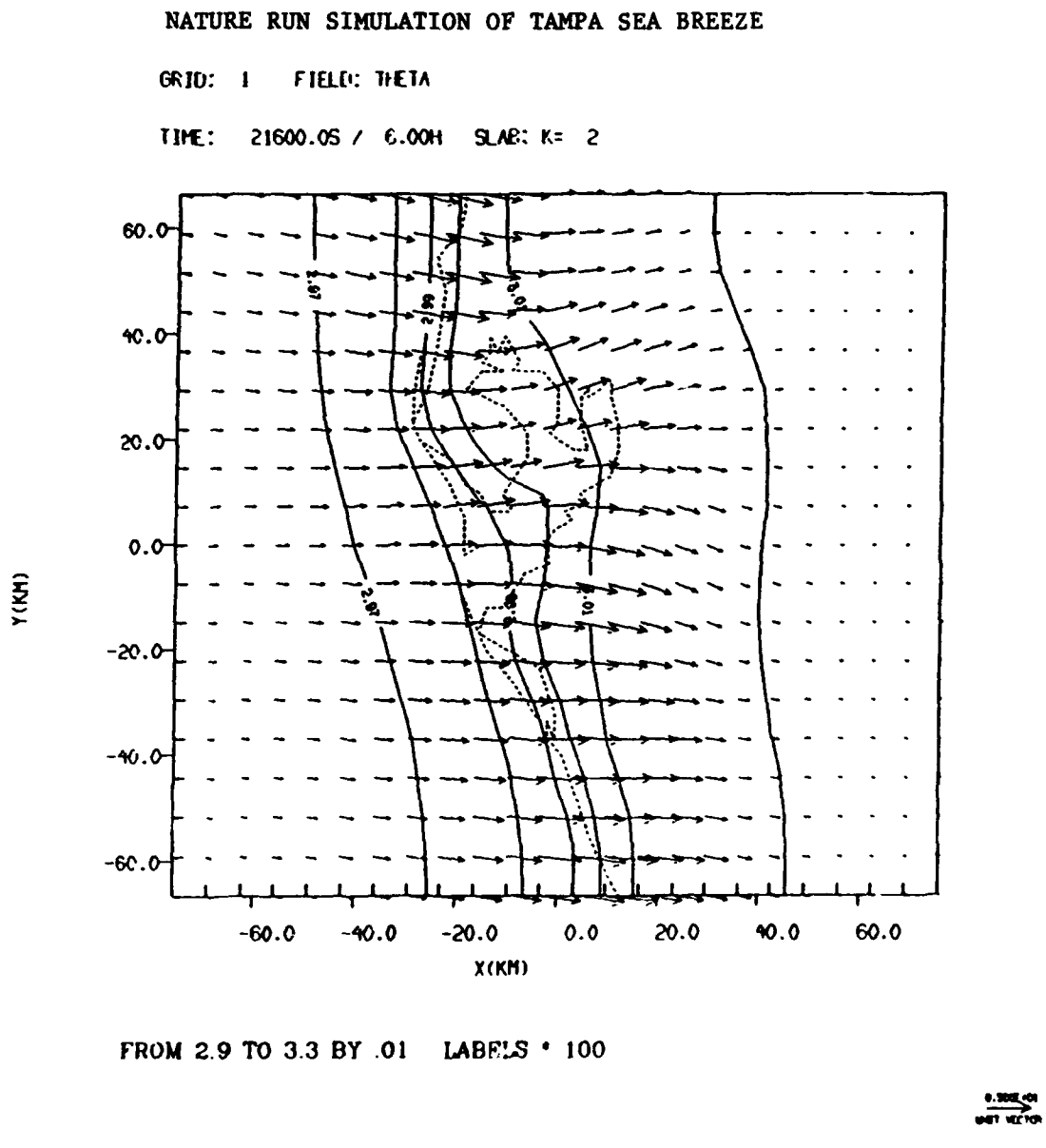

Figure 9 Continued

(c)

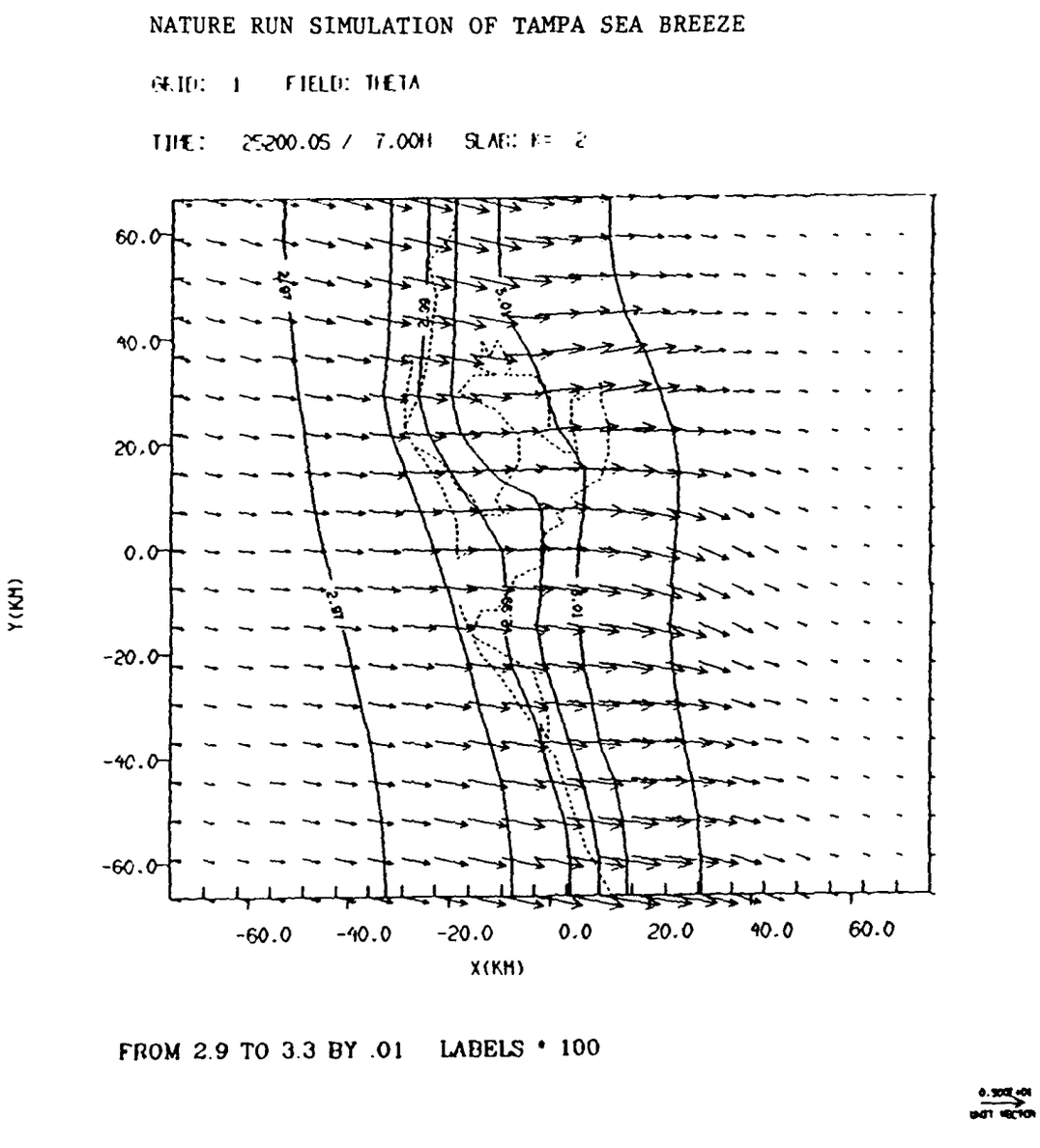

Figure 9 Continued

(d)

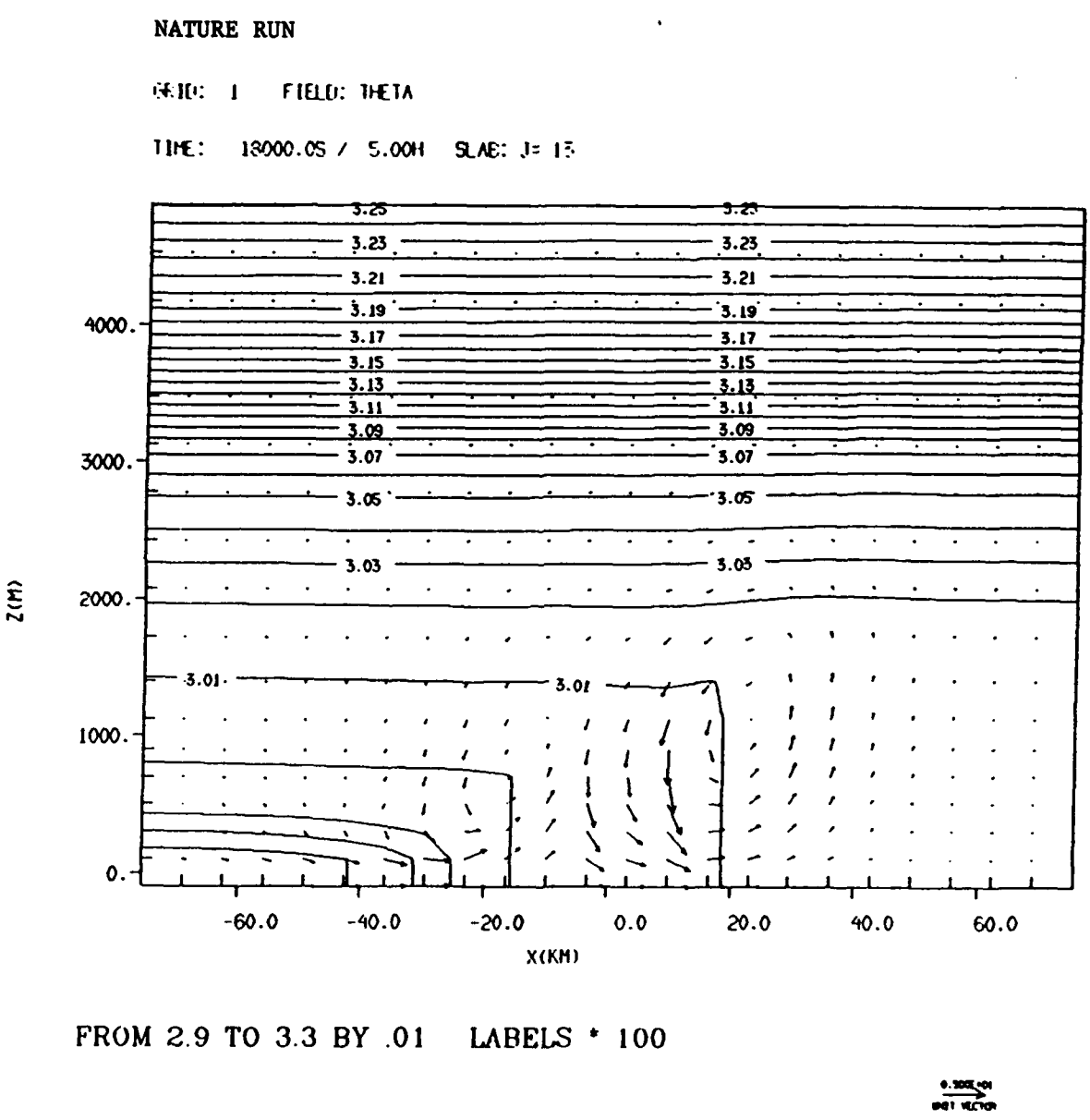

Figure 9 Continued

(e)

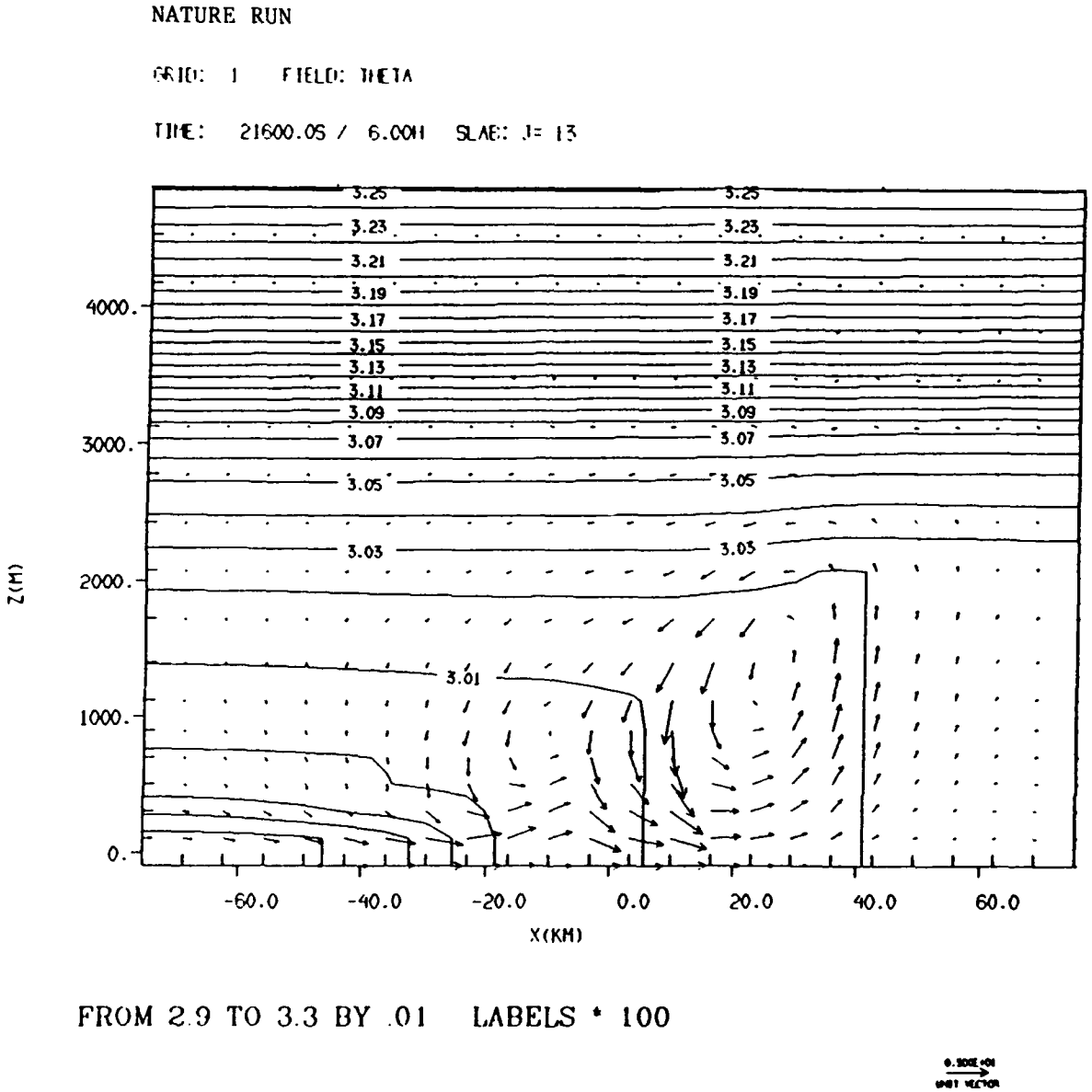

Figure 9 Continued

(f)

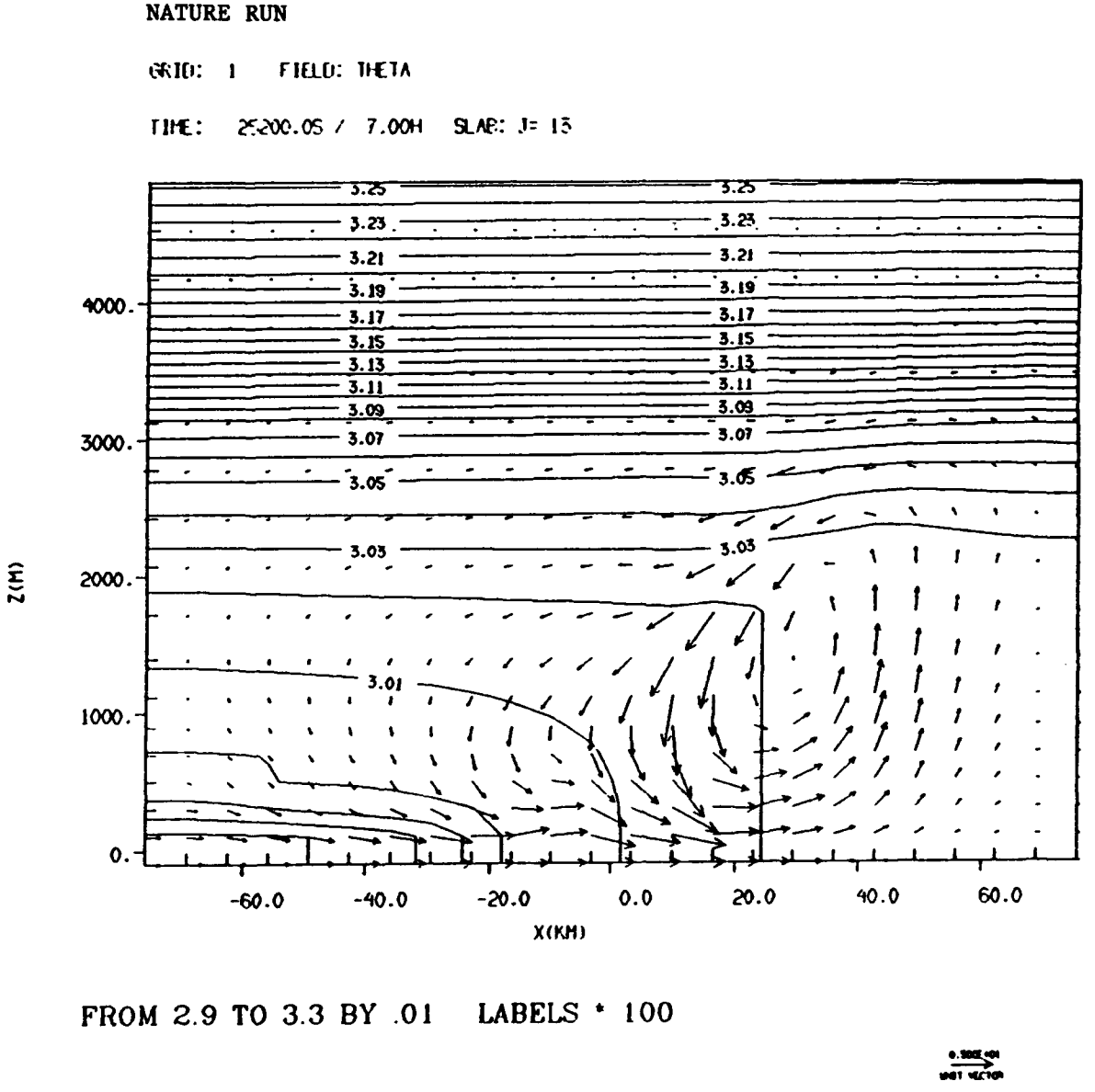

Figure 9 Continued

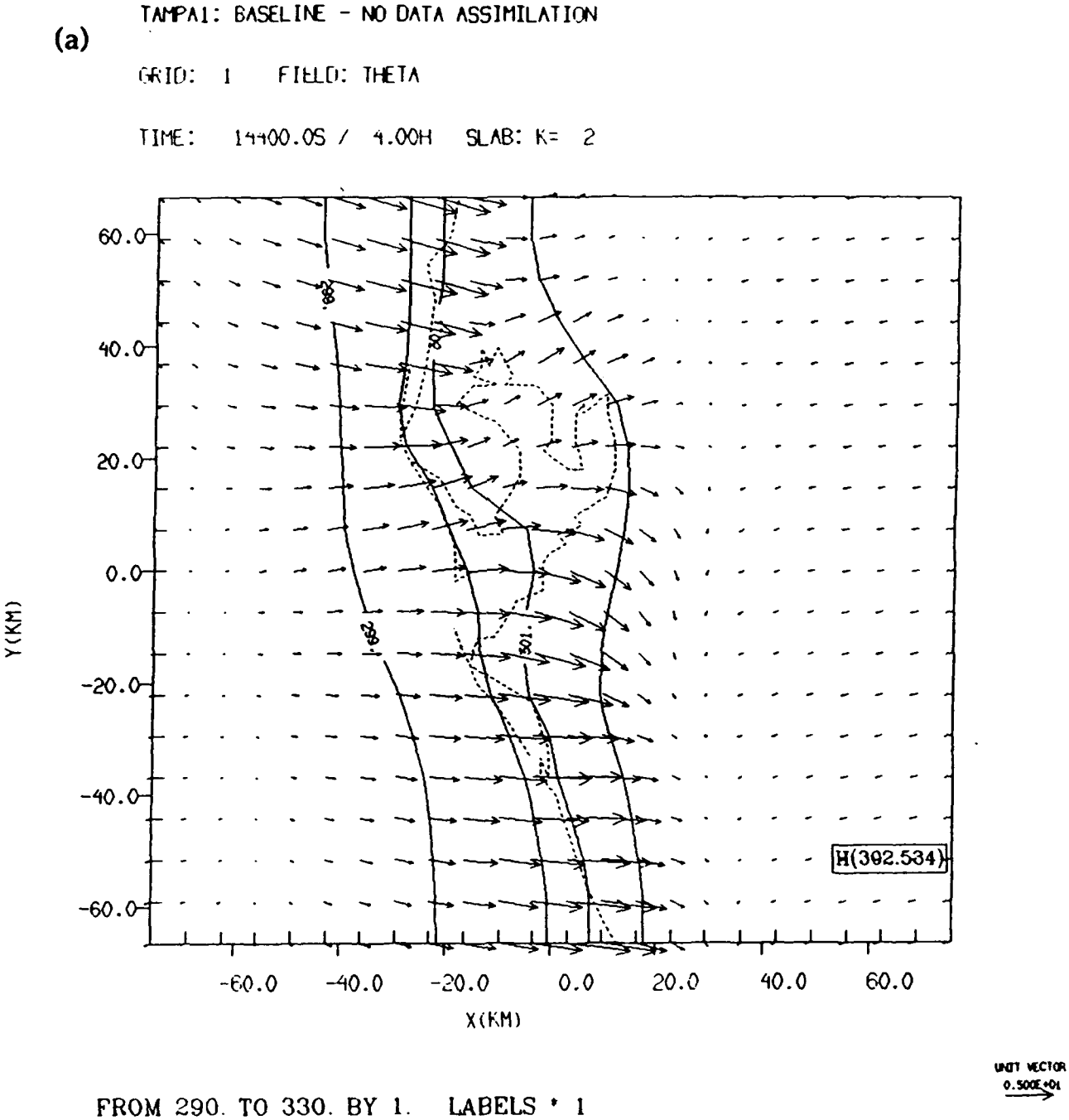

Figure 10: Experiment 1 output. Baseline run of the forecast model with no data assimilation. (a) horizontal cross-section of 4-hour forecast, valid at 1400 LST, and (b) corresponding vertical cross-section.

(b)

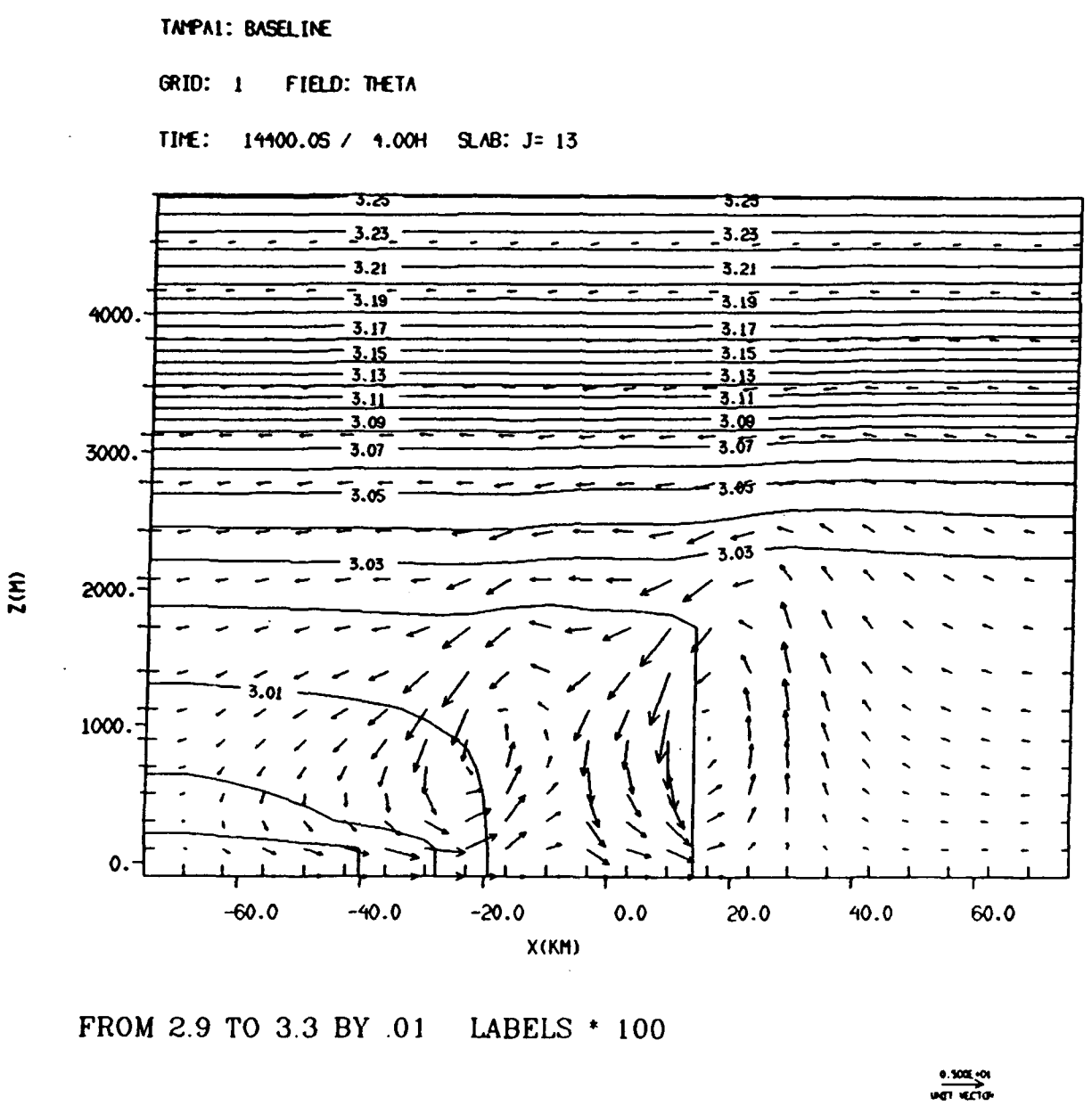

FROM 2.9 TO 3.3 BY .01 LABELS * 100

Figure 10 Continued

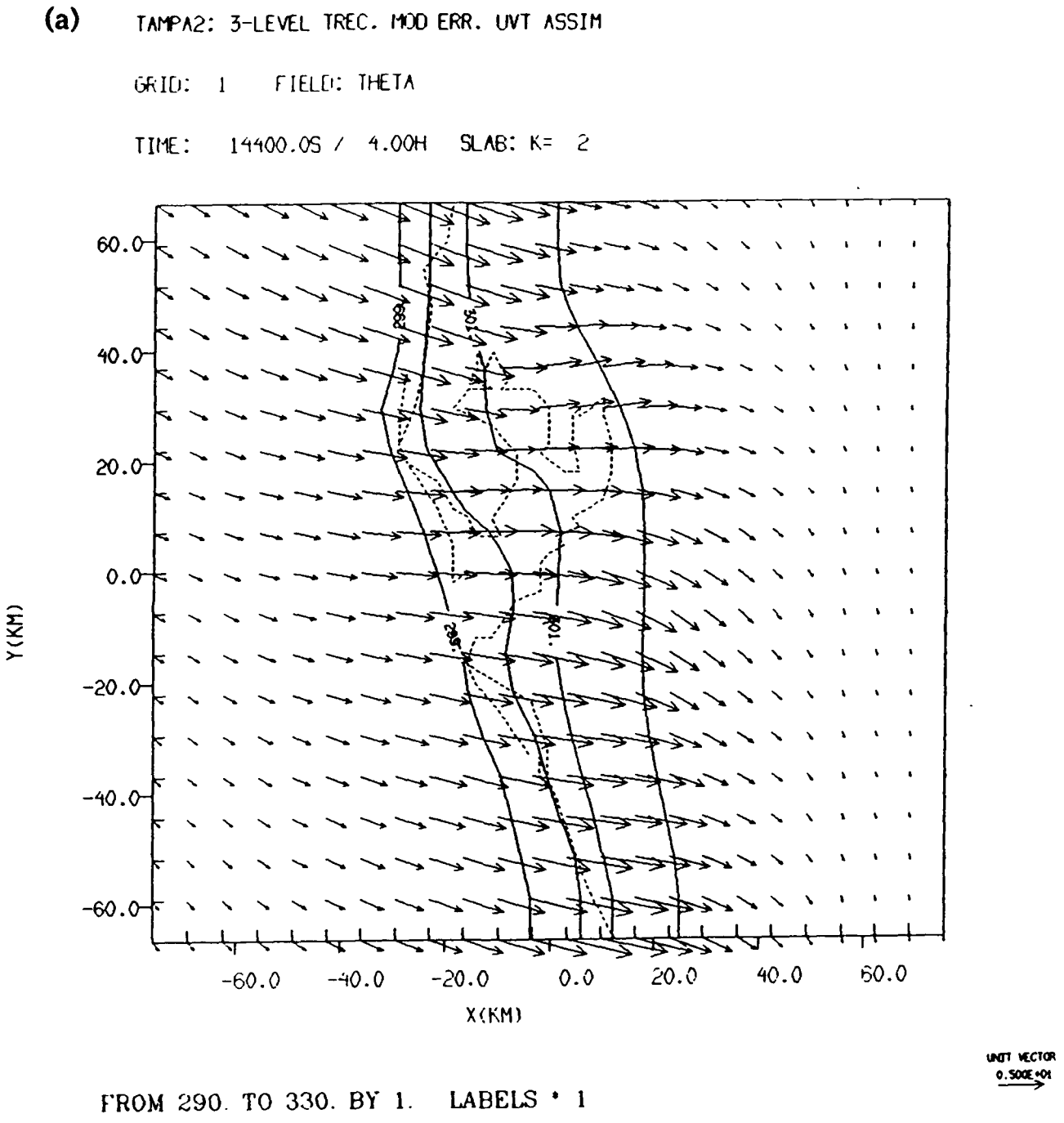

Figure 11: Experiment 2 output: 3-level TREC data assimilation experiment. (a) horizontal cross-section of 4-hour forecast, valid at 1400 LST, and (b) corresponding vertical cross-section.

(b)

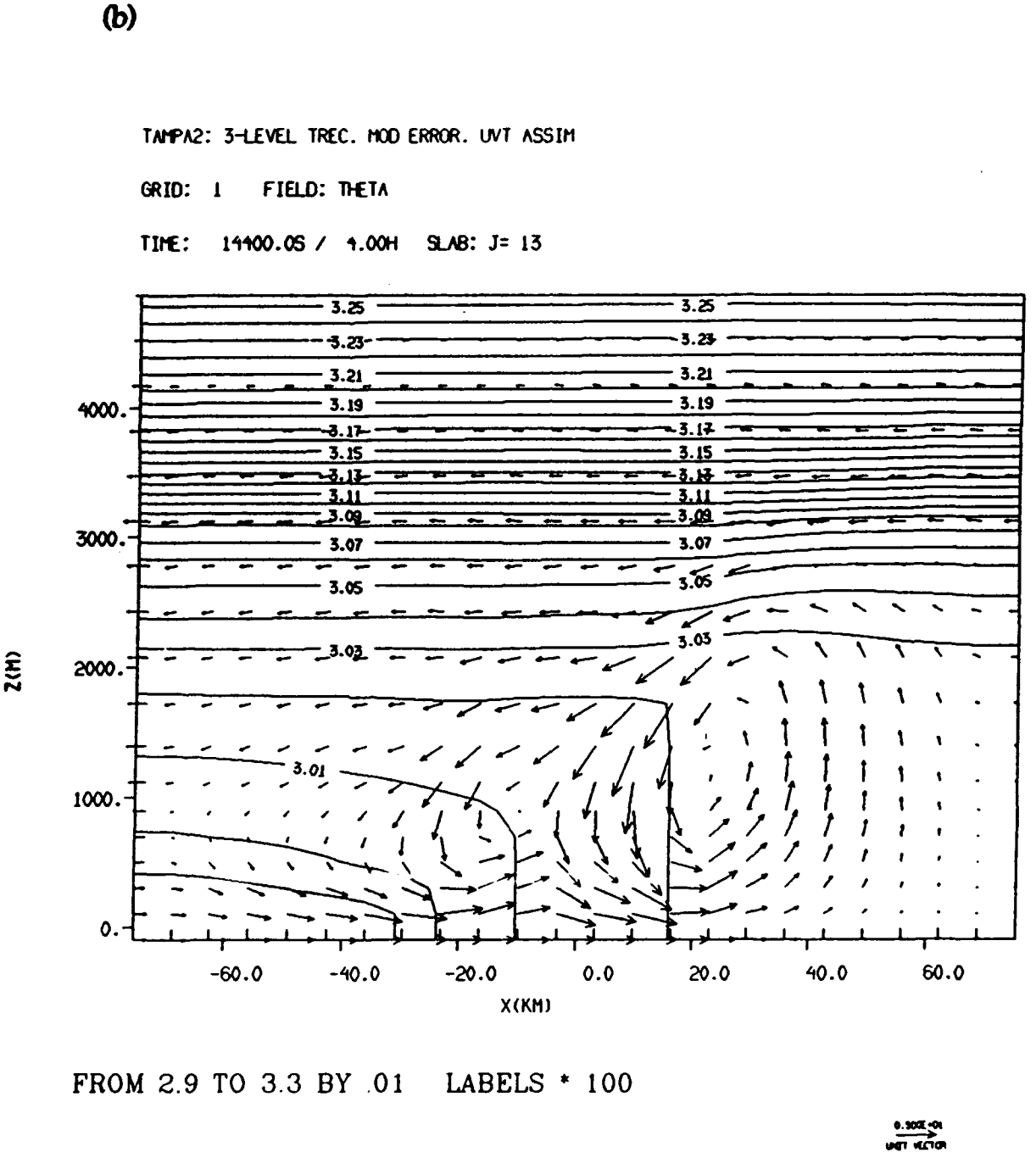

Figure 11 Continued

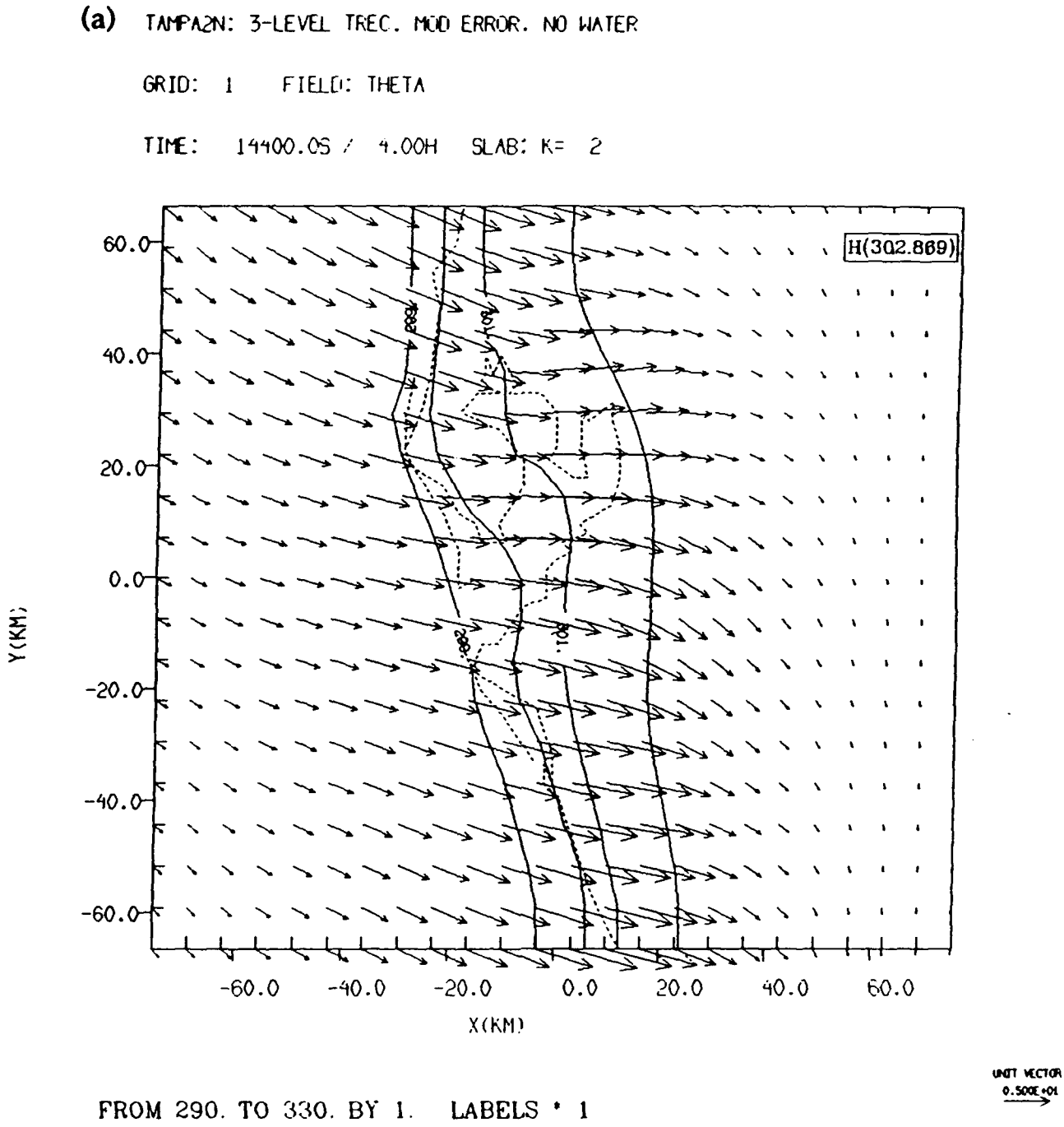

Figure 12: Experiment 2N output: 3-level TREC data assimilation experiment with no observations over water used. (a) horizontal cross-section of 4-hour forecast, valid at 1400 LST, and (b) corresponding vertical cross-section.

(b)

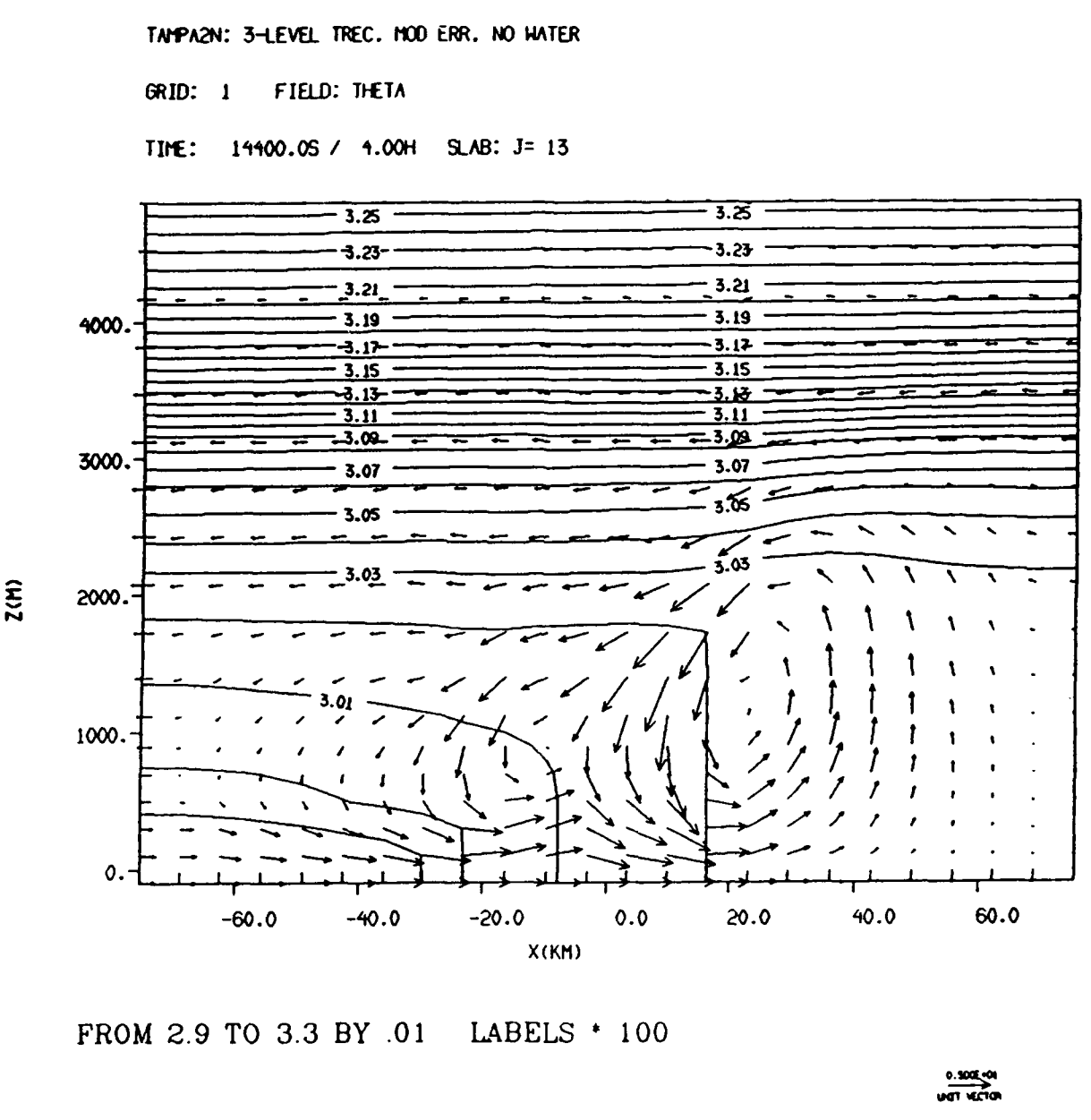

Figure 12 Continued

(a)

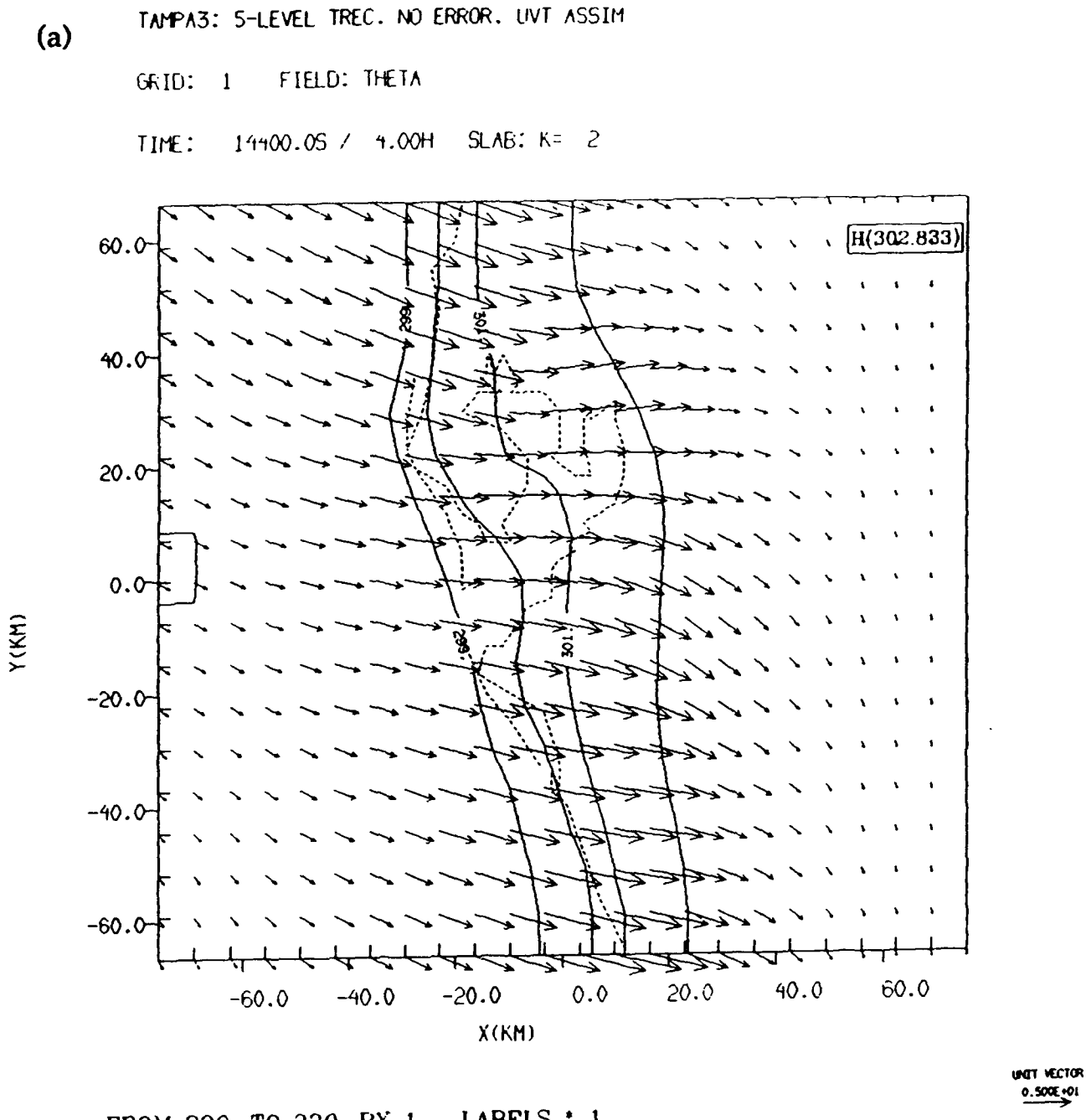

Figure 13: Experiment 3 output: 5-level TREC data assimilation experiment with no error. (a) horizontal cross-section of 4-hour forecast, valid at 1400 LST, and (b) corresponding vertical cross-section.

(b)

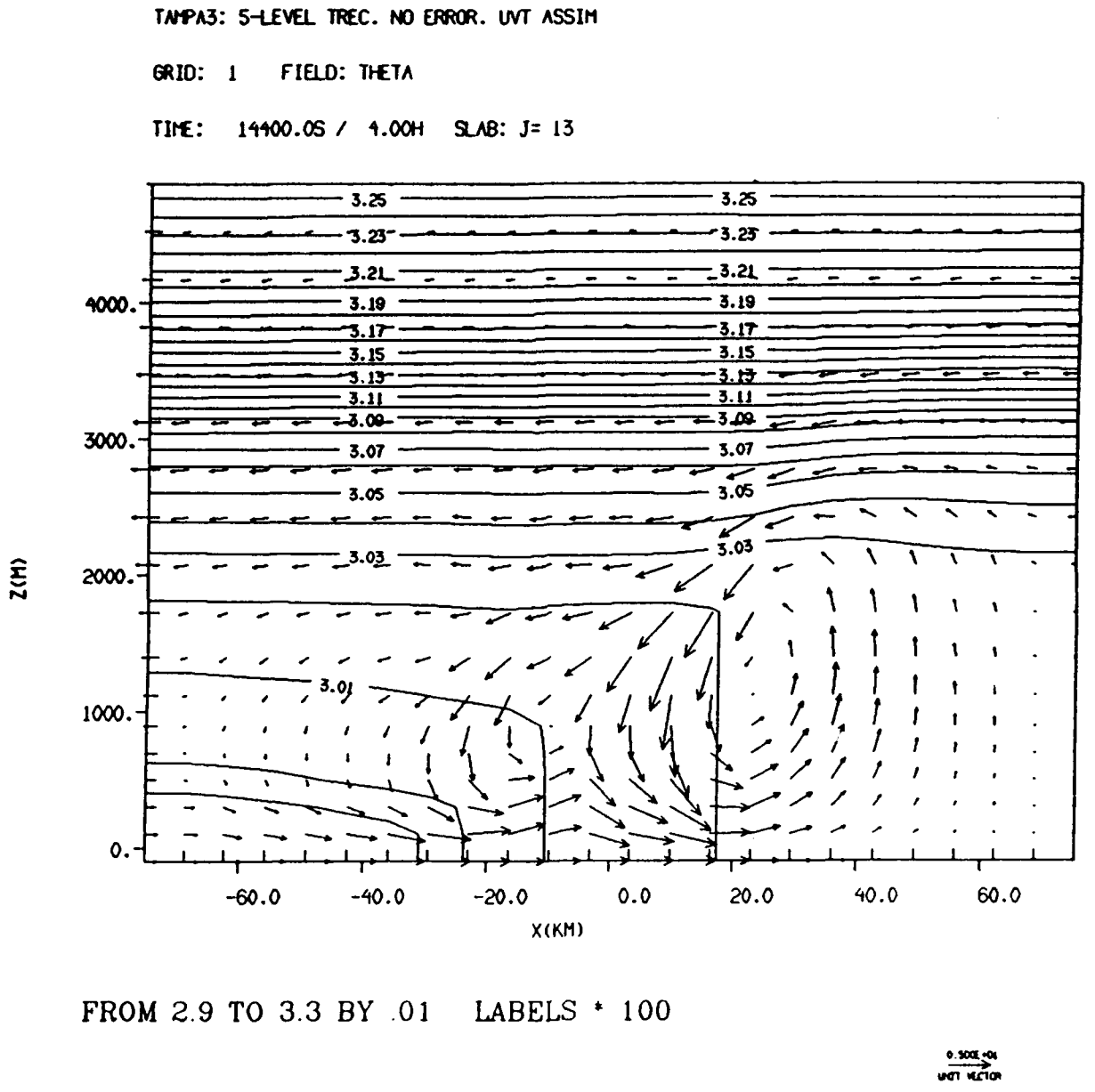

Figure 13 Continued

(a)

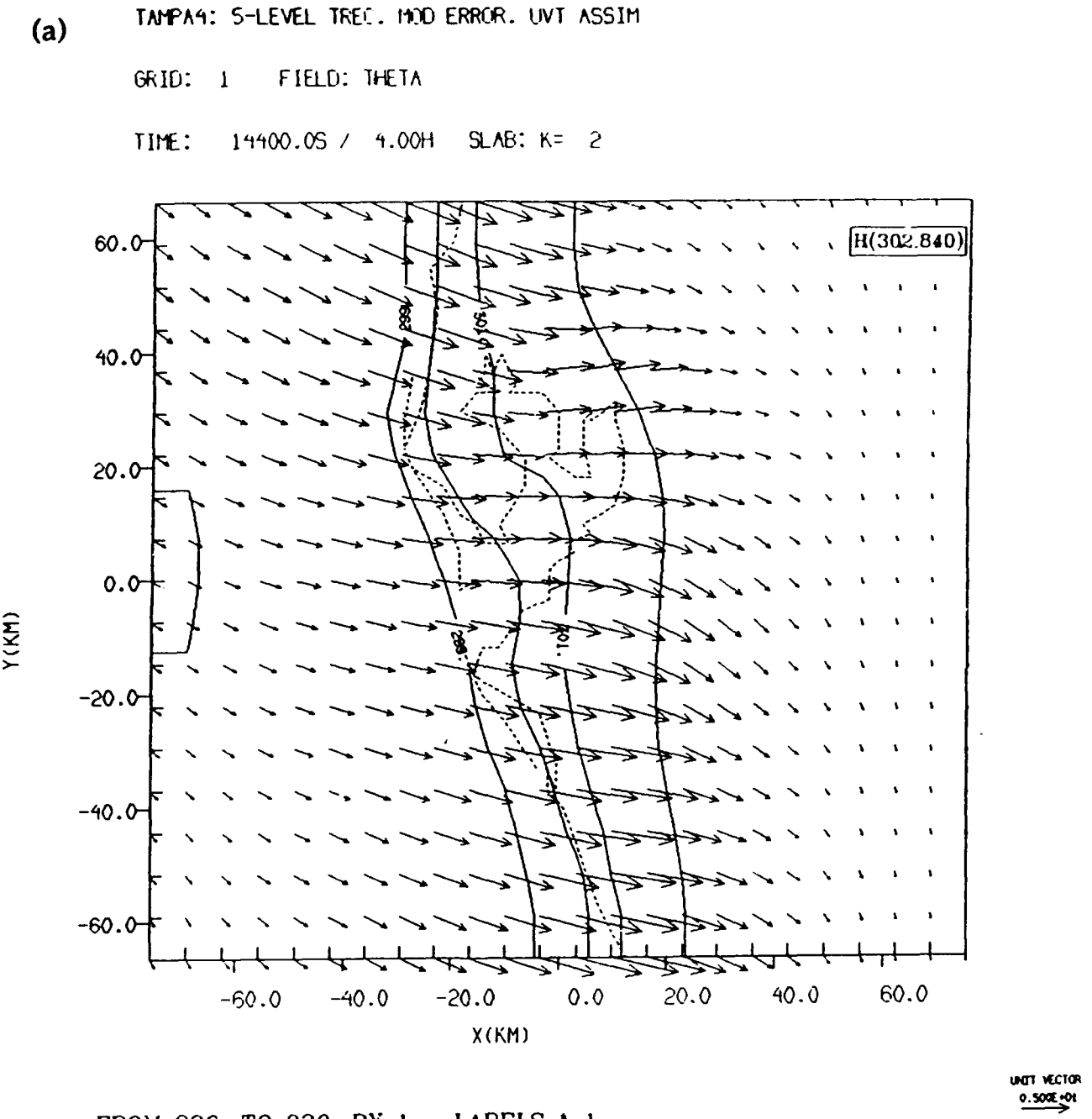

Figure 14: Experiment 4 output: 5-level TREC data assimilation experiment with moderate errors. (a) horizontal cross-section of 4-hour forecast, valid at 1400 LST, and (b) corresponding vertical cross-section.

(b)

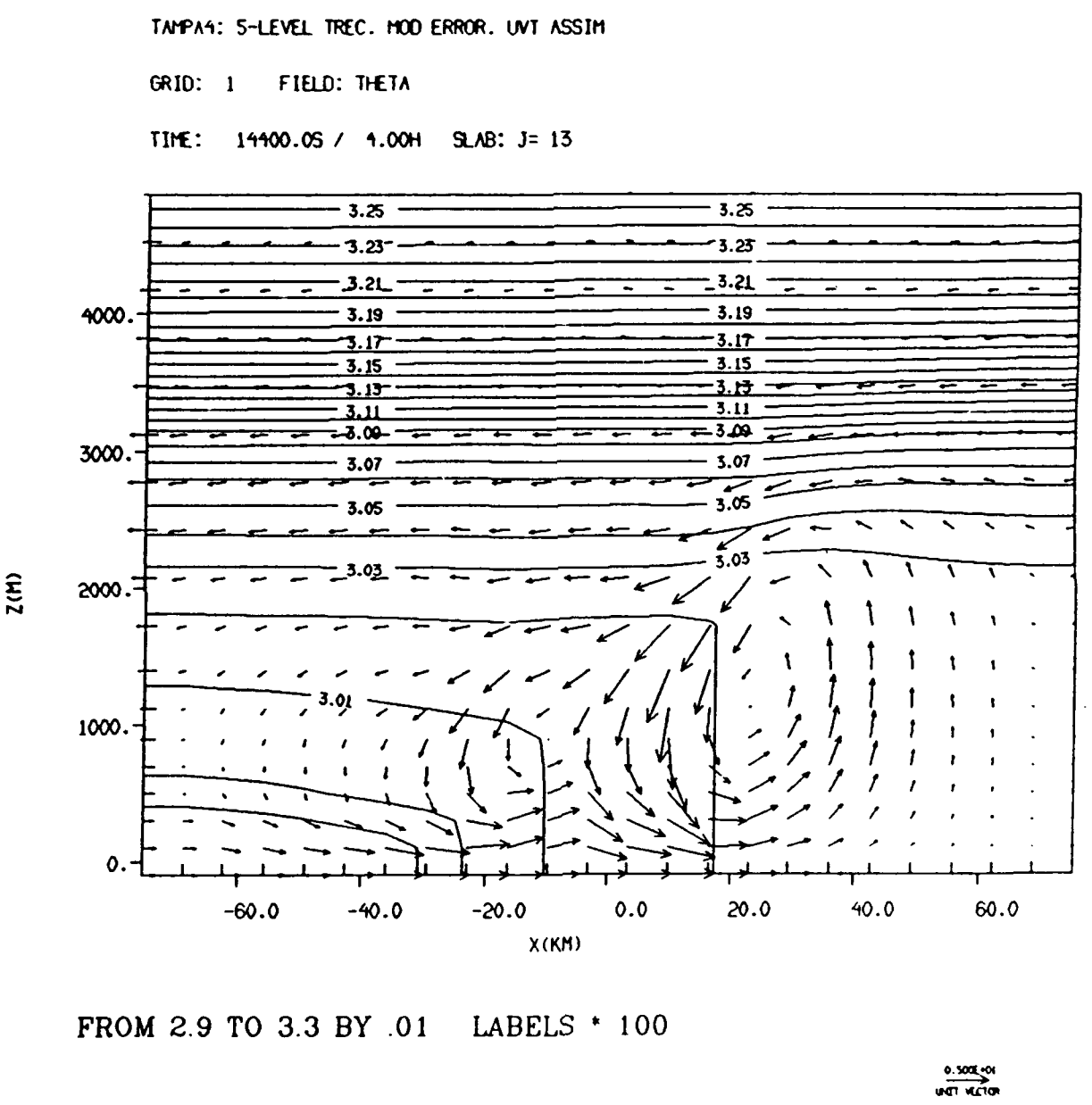

Figure 14 Continued

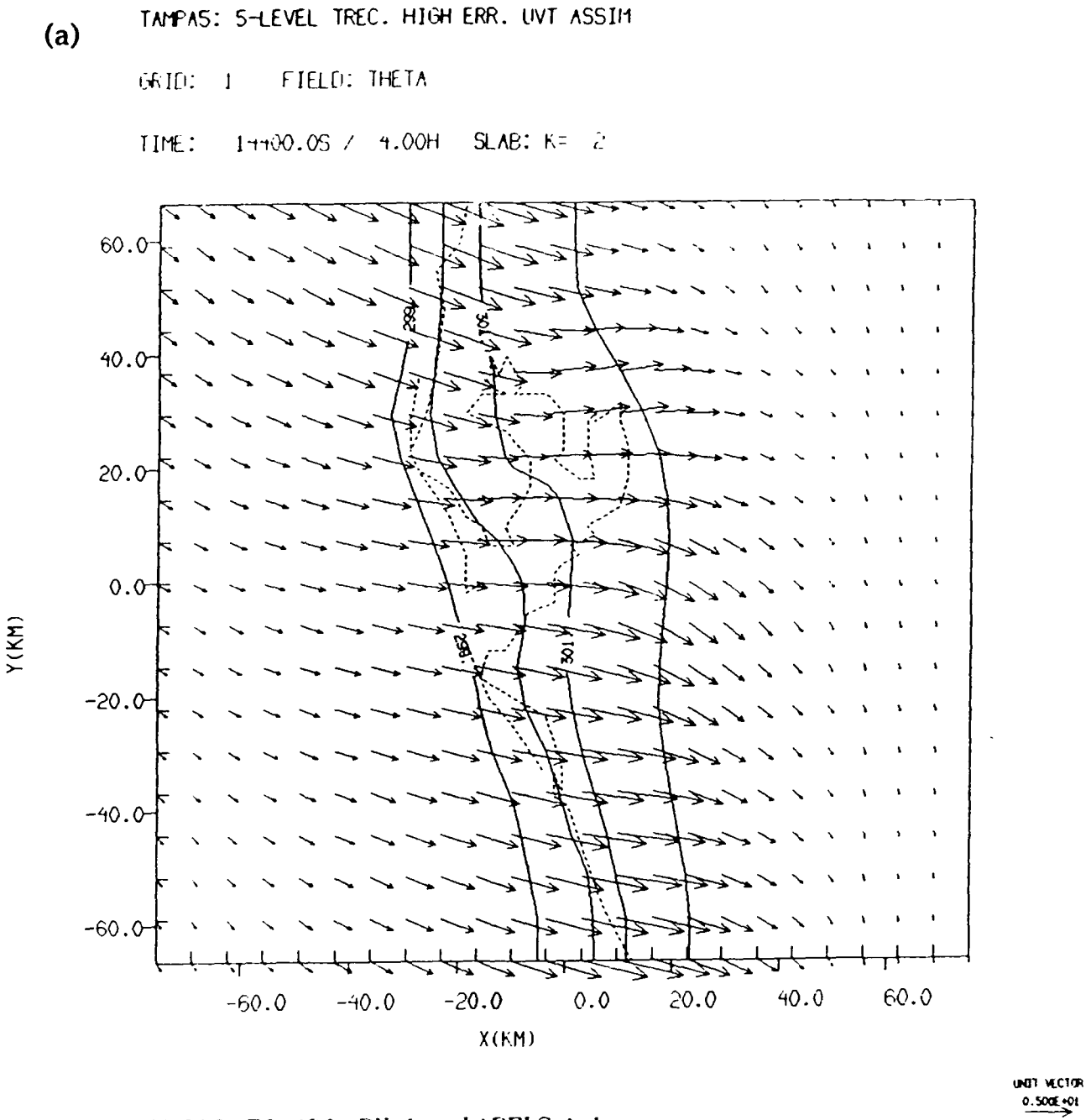

Figure 15: Experiment 5 output: 5-level TREC data assimilation experiment with high errors. (a) horizontal cross-section of 4-hour forecast, valid at 1400 LST, and (b) corresponding vertical cross-section.

(b)

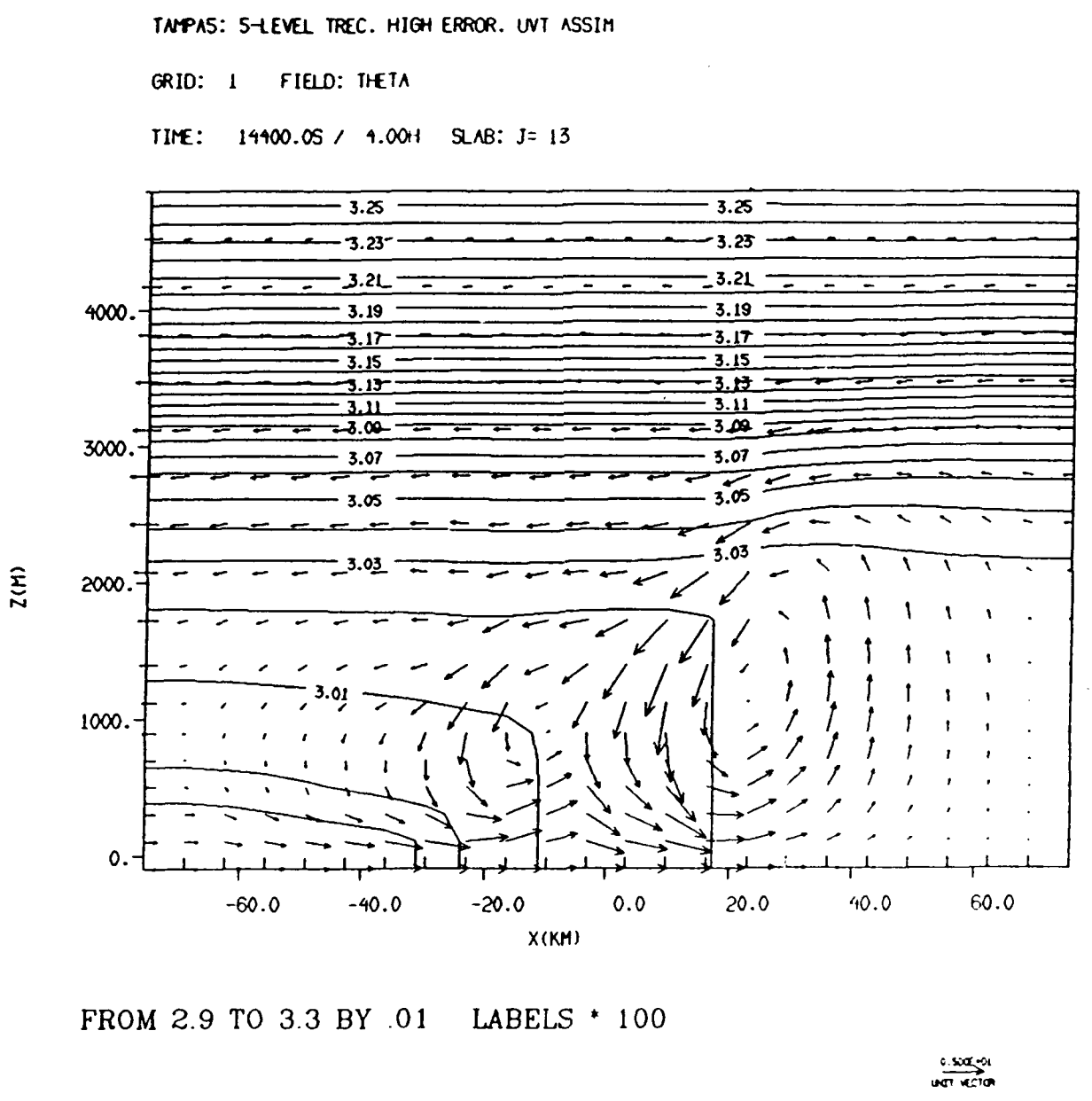

Figure 15 Continued

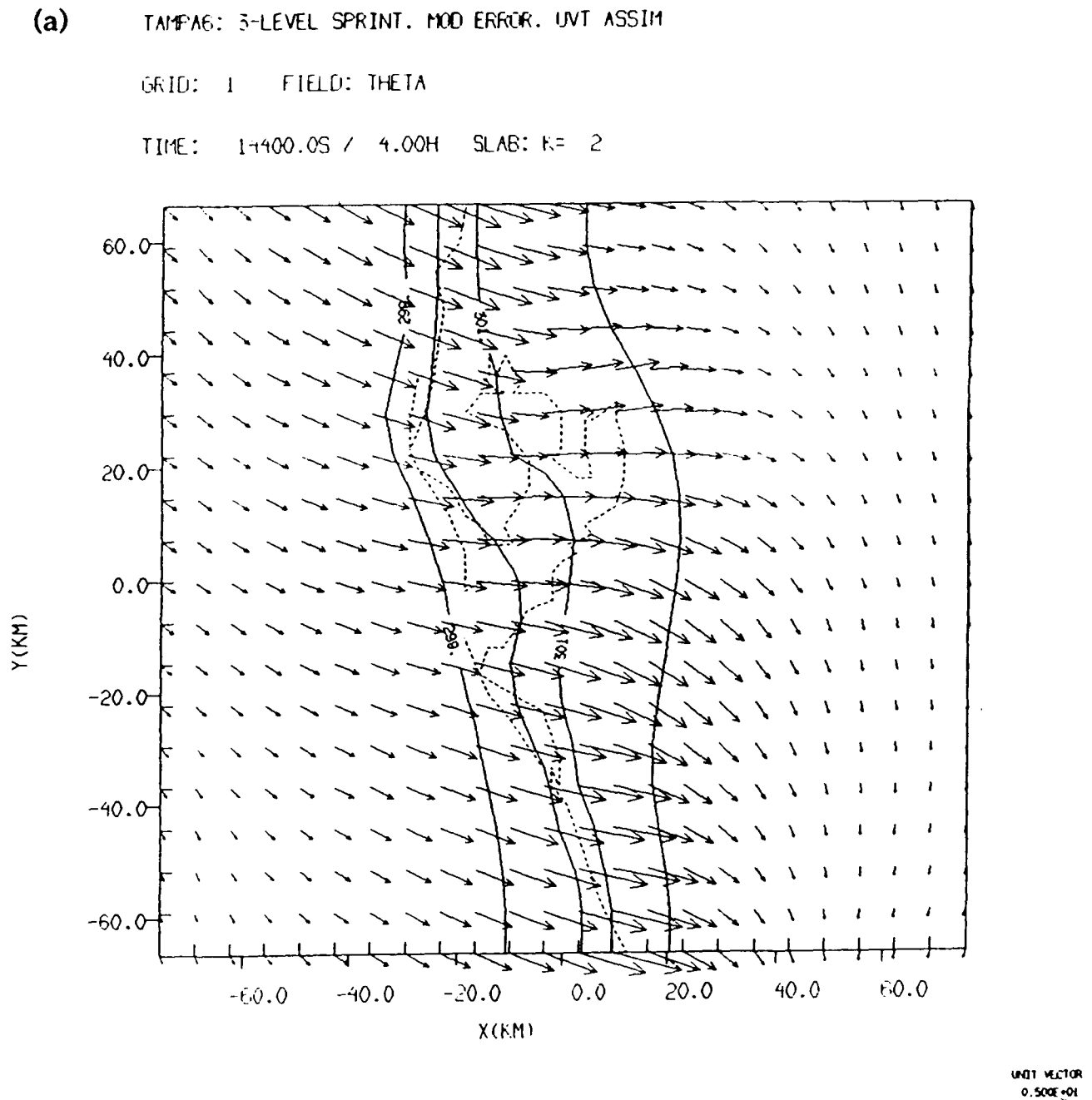

Figure 16: Experiment 6 output: 3-level SPRINT data assimilation experiment with moderate errors. (a) horizontal cross-section of 4-hour forecast, valid at 1400 LST, and (b) corresponding vertical cross-section.

(b)

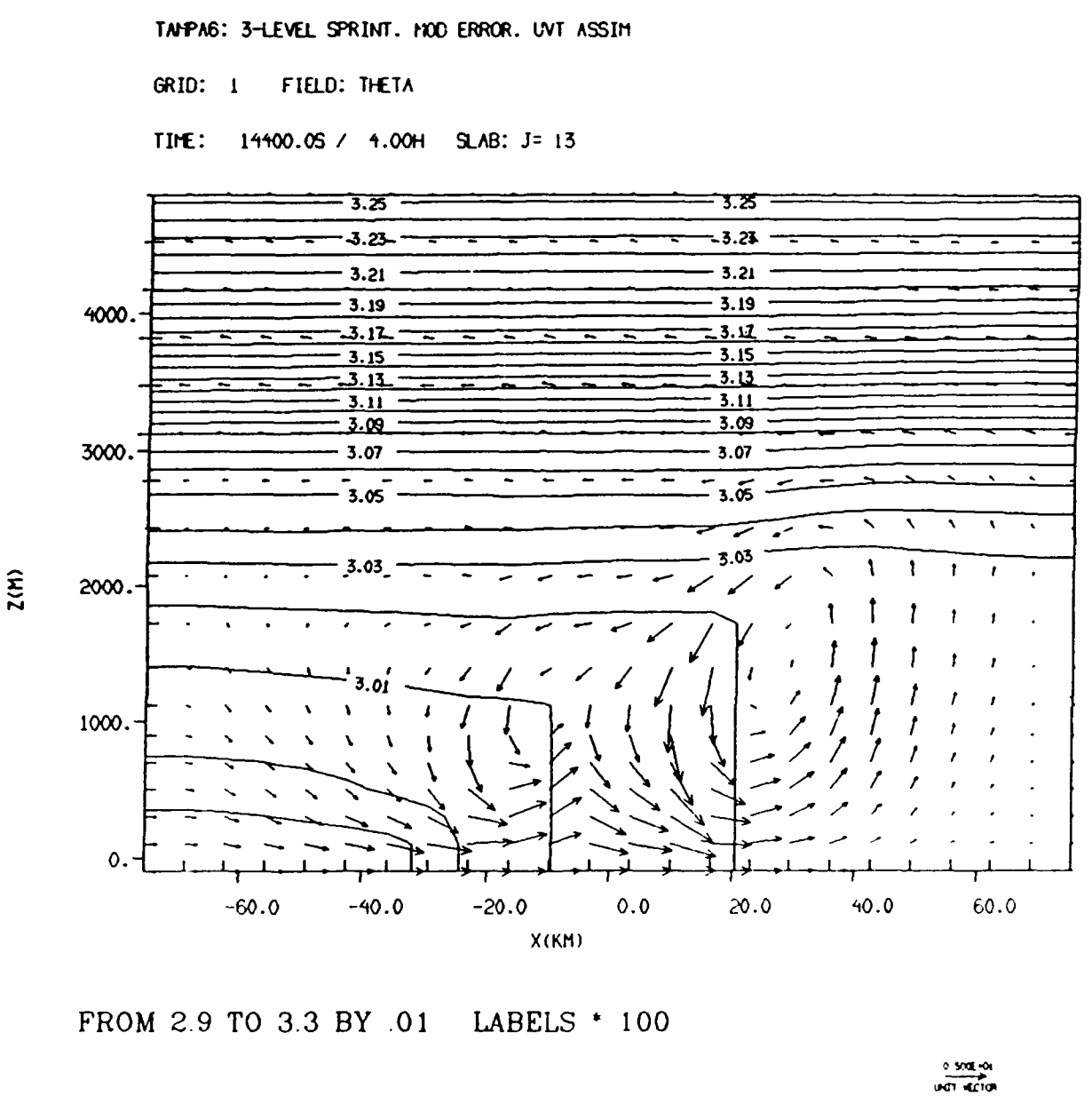

Figure 16 Continued

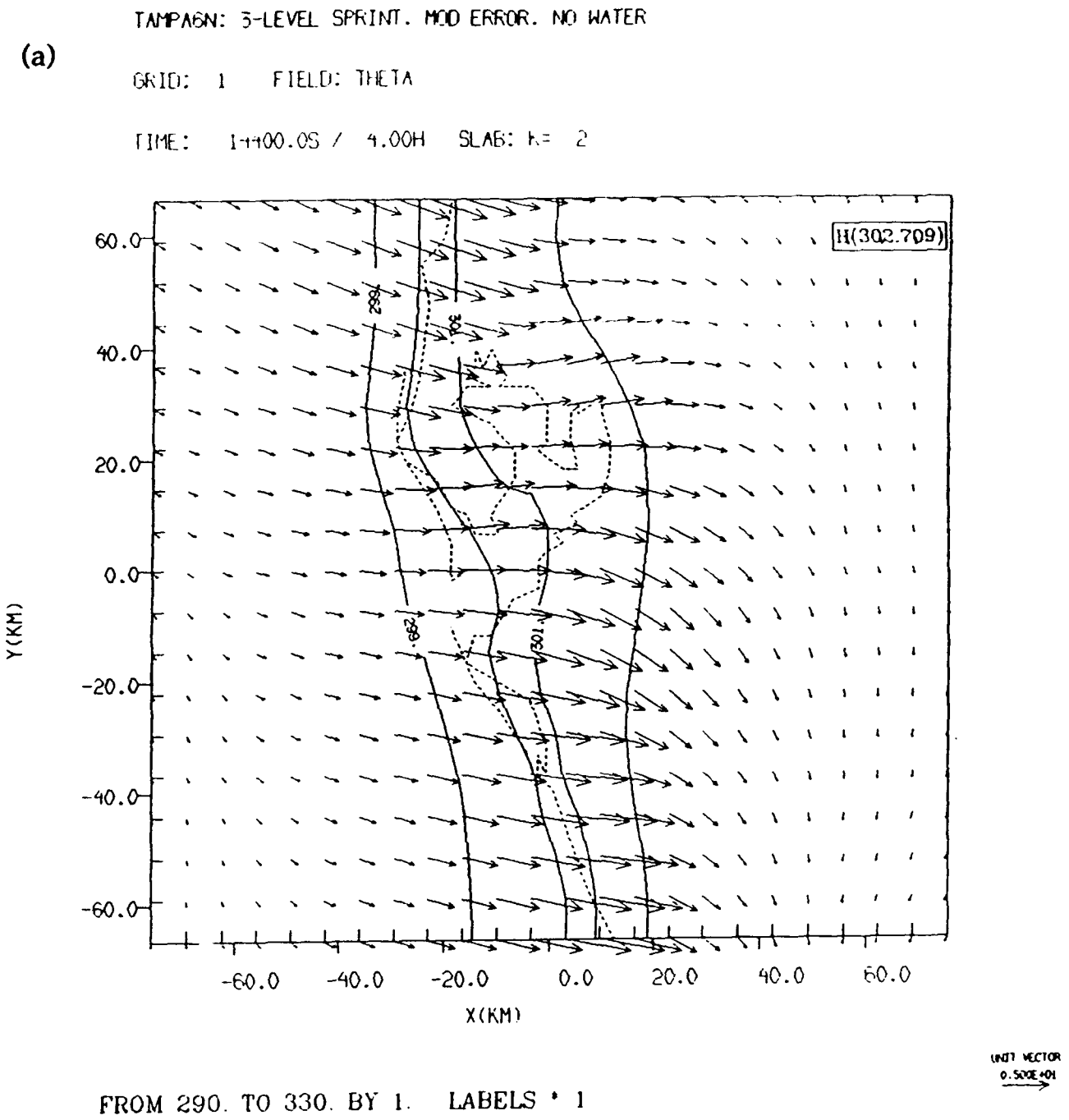

Figure 17: Experiment 6N output: 3-level SPRINT data assimilation experiment with moderate errors and no observations over water used. (a) horizontal cross-section of 4-hour forecast, valid at 1400 LST, and (b) corresponding vertical cross-section.

(b)

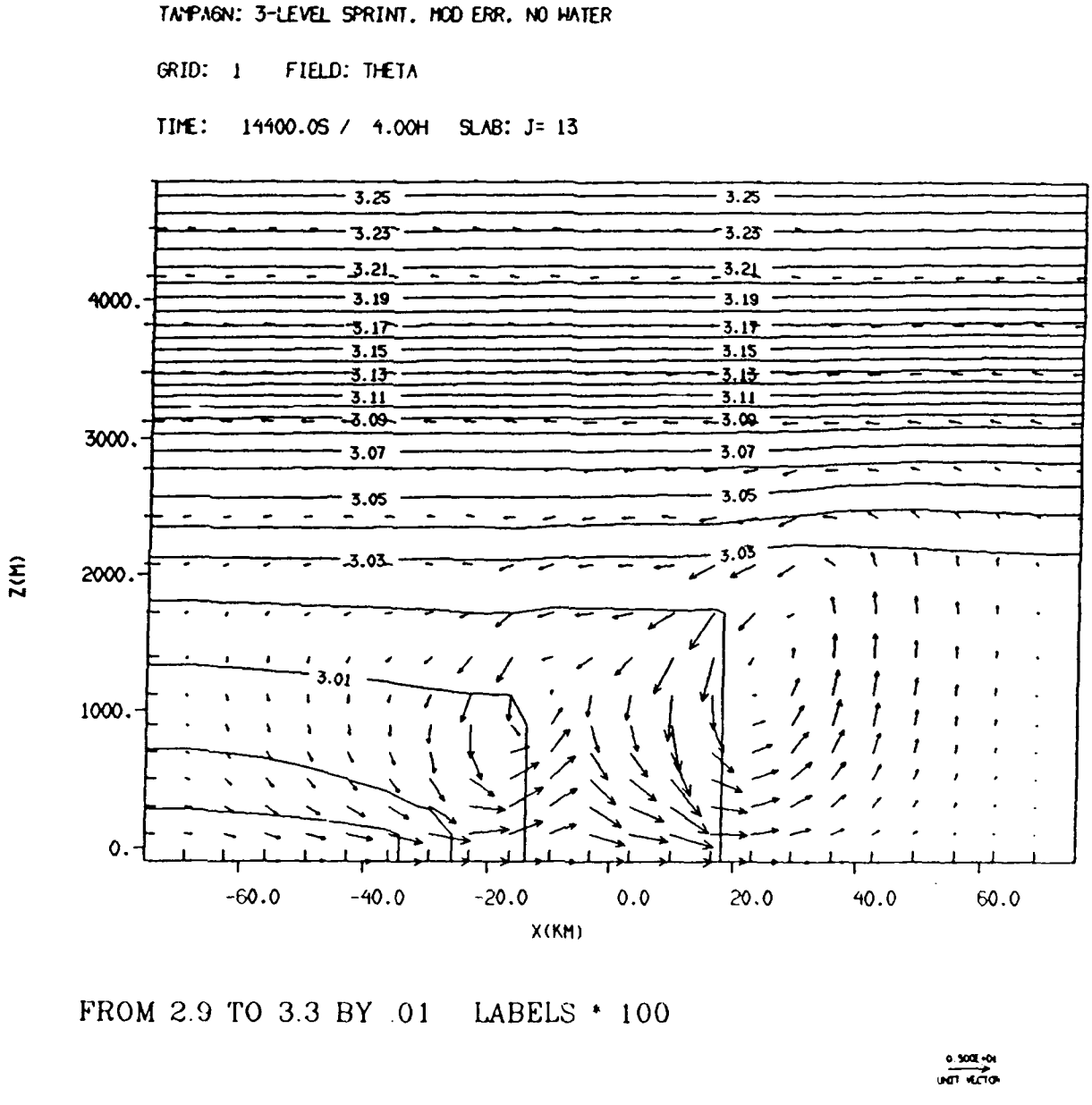

Figure 17 Continued

(a)

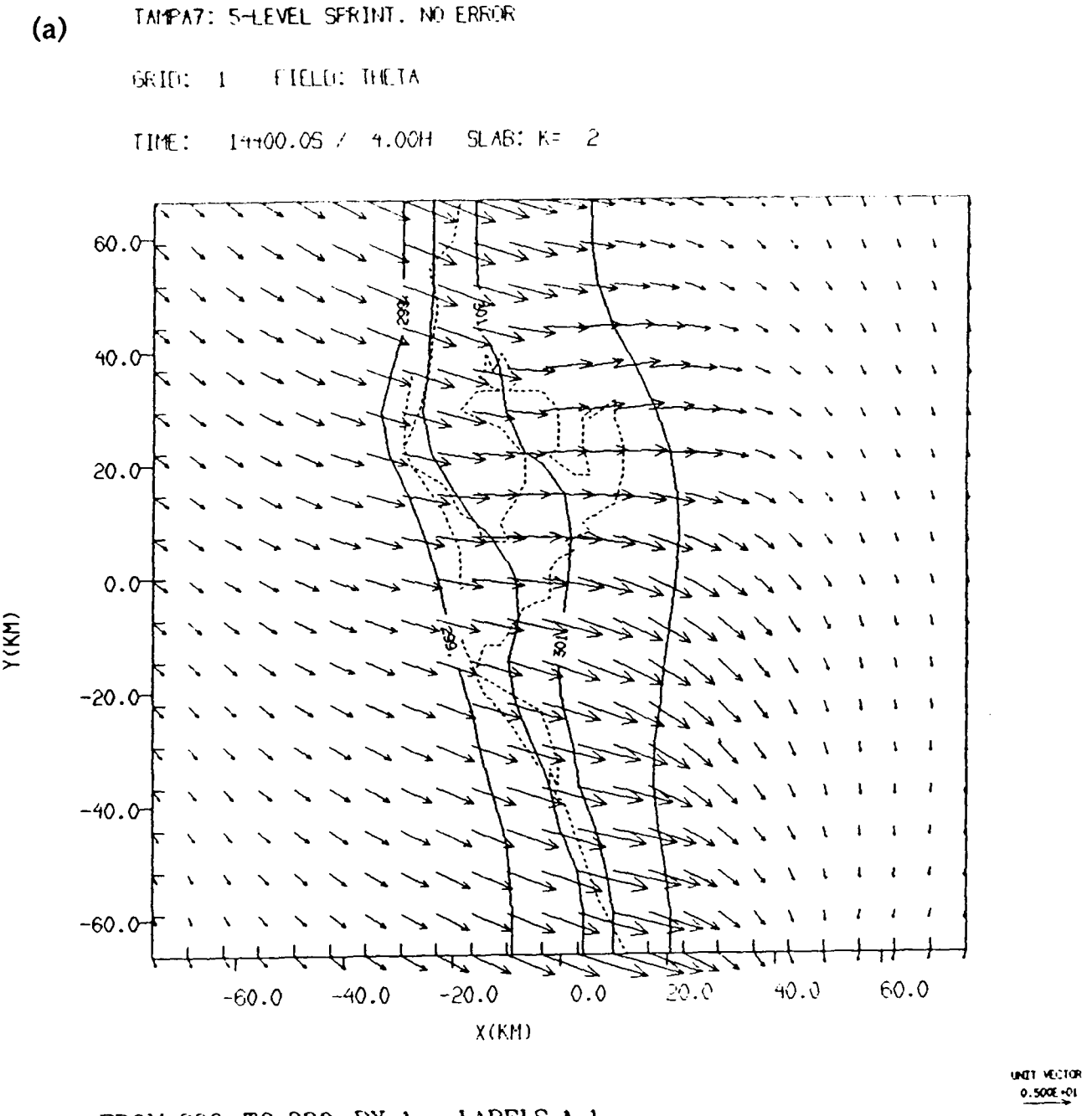

Figure 18: Experiment 7 output: 5-level SPRINT data assimilation experiment with no errors. (a) horizontal cross-section of 4-hour forecast, valid at 1400 LST, and (b) corresponding vertical cross-section.

(b)

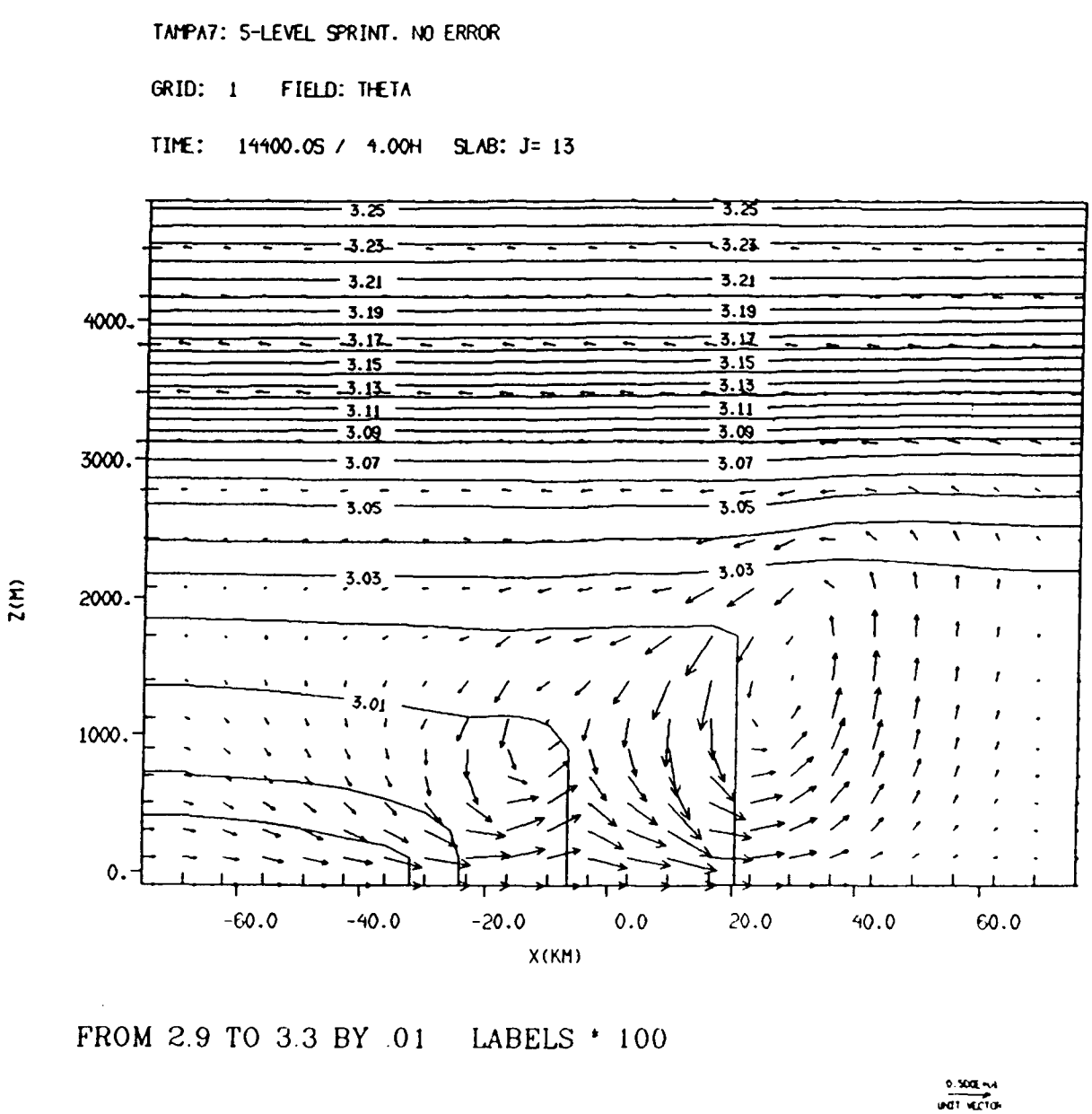

Figure 18 Continued

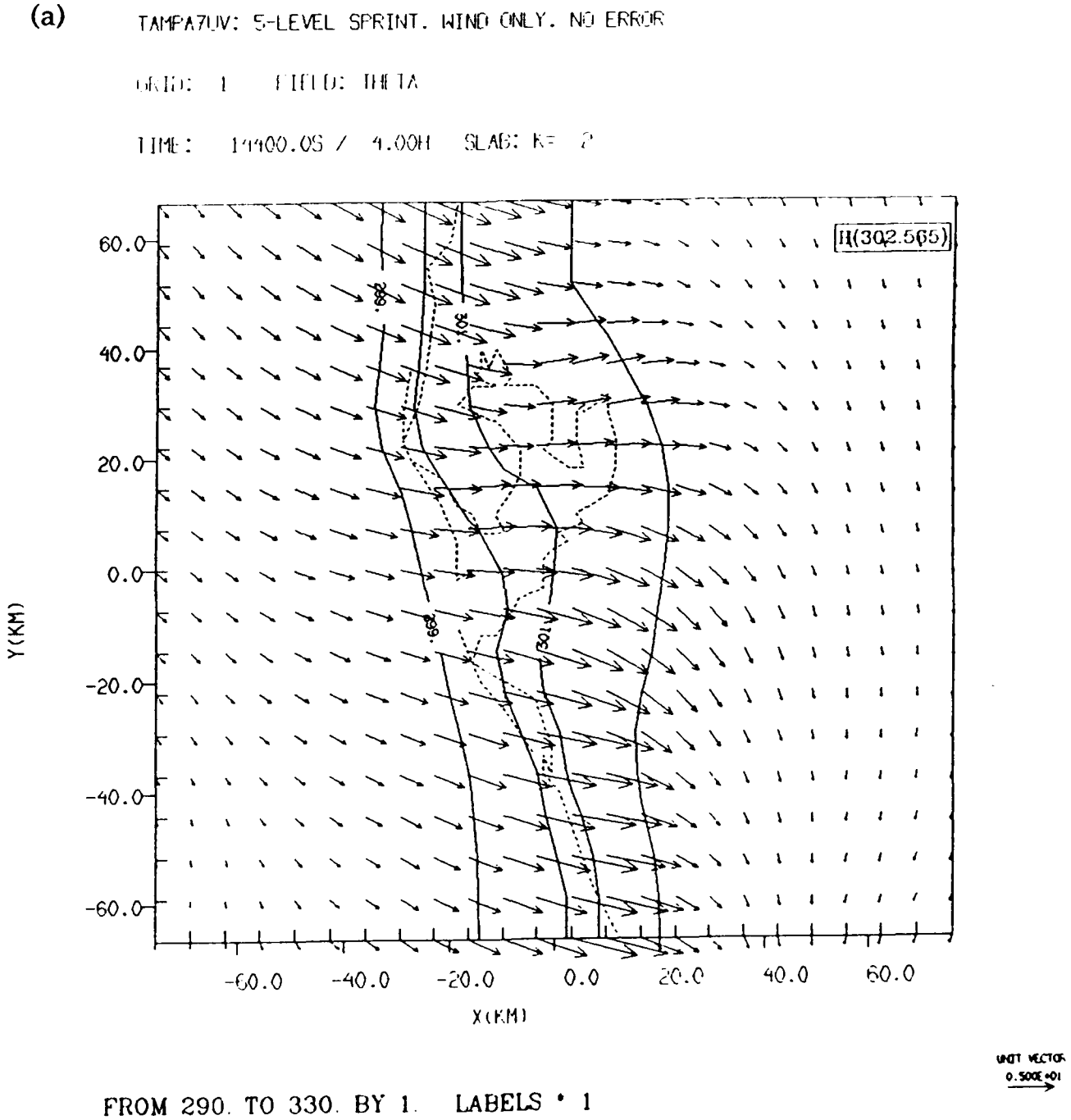

Figure 19: Experiment 7UV output: 5-level SPRINT data assimilation experiment with no errors and no temperature assimilation. (a) horizontal cross-section of 4-hour forecast, valid at 1400 LST, and (b) corresponding vertical cross-section.

(b)

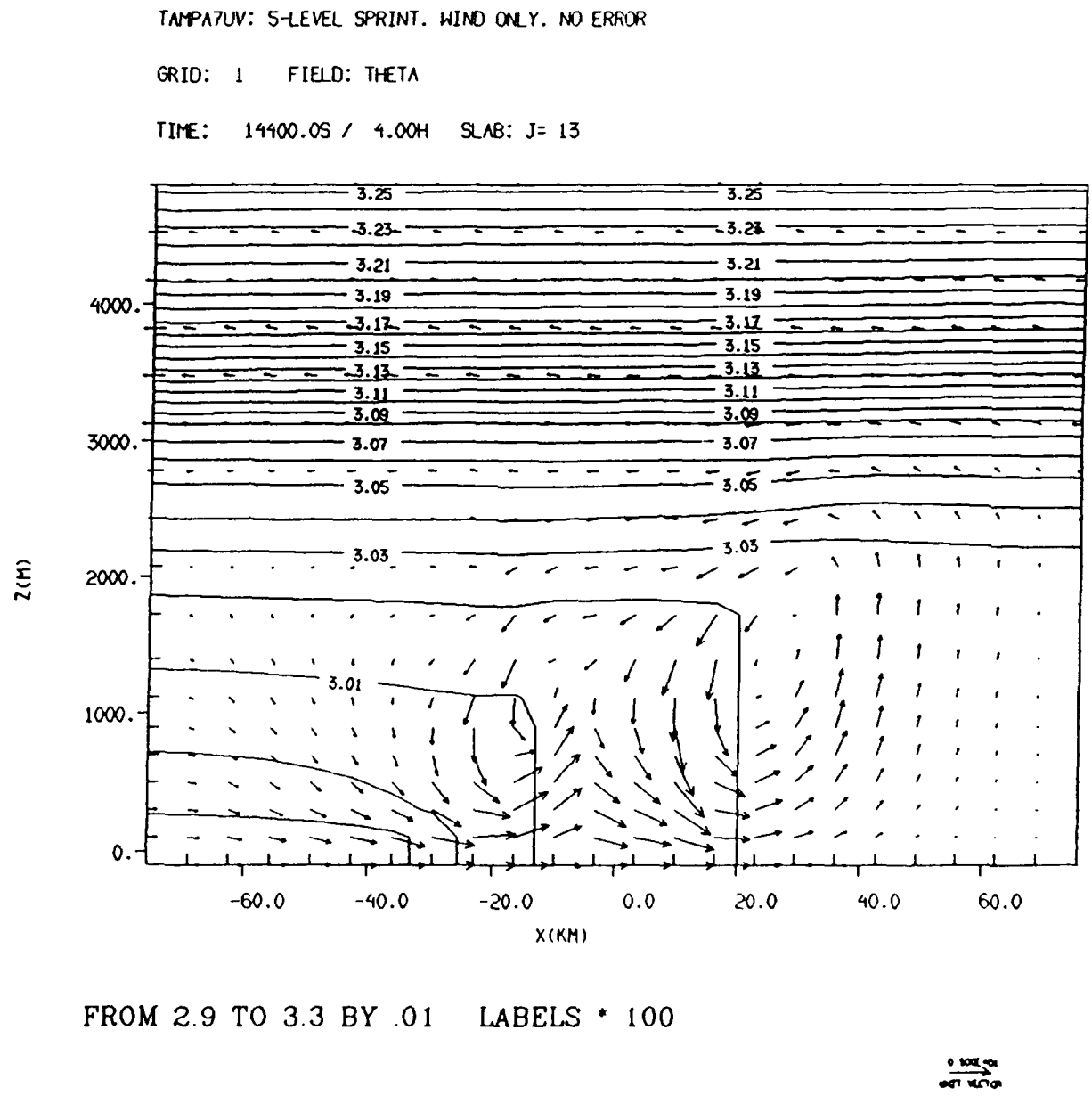

Figure 19 Continued

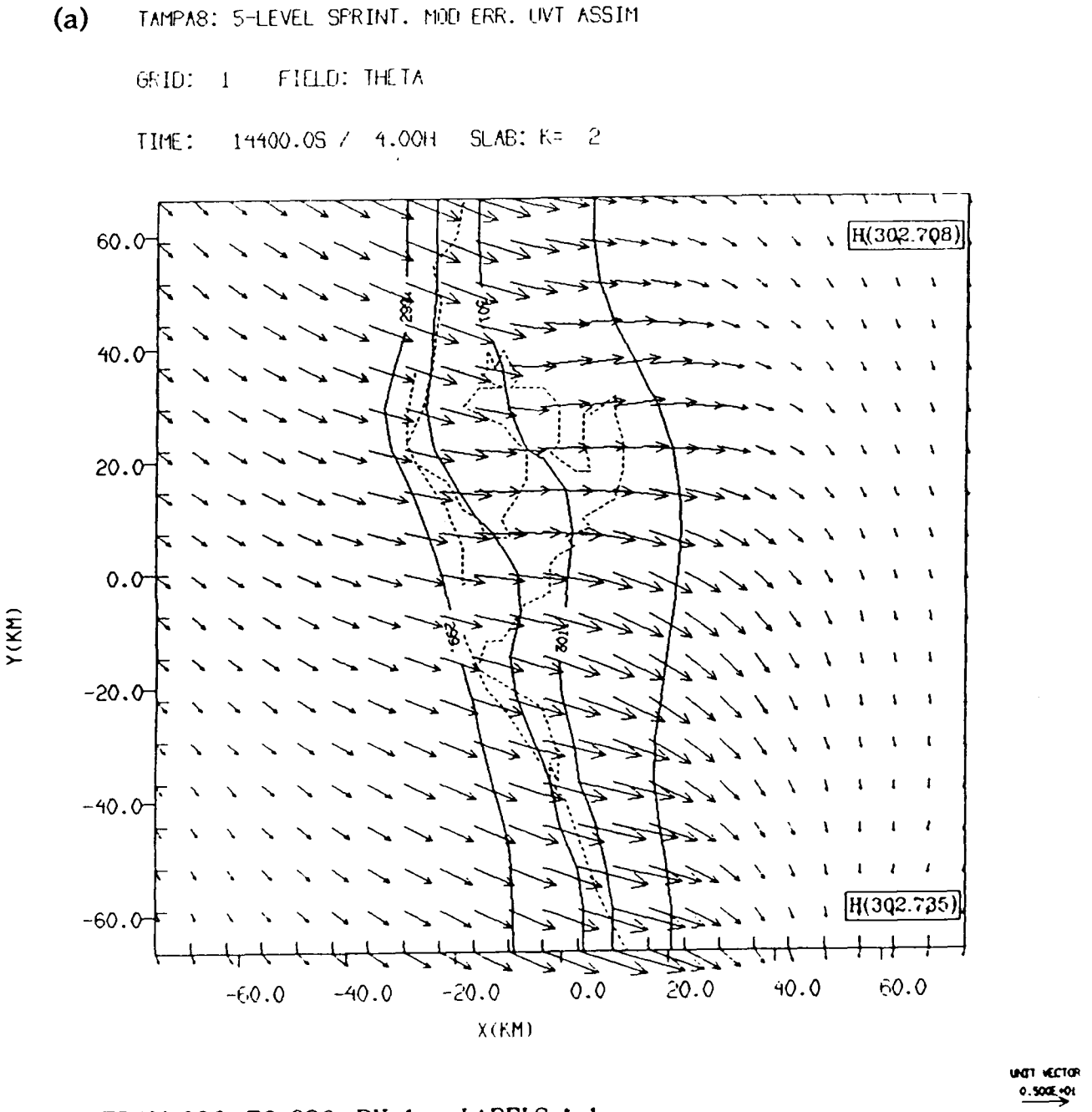

Figure 20: Experiment 8 output: 5-level SPRINT data assimilation experiment with moderate errors. (a) horizontal cross-section of 4-hour forecast, valid at 1400 LST, and (b) corresponding vertical cross-section.

(b)

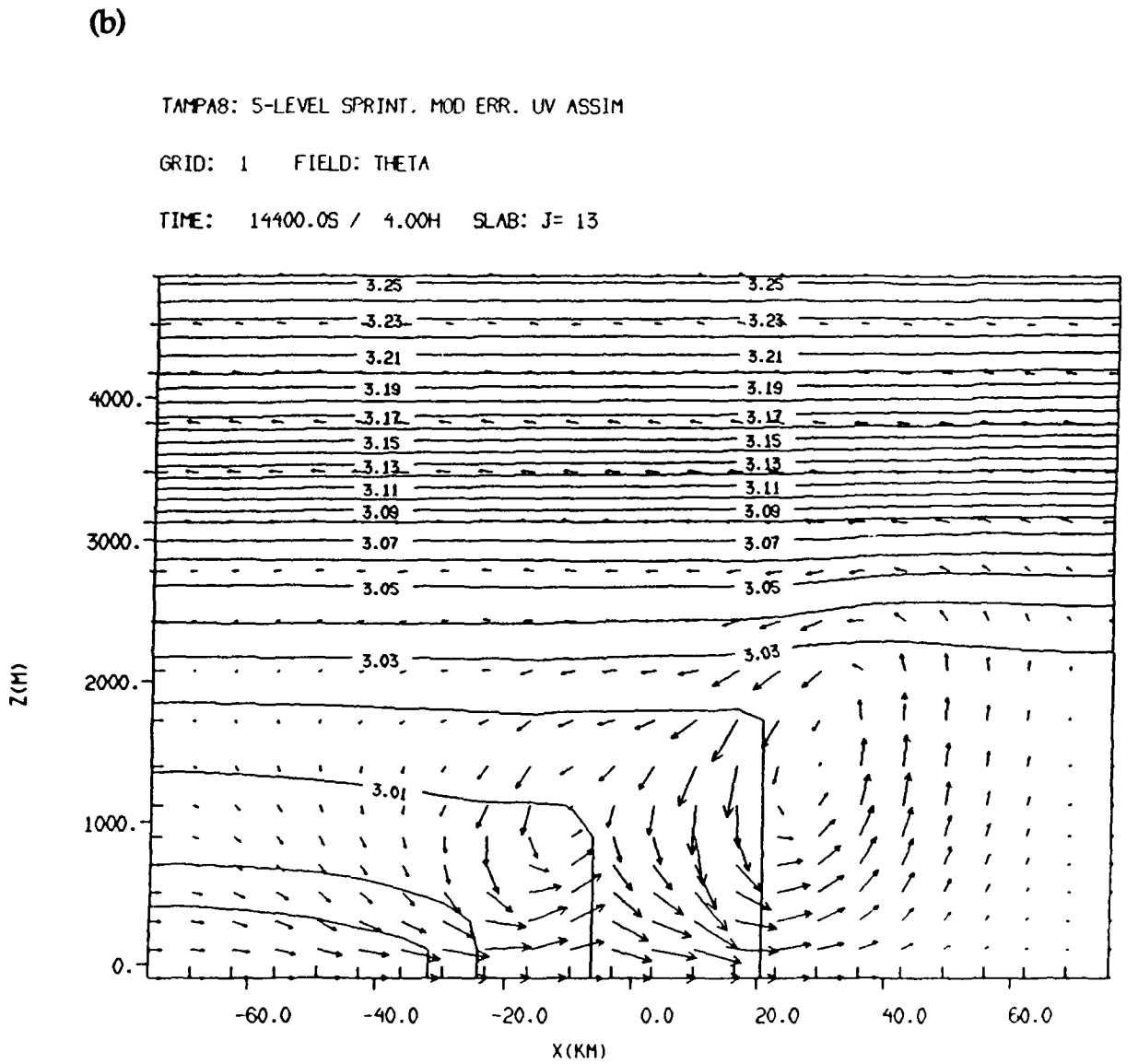

Figure 20 Continued

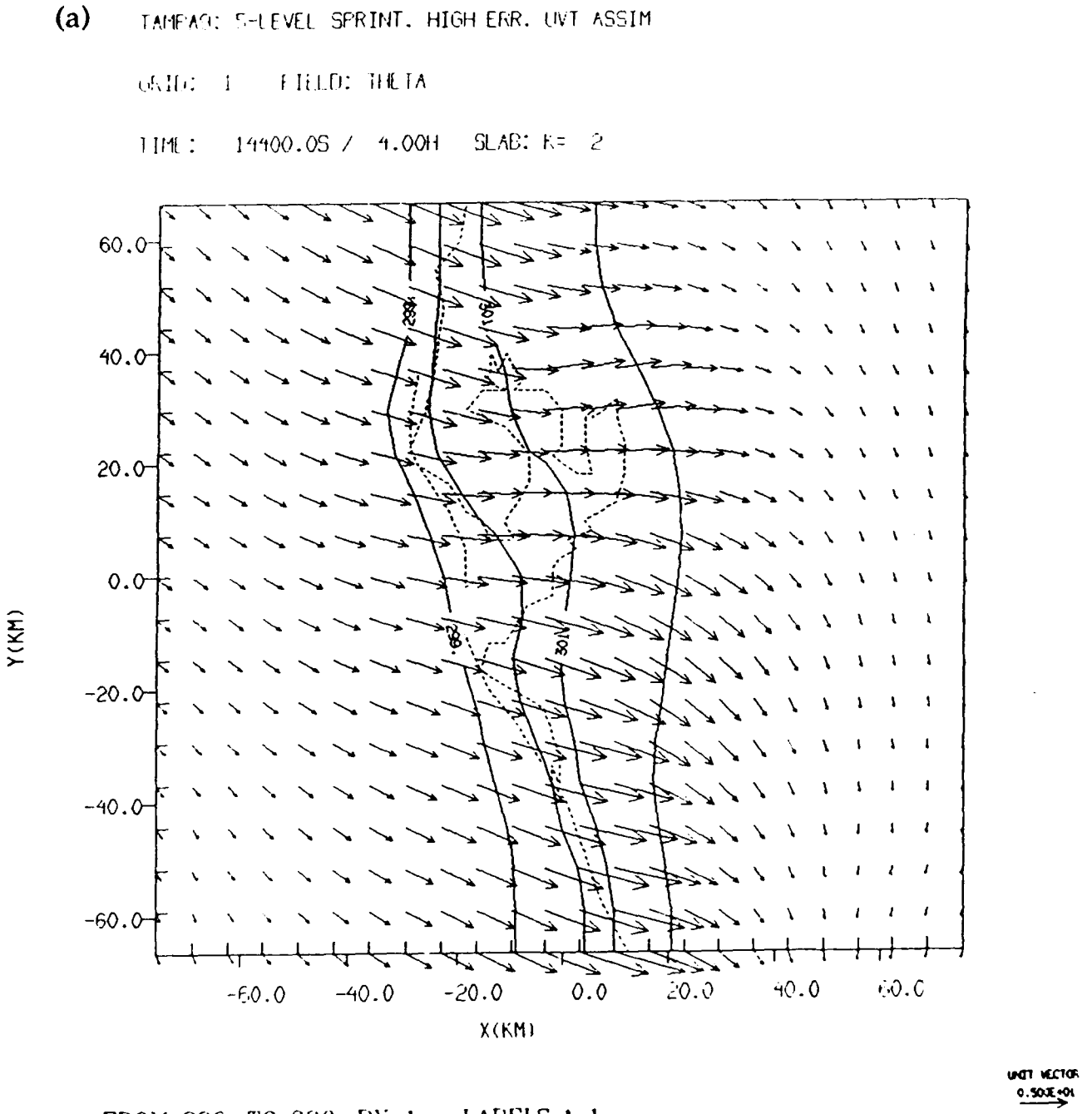

Figure 21: Experiment 9 output: 5-level SPRINT data assimilation experiment with high errors. (a) horizontal cross-section of 4-hour forecast, valid at 1400 LST, and (b) corresponding vertical cross-section.

(b)

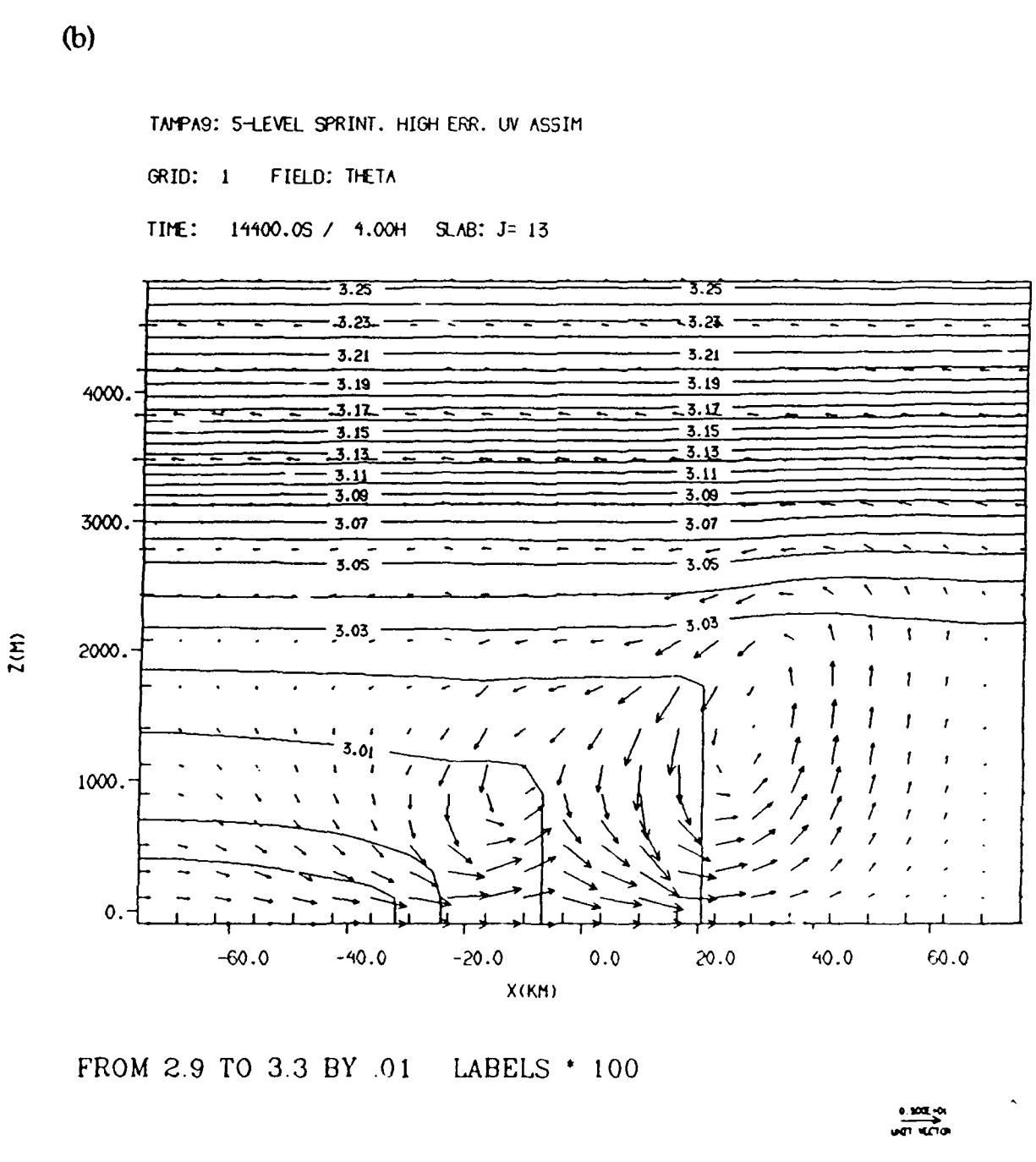

Figure 21 Continued

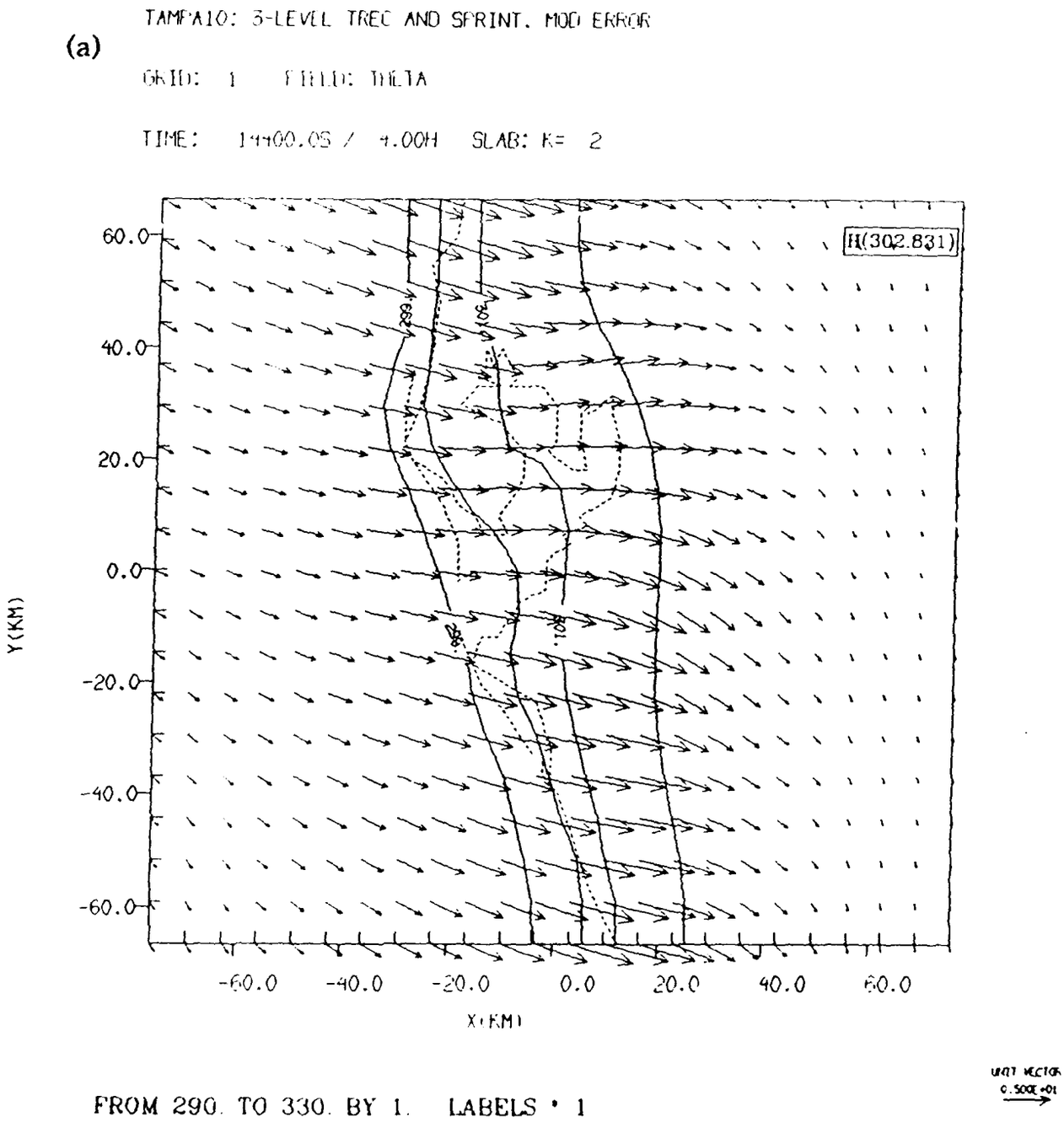

Figure 22: Experiment 10 output: 3-level SPRINT and TREC data assimilation experiment with moderate errors. (a) horizontal cross-section of 4-hour forecast, valid at 1400 LST, and (b) corresponding vertical cross-section.

(b)

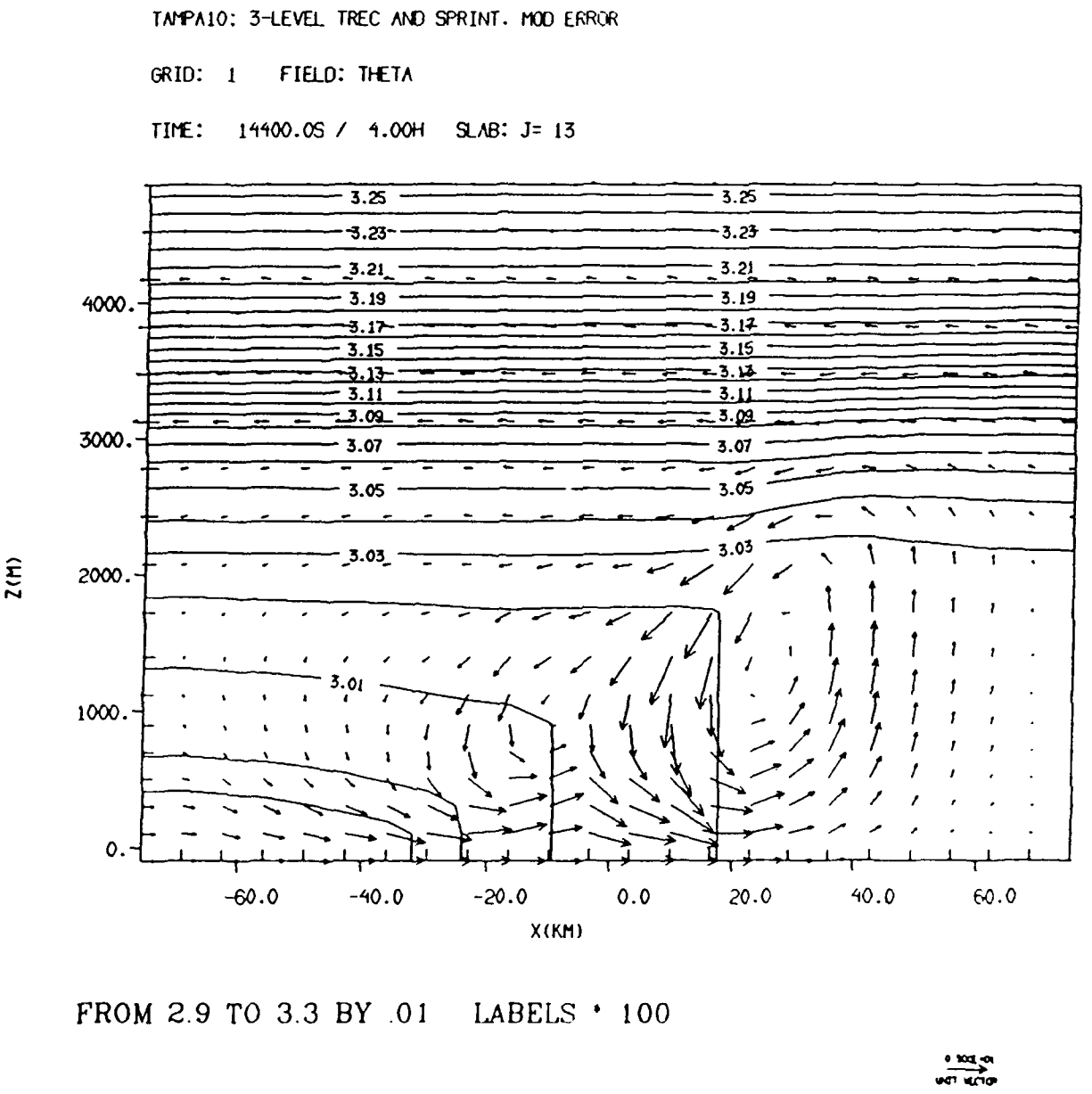

Figure 22 Continued

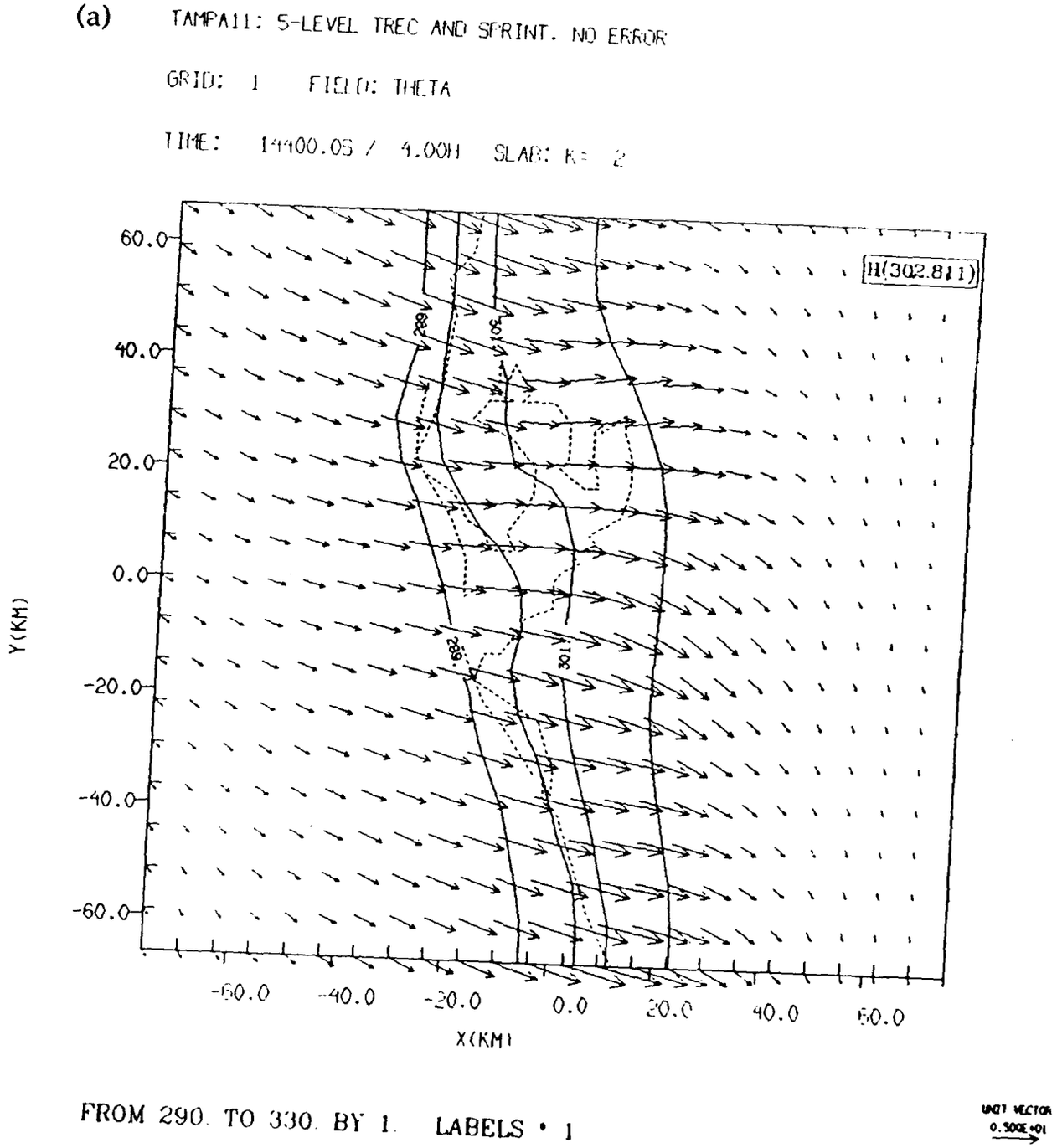

Figure 23: Experiment 11 output: 5-level SPRINT and TREC data assimilation experiment with no errors. (a) horizontal cross-section of 4-hour forecast, valid at 1400 LST, and (b) corresponding vertical cross-section.

(b)

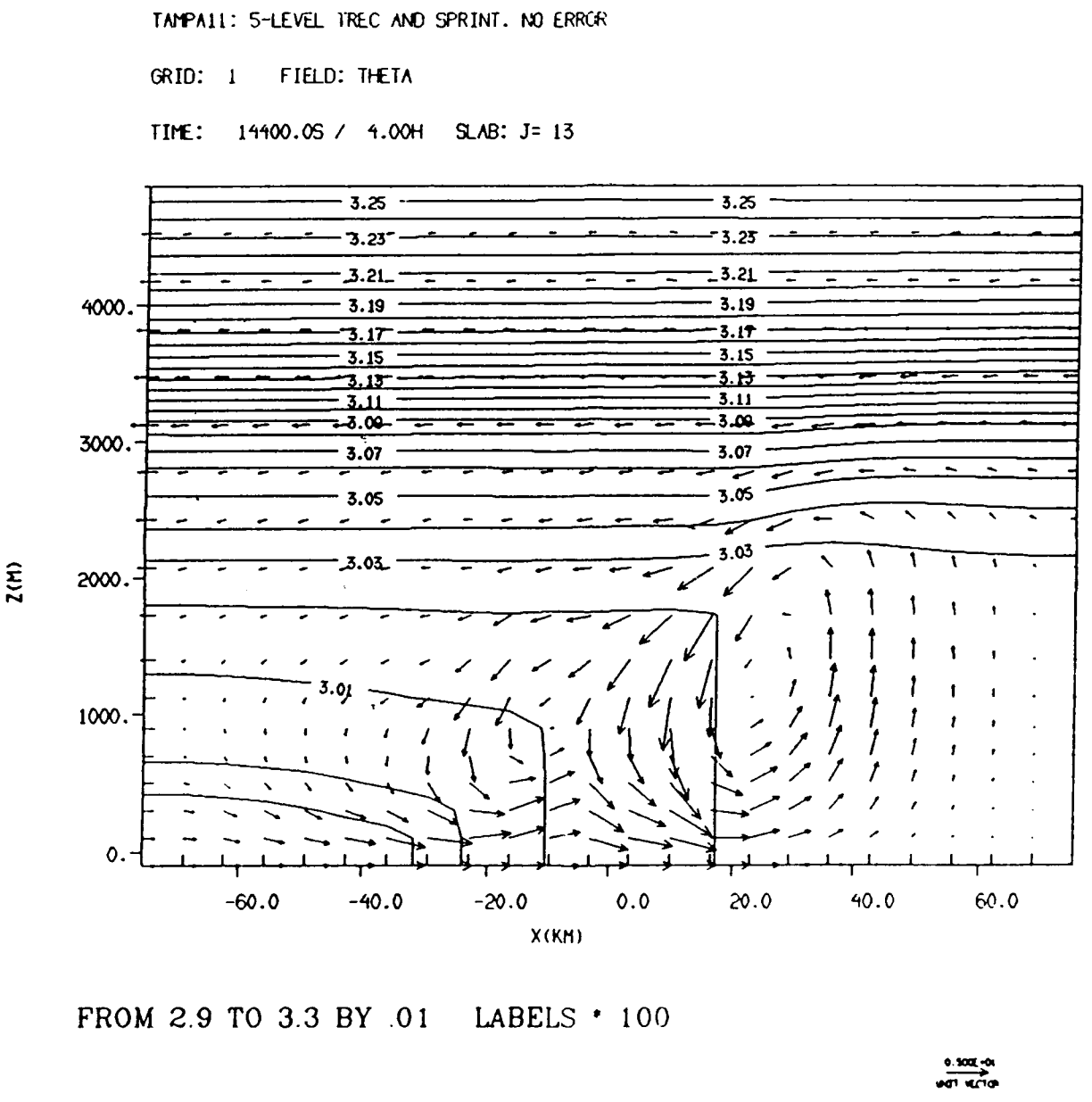

Figure 23 Continued

(a)

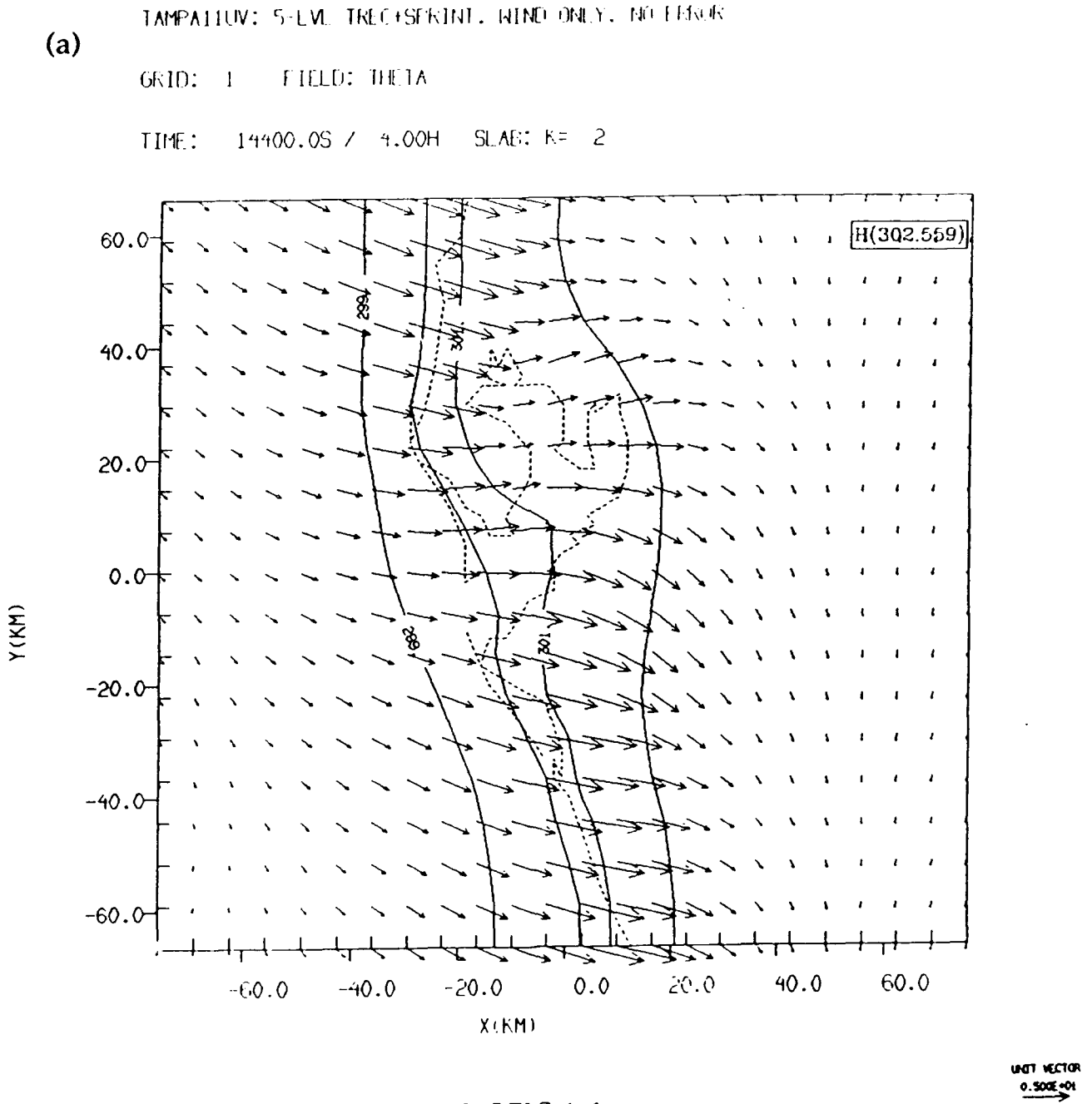

Figure 24: Experiment 11UV output: 5-level SPRINT and TREC data assimilation experiment with no errors and no temperature assimilation. (a) horizontal cross-section of 4-hour forecast, valid at 1400 LST, and (b) corresponding vertical cross-section.

(b)

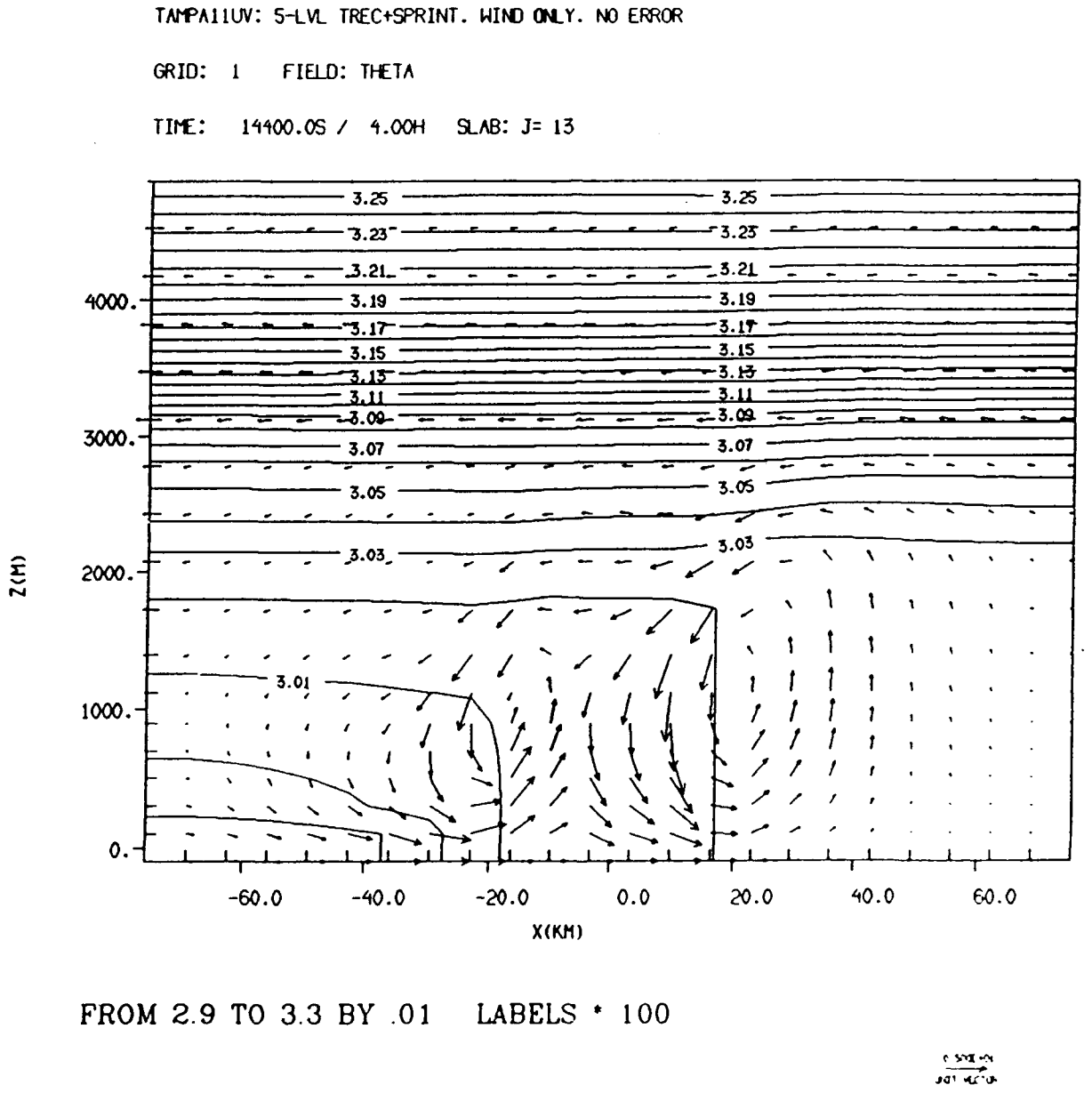

Figure 24 Continued

(a)

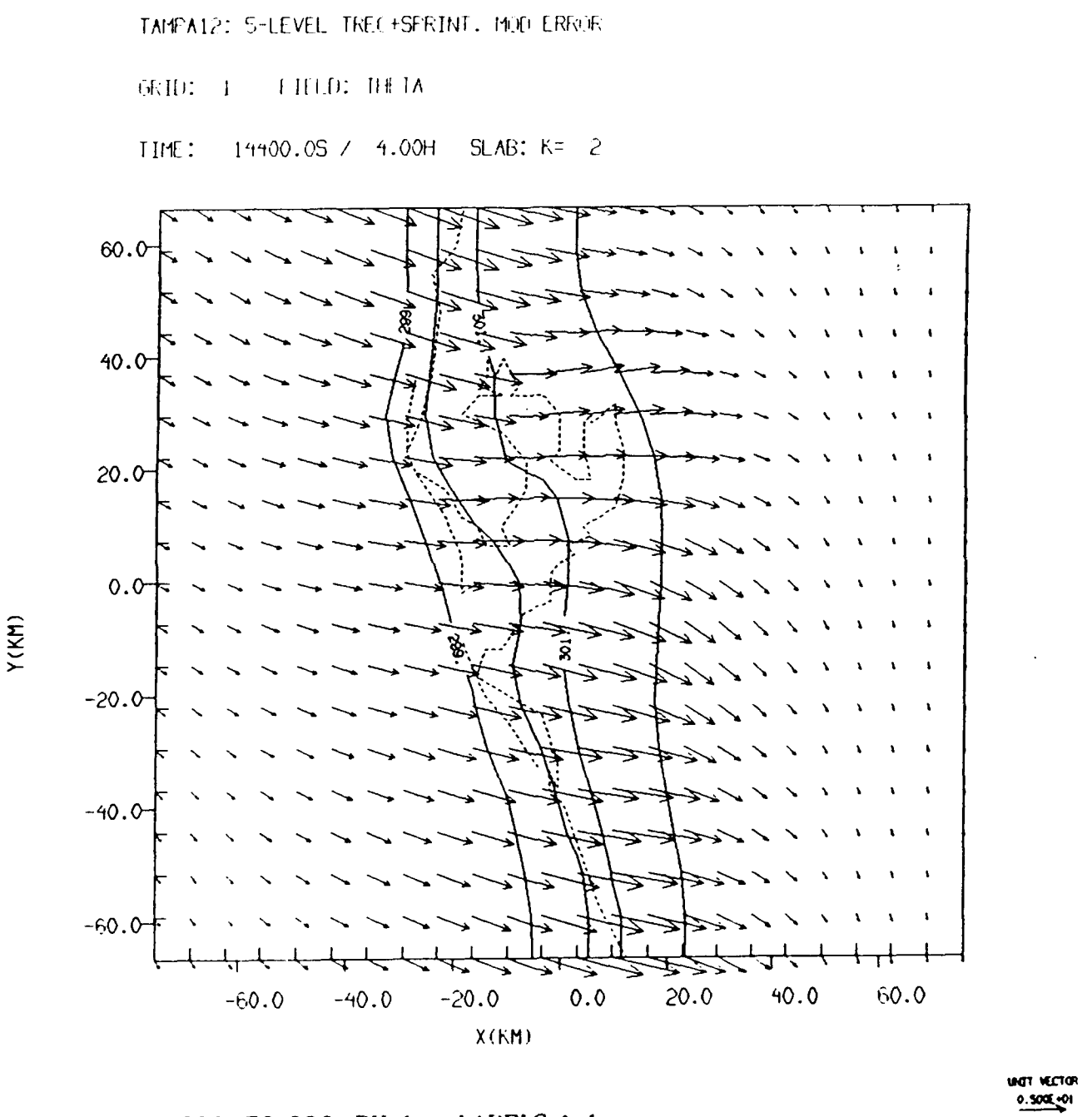

Figure 25: Experiment 12 output: 5-level SPRINT and TREC data assimilation experiment with no errors. (a) horizontal cross-section of 4-hour forecast, valid at 1400 LST, and (b) corresponding vertical cross-section.

(b)

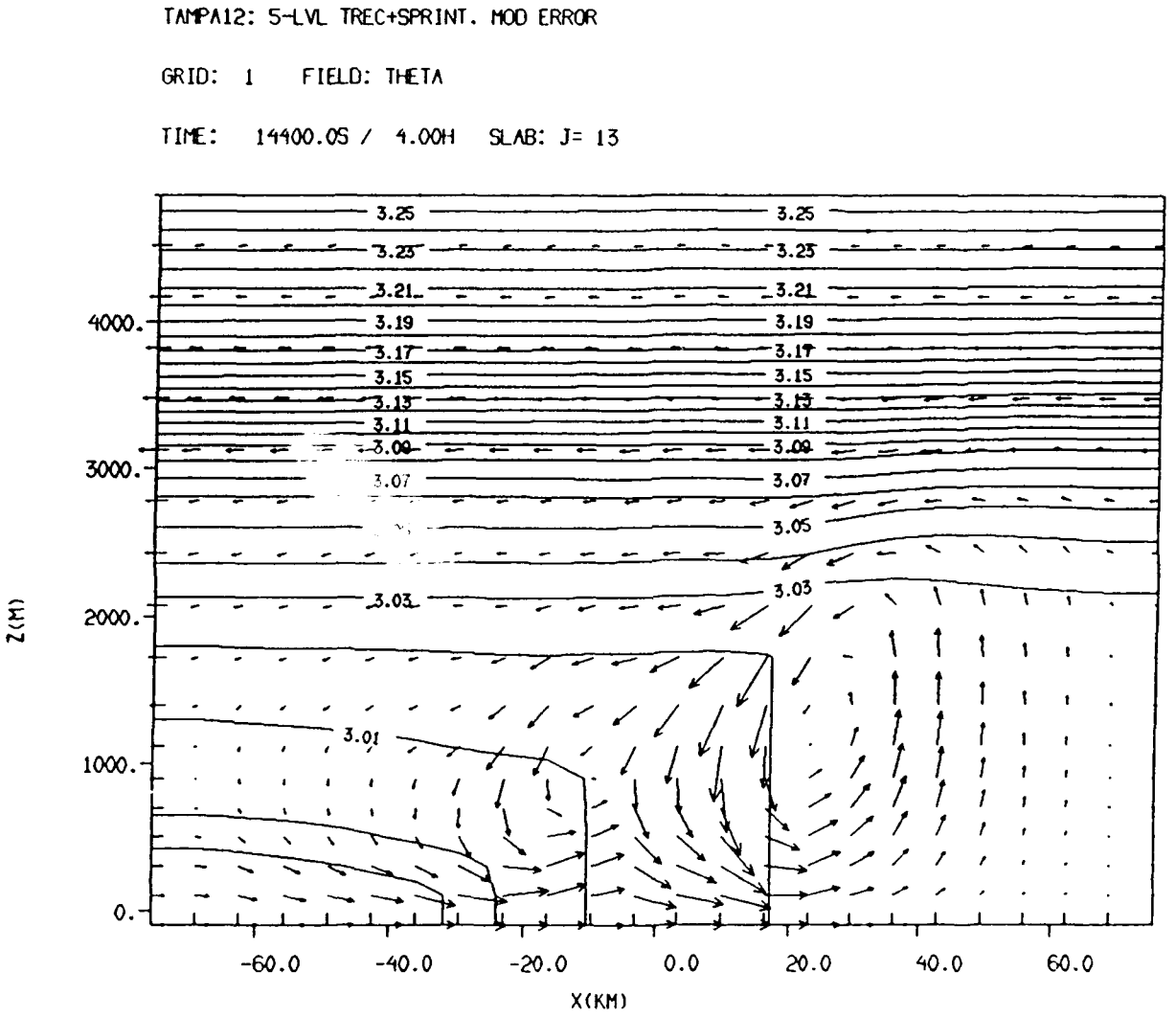

Figure 25 Continued

(a)

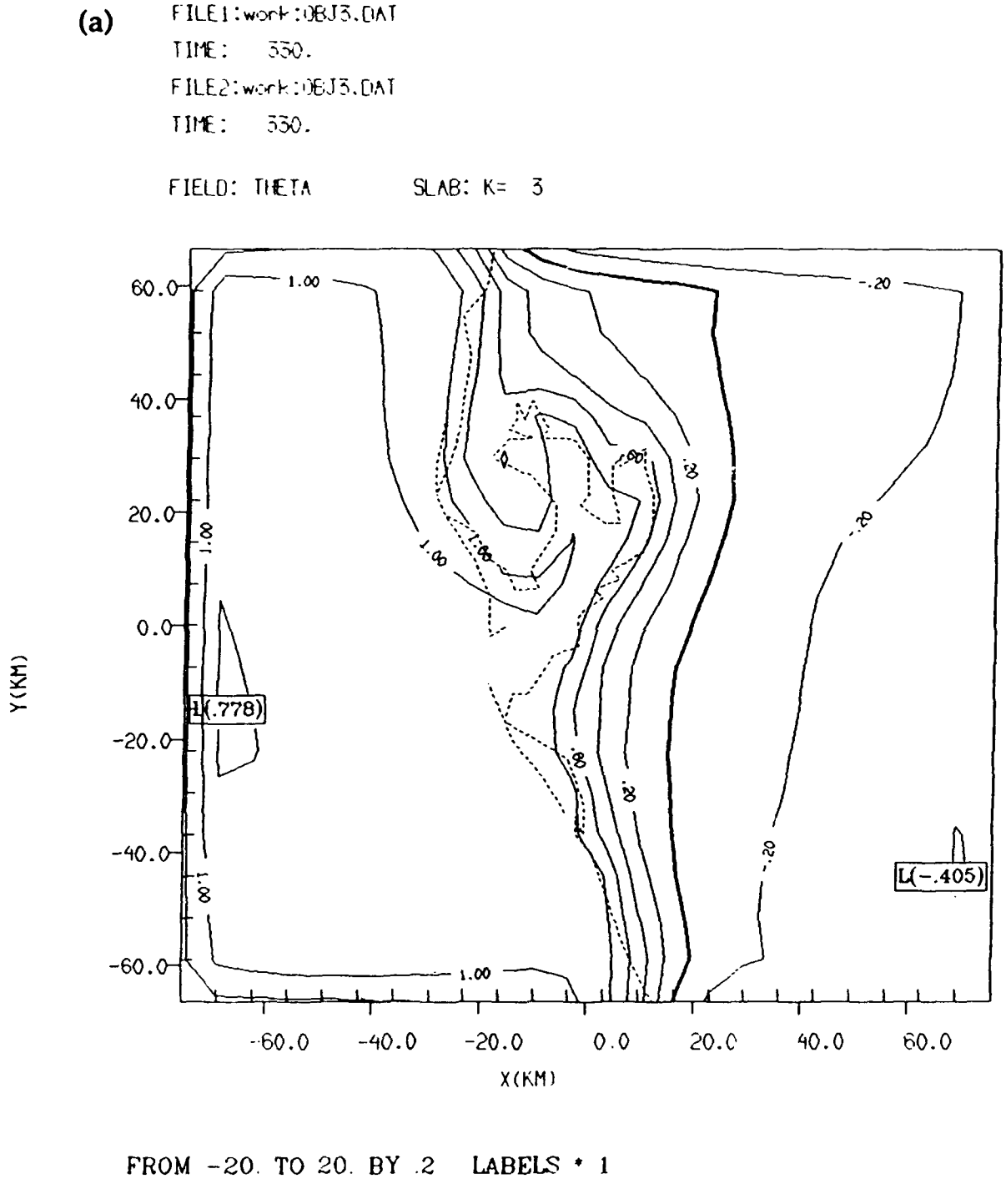

Figure 26: Plot of retrieved temperature errors at level z=3 for experiment 3. (a) Plot at time t=330 s, and (b) plot at time t=3630 s.

(b)

FILE1:work:OBJ3.DAT
TIME: 3630.
FILE2:work:OBJ3.DAT
TIME: 3630.

FIELD: THETA SLAB: K= 3

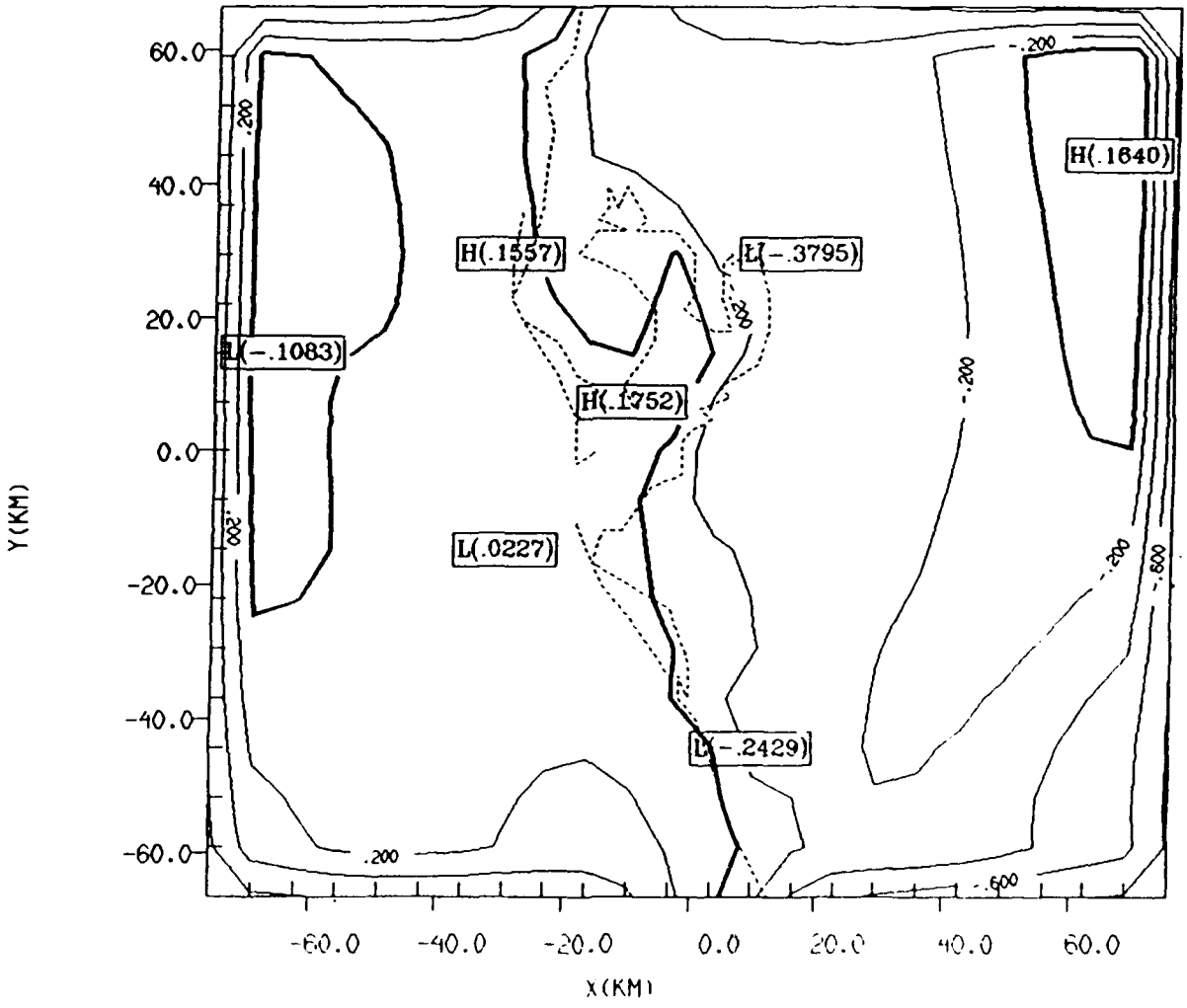

FROM -20. TO 20. BY 2 LABELS * 1

Figure 26 Continued

(a)

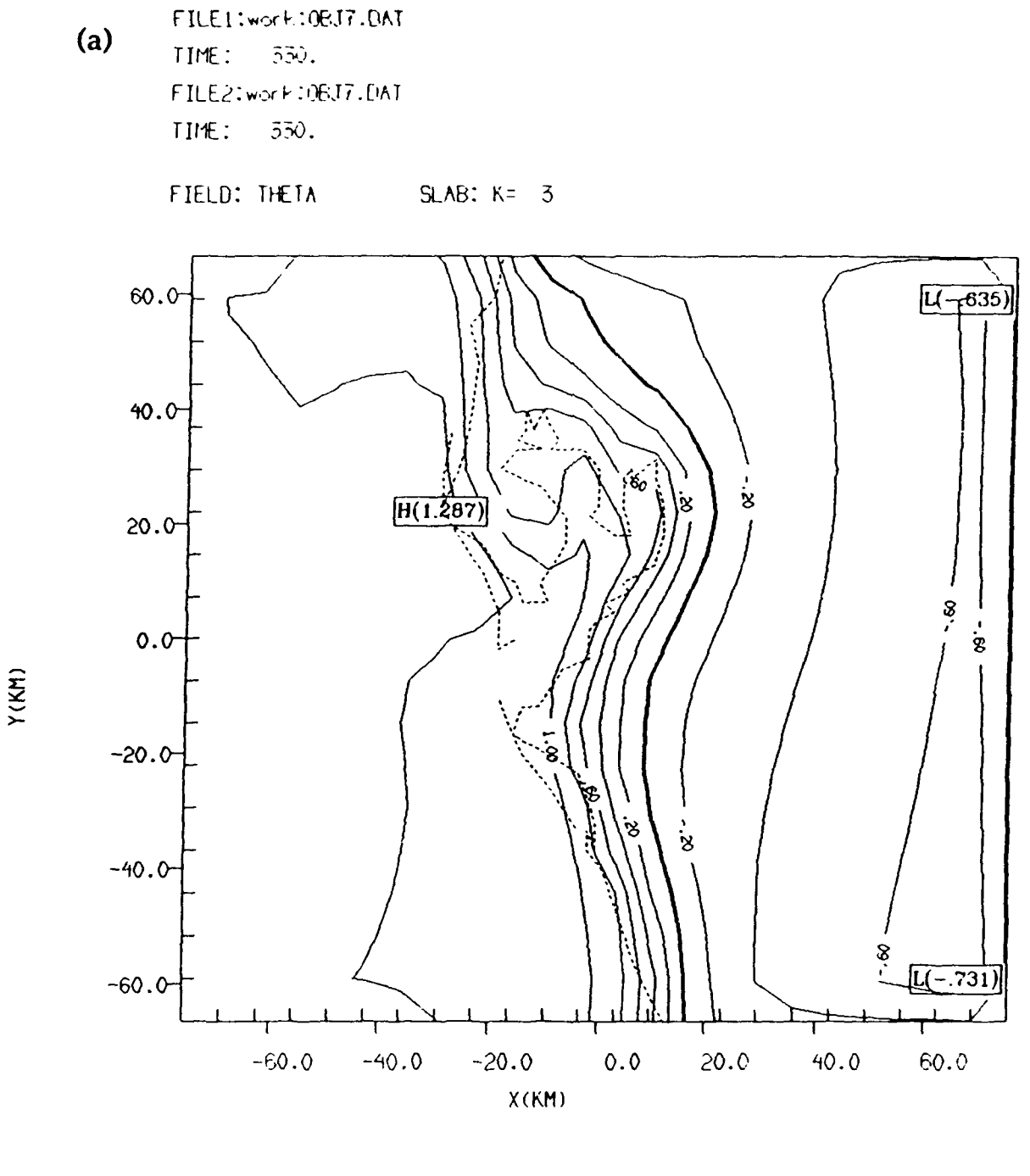

Figure 27: Plot of retrieved temperature errors at level z=3 for experiment 7. (a) Plot at time t=330 s, and (b) plot at time t=3630 s.

(b)

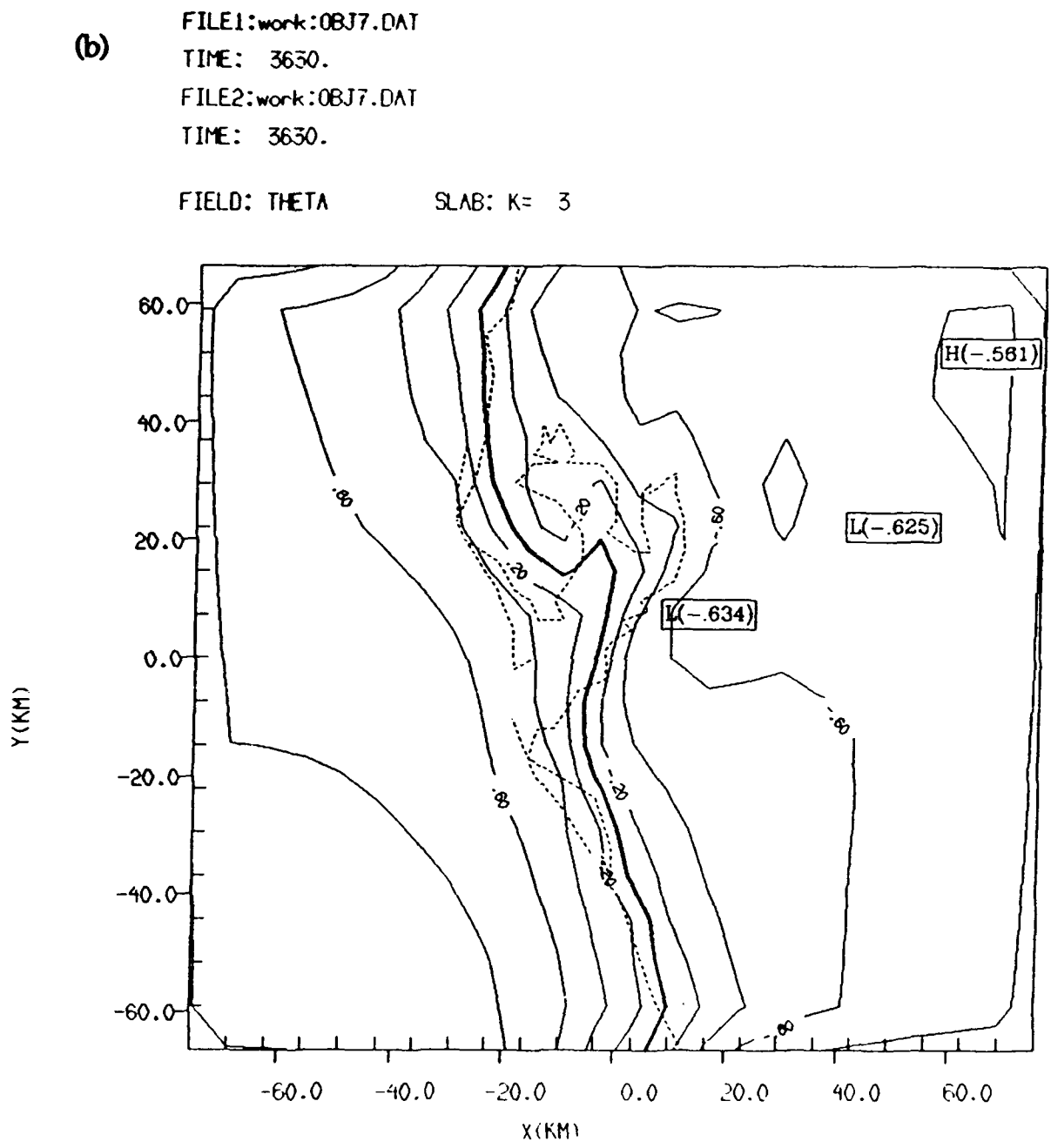

Figure 27 Continued